Mucosal macrophages govern intestinal regeneration in response to injury

Ilias Moraitis

regenerative state, and ultimately whether these processes are conserved in human as well.

In this study we identify a novel crosstalk between macrophages and the intestinal epithelial cells that regulates intestinal regenerative program in mouse and humans. Upon injury macrophages are recruited near the intestinal epithelium to express nrg1 and spp1 that induces the regenerative genetic program and the subsequent restoration of homeostatic conditions. Our findings revealed that macrophages are recruited around the intestinal stem cell compartment upon radiation injury, promoting a fetal-like reprogramming and proliferation of epithelial cells that drives the regeneration process. Collectively, this study identifies macrophages as essential contributors to intestinal regeneration beyond their innate immune response. Targeting macrophages therapeutically may hold promise in enhancing regeneration and improving the quality of life for cancer survivors.

Keywords: Gastrointestinal Physiology, Immunology, Radiotherapy, Gastroenterology

Resumen

La radioterapia es un tratamiento eficaz contra el cáncer. Sin embargo, induce toxicidad en los tejidos sanos que rodean el campo irradiado. La enteritis inducida por radiación es una complicación común de la radioterapia abdominal. Los síntomas incluyen sangrado, malabsorción, diarrea y dolor abdominal, los cuales afectan significativamente la calidad de vida de los pacientes. Además, debido a la gravedad de estos síntomas en algunos pacientes, el tratamiento debe interrumpirse, lo que pone en peligro la eficacia del tratamiento contra el cáncer. Actualmente, los tratamientos son sintomáticos porque no existe una cura médica. Nuestra hipótesis es que los pacientes con enteritis inducida por radiación se beneficiarían de terapias que mejoren la regeneración intestinal.

Tras una lesión, el epitelio se reprograma transitoriamente hacia un estado primitivo similar al fetal. La regeneración epitelial se logra mediante la proliferación de células madre intestinales (ISCs, por sus siglas en inglés) o mediante la dediferenciación de progenitores y células diferenciadas, las cuales adquieren un programa genético regenerativo para producir *de novo* ISCs, mostrando así una notable plasticidad celular. Esto nos llevó a plantear que, si comprendemos plenamente los mecanismos celulares y moleculares que impulsan la plasticidad celular, sería posible potenciar la regeneración intestinal tras una lesión intestinal.

En la última década, los macrófagos han recibido una atención significativa debido a sus funciones multifacéticas y a su diverso papel en procesos como la inflamación, la reparación y la remodelación. No

obstante, carecemos de un marco integral que describa cómo los macrófagos pueden influir en el proceso de regeneración intestinal a niveles celular y molecular, su posible papel en la adquisición de un estado regenerativo y, por último, si estos procesos también se conservan en humanos.

En este estudio identificamos una nueva interacción entre los macrófagos y las células epiteliales intestinales que regula el programa regenerativo intestinal en ratones y humanos. Tras una lesión, los macrófagos son reclutados cerca del epitelio intestinal para expresar nrg1 y spp1, lo que induce el programa genético regenerativo y la posterior restauración de las condiciones homeostáticas. Nuestros hallazgos revelaron que los macrófagos son reclutados alrededor del compartimento de células madre intestinales tras una lesión por radiación, promoviendo una reprogramación similar al estado fetal y la proliferación de células epiteliales que impulsan el proceso de regeneración. En conjunto, este estudio identifica a los macrófagos como contribuyentes esenciales a la regeneración intestinal más allá de su respuesta inmune innata. Dirigir terapéuticamente a los macrófagos podría ser prometedor para mejorar la regeneración y la calidad de vida de los sobrevivientes de cáncer.

Palabras clave: Fisiología Gastrointestinal, Inmunología, Radioterapia, Gastroenterología

Resum

La radioteràpia és un tractament anticancerigen eficaç. No obstant això, indueix toxicitat en el teixit sa que envolta el camp irradiat. L'enteritis induïda per radiació és una complicació comuna de la radioteràpia abdominal. Els símptomes inclouen sagnat, mala absorció, diarrea i dolor abdominal, que deterioren significativament la qualitat de vida dels pacients. A més, a causa de la gravetat d'aquests efectes en alguns pacients, s'ha d'interrompre el tractament, comprometent així l'eficàcia del tractament anticancerigen. Actualment, els tractaments són simptomàtics perquè no existeix una cura. Hipotetitzem que els pacients amb enteritis induïda per radiació es podrien beneficiar de teràpies que millorin la regeneració intestinal.

Després d'una lesió, l'epiteli és reprogramat transitòriament cap a un estat primitiu similar al fetal. La restitució epitelial s'aconsegueix mitjançant la proliferació de cèl·lules mare intestinals (CMI) actives o mitjançant la desdiferenciació de progenitors i cèl·lules diferenciades que adquireixen un programa genètic regeneratiu per produir de nou CMIs, mostrant així una notable plasticitat cel·lular. Això ens porta a plantejar que, si comprenem completament els mecanismes cel·lulars i moleculars que impulsen la plasticitat cel·lular, pot ser possible potenciar la regeneració intestinal després d'una lesió. En l'última dècada, els macròfags han atret una atenció significativa per les seves múltiples funcions i els seus diversos rols en processos com la inflamació, la reparació i la remodelació de teixits. No obstant això, no es coneix si els macròfags poden influir en el procés de regeneració

intestinal a nivell cel·lular i molecular, el seu paper potencial en l'adquisició d'un estat regeneratiu, i, en última instància, si aquests processos també es conserven en humans.

En aquest estudi identifiquem una nova interacció entre els macròfags i les cèl·lules epitelials intestinals que regula el programa regeneratiu intestinal en ratolins i humans. Després d'una lesió, els macròfags són reclutats prop de l'epiteli intestinal per expressar *nrg1* i *spp1*, que indueixen el programa genètic regeneratiu i la posterior restauració de les condicions homeostàtiques. Les nostres troballes han revelat que els macròfags són reclutats al voltant de cèl·lules mare intestinals després d'una lesió per radiació, promovent una reprogramació similar al desenvolupament fetal i la proliferació de cèl·lules epitelials que impulsa el procés de regeneració. Col·lectivament, aquest estudi identifica els macròfags com a contribuents essencials a la regeneració intestinal més enllà de la seva resposta immune innata. L'ús terapèutic de macròfags podria tenir potencial per augmentar la regeneració i millorar la qualitat de vida dels supervivents del càncer.

Paraules clau: Fisiologia Gastrointestinal, Immunologia, Radioteràpia, Gastroenterologia

Acknowledgments

I would like to thank Jordi's lab (Cell Plasticity and Regeneration Group), and all its members, for their support and help, and for creating an environment that encourages growth, success, and enjoyable moments.

I would like to thank my extremely positive supervisor, Jordi Guiu, for his guidance, support, and encouragement throughout my PhD. He is an excellent mentor, an inspiring motivator, and a person with great character, three qualities that are rarely found together in a PI. Your mentorship has been instrumental in my journey, and if I continue in academia and research, your influence will have played a significant role.

Thank you Monica, for all your help over these years. You taught me so many techniques and protocols and showed me how to work in the lab. I don't know how I would have managed without your support and advice. You've been such an important part of my PhD.

Borja, you've been an amazing colleague and an even better person. My PhD experience wouldn't have been the same without you. I can't even count the number of times you helped me with experiments or the great moments we shared both in and out of the lab. I wish everyone could have a colleague like you.

Thank you Olga for all your help and for being part of my PhD. I really enjoyed the time we spent together and appreciate everything you did.

Thank you Jasin for your help, feedback, and comments, as well as for the great time in the lab. I truly appreciate your support.

Thank you, Loris, for the incredible work you did and for analyzing and generating all these data. Without your efforts, it wouldn't have been possible for me to finish.

Thank you to everyone in the PCMR-C program, both former and current members, for all your help with the project whether it was lending reagents, providing valuable feedback and help or offering encouragement. Thank you, Yanis, Lea, Edgar, Mariana, Alba, Damia, Franz, Angel, A(n)dri for the great times we had in and out of the lab.

Paula and Priscila, thank you for the nice time in the lab, even though it was for a short while. I really enjoyed working with you.

Thanks to all facilities of IDIBELL, mouse lab (Juani Fernandez, Antoni Ventura, Aida Lopez and Marina Peñafiel) histology platform (Lola Mulero, José Antonio Llamas and Mireia Torres) optical microscopy platform (Jaume Boix Saioa Mendizuri and Joan Repullés) flow cytometry platform (José Vaquero) for their assistance and for training me to use the equipment. Your support was greatly appreciated.

Thank you my tutora Meritxel Rovira, for your feedback, comments, support, and guidance throughout my PhD. I appreciate your help.

Ευχαριστώ την ελληνική μαφία, Γιάννη, Βαγγέλη, Νικολέτα και Κατερίνα για όλες τις όμορφες στιγμές που περάσαμε Βαρκελώνη για την βοήθεια και την υποστήριξή σας όλα αυτά τα χρόνια σίγουρα δεν θα ήταν το ίδιο χωρίς εσάς.

Ένα μεγάλο ευχαριστώ στην οικογένεια και στους φίλους μου για την υποστήριξη και την βοήθεια που μου έδειξαν την περίοδο του διδακτορικού μου.

1 Table of Contents

1. Introduction

1.1 Small intestine

1.1.1 Digestive System, the Structure, and Functions of Intestine

The small and large intestine form a major part of the gastrointestinal (GI) tract and are located in the abdomen cavity. They are the biggest site of digestion and absorption of nutrients from ingested food [1]. The small intestine is composed of three anatomical and functionally disctint regions: duodenum, jejunum, and ileum [2] (Figure 1). The duodenum, the first and the shortest section of small intestine, receives partially digested food from the stomach along with pancreatic secretions rich in digestive enzymes. Positioned between the duodenum and ileum, the jejunum occupies the middle portion of the intestine. It contains circular folds and villi similarly to duodenum to increase surface area for absorbing of small nutrient particles that were enzymatically digested in the duodenum. These nutrients are subsequently transported to the liver through enterohepatic circulation. The ileum is the third part of the small intestine and contains villi like those in duodenum and jejunum. Functionally, the ileum absorbs vitamin B12, bile acids, and other remaining nutrients that not absorbed by jejunum [2].

A cross-sectional structure of small intestine contains four layers: mucosa, submucosa, muscularis, and serosa [3]. The mucosa consists of epithelial cells, that produce a thick protective fluid known as mucus. Its primary roles include absorbing and transporting nutrients, maintaining tissue moisture, and protecting the body from pathogens and foreign substances [4]. The submucosa is a relatively thin, and contains the blood vessels, nerves, and lymphatics. Submucosa supports the mucosa and joins it to the muscular

layer. The muscular layer consists of muscle tissue, and it is responsible for gut movement such as peristalsis. Finally, serosa is the outside layer of the small intestine and consists of mesothelium and epithelium [3].

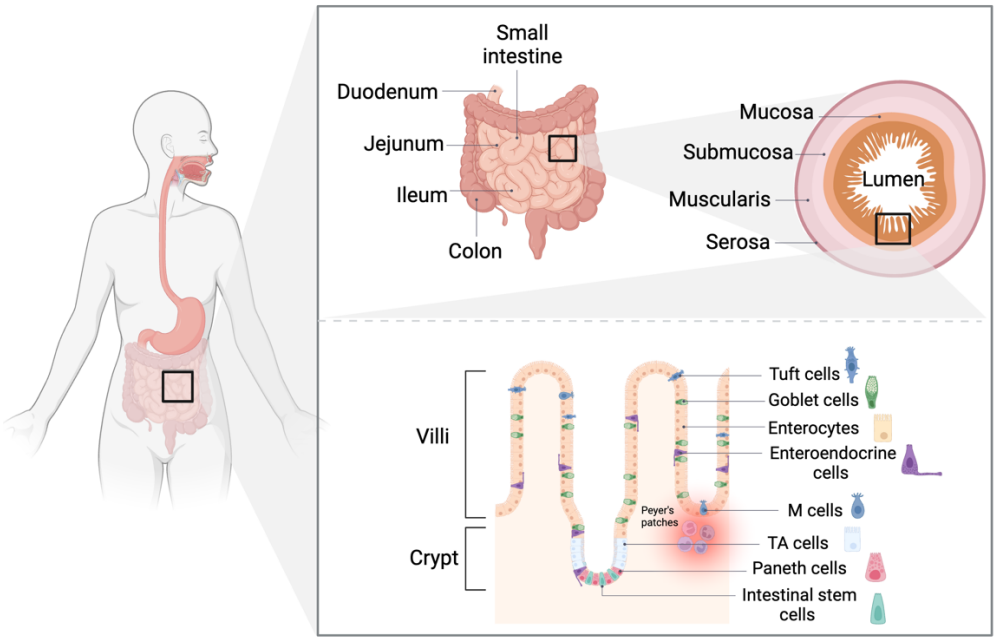

Figure 1: The structure of the small intestine. The small intestine is a long tube-like organ that connects the stomach to the colon. The small intestine includes the duodenum, jejunum, and ileum. The cross-sectional structure of small intestine contains four layers: mucosa, submucosa, muscularis, and serosa. Small intestine is composed of two connected structures, the villi and the crypts. In the crypt compartment are located intestinal stem cells, Paneth cells and transit amplifying (TA) cells. in the villi compartment are located differentiated cells: Goblet cells, Enteroendocrine, Enterocytes, Tuft and M cells. Illustration created using BioRender.

1.1.2 Intestinal Epithelial Cells (IECs)

The intestinal epithelium, the largest of the body's mucosal surfaces, covers approximately 400 m^2 and is equipped with specialized structures to optimize nutrient absorption. These structures include villi and crypts, each contributing uniquely to intestinal function.

Villi are small, finger-like projections extending into the lumen of the small intestine, covered by a single layer of epithelial cells. Their primary roles are the absorption and transport of nutrients, facilitated by their extensive surface area.

Crypts are tubular invaginations located between the bases of adjacent villi. Their main functions include cell renewal, as they house stem cells that regenerate the epithelium, and secretion of antimicrobial to maintain the intestinal homeostasis.

The intestinal epithelium is continually renewed by ISC that reside in the base of crypts. These cells give rise to differentiated cells through a well-orchestrated series of states from undifferentiated to fully mature cells [5, 6]. ISCs divide symmetrically to maintain their pool and produce progenitors that called transit-amplifying (TA) cells [7, 8]. TA cells start proliferating extensively to generate a large number of precursors for differentiated epithelial cells, losing their self-renewal capacity and retaining multipotency. This proliferation ensures rapid replenishment of the intestinal epithelium. Therefore, TA cells begin to lose their proliferative capacity and to transitioning into early differentiation where they begin to specialize into distinct lineages, including absorptive and secretory lineages. Finally, as these cells migrate upward from the crypt to the villus, they fully differentiate

epithelial cells. Terminally differentiated cells (i.e. Goblet cells, Tuft cells, Enterocytes, M cells, and Enteroendocrine except for Paneth cells) migrate up the crypt–villus axis until they are lost from the epithelial layer. This continuous renewal, taking approximately 4-5 days, ensures the intestinal epithelium remains functional and robust despite the harsh environment of the gut. For this process to be maintained, epithelial stem cells must be able to undergo repeated rounds of replication and possess the capacity for continuous self-renewal. The patterning and distribution of proliferating crypts in the intestine depend on paracrine signaling between the epithelium and the underlying mesenchyme. A balance between bone morphogenetic protein signals and antagonists, such as noggin and gremlin, provides a niche for proliferating stem cells while limiting ectopic crypt formation [5]. ISCs further depend on signaling through both the WNT–β-catenin and the Notch pathways for promoting self-renewal and directing differentiation towards secretory versus non-secretory lineage IEC fates [6] (Figure 7).

1.1.2.1 Intestinal stem cells (ISCs)

Intestinal stem cells were first reported in the 1970s by Cheng and Leblond [9]. Using electron microscopy, they identified slender cells interspersed between the granular Paneth cells at the bottom of the crypt or the so-called crypt base columnar (CBC) cells and were proposed as intestinal stem cells. Later, Bjerknes and Cheng provided additional information on these specialized cells using radioactive clonal marking techniques [10]. On 2007, Barker and colleagues described the leucine-rich repeat-containing G protein-coupled receptor 5 (Lgr5), the first bona fide marker of ISCs (Figure

2). Since then, other markers have been described, including olfactomedin 4 (OLFM4) [11], calcium-binding protein 2 (SMOC2) [12] among others. Besides the CBC cells, cells residing at the +4 position and expressing markers such as (Bmi1, mTert, Lrig1, and Hopx) [13] were proposed as a quiescent ISC population. This non-proliferative label-retaining cells were subsequently characterized as secretory progenitors that differentiate towards Paneth and enteroendocrine cells[14, 15]. Interestingly, after intestinal injury, these secretory progenitors can rapidly proliferate and generate clones of all major epithelial cell types, demonstrating their ability to revert to a stem-cell state and contribute to tissue regeneration [15].

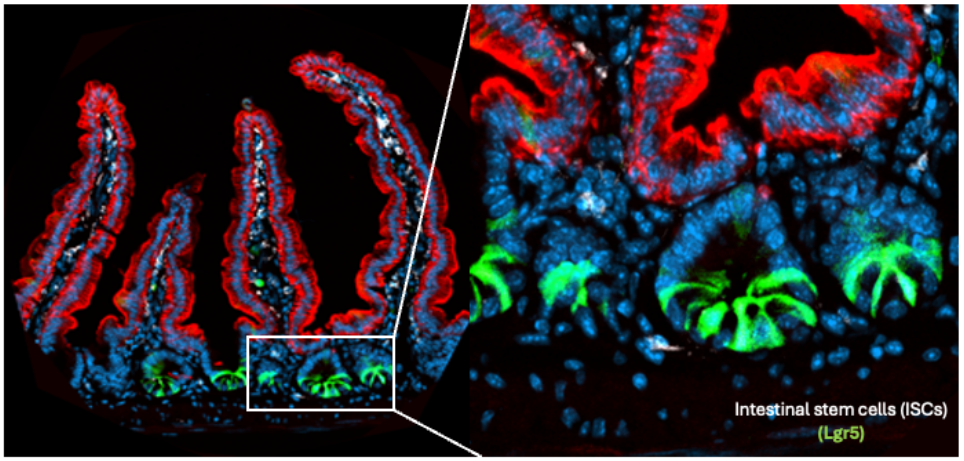

Figure 2: Lgr5+ intestinal stem cells are located in the crypt. Detection of KRT20 (differentiated epithelial cells, red), Lgr5-EGFP (ISCs, green), F4/80 (macrophages, white) and DAPI (blue) in tissue section from small intestine from Lgr5-eGFP-ires-creERT2 mouse demonstrate the location of ISCs in crypt compartment and differentiated cells in the villi compartment. Image generated during the thesis.

ISC divisions occur symmetrically and do not align with a model where two daughter cells resulting from an ISC cell division adopt divergent fates [8] [7].

In other words, both daughter cells retain the same stem cell properties and have the potential to continue self-renewal or differentiate into specialized cell types. Lineage tracing experiments have shown that crypts characterized by monoclonality [8]. This monoclonality is achieved by neutral competition of the space. Stem cells follow a stochastic pattern of behavior known as “neutral drift dynamics.” Which means that, if the last stem cell in a clone is lost (if the two daughters cells differentiated), that particular clone becomes extinct [8]. Therefore, crypts inevitably drift toward clonality. However, as demonstrated by Laila Ritsma and her colleagues, the process is not entirely neutral [16]. Their research reveals a positional bias in which stem cells positioned centrally within the crypt are more likely to persist compared to those located at the crypt's edges. This is because the central stem cells have a better access to the niche signals that regulate their maintenance and proliferation, giving them a competitive advantage over the border cells. Therefore, stem cell neutral competition in part ensures the maintenance of tissue homeostasis by allowing for the continuous turnover of cells while preventing the expansion of any single stem cell population. Recently findings challenges the previous model that attributed the renewal of the intestinal epithelium exclusively to Lgr5+ stem cells at the crypt base [17]. Using advanced fate-mapping techniques, the study identifies Fgfbp1+/Lgr4+ cells in the upper crypt zone as the root of the intestinal cellular lineage tree, rather than Lgr5+ cells. However, this discovery raises several important questions. For instance, are Fgfbp1+/Lgr4+ upper crypt cells a type of transit-amplifying (TA) cell? How do we reconcile their new characterization with their roles as stem cells? Since TA cells have historically been considered absorptive progenitors, could the process of generating an Lgr5+ cell from an

Fgfbp1+ cell represent a dedifferentiation event? We must be very caution with terminology and avoid making fast assumptions that could undermine years of well-characterized and established studies on intestinal cellular hierarchy. Nonetheless, this study highlights the truly remarkable plasticity of intestinal epithelial cells, not only during injury but also under homeostasis. With this study, it is an opportune to begin redefining what "stemness" truly means in the context of the intestine, embracing a more dynamic understanding of epithelial cells roles in regeneration and maintenance.

ISCs rely on various signaling pathways to maintain their stemness and regulate their differentiation into specialized cell types [18]. The mains keys signaling pathways that are involved in this process are: Wnt, Notch, Bone morphogenetic protein (BMP) and Hedgehog signaling. These signaling pathways work together in a coordinated manner to maintain the balance between stem cell self-renewal and differentiation, ensuring the proper function and homeostasis of the intestinal epithelium (Figure 7).

Wnt signaling: The Wnt gradient extending from the bottom of the crypt to the crypt-villus junction is crucial for the proliferation and maintenance of ISCs [19, 20]. Wnt ligands, which activate both the canonical and non-canonical pathways, are secreted into the surrounding niche by epithelial cells (Paneth cells) as well as stromal cells [21-23]. Lgr5 as a stem cell-specific receptor plays a critical role on Wnt signaling. It acts by enhancing Wnt signaling through its interaction with R-spondin proteins (RSPO1-4), which are ligands that amplify Wnt receptor activity [24]. When R-spondins bind to Lgr5 and its homologs, this interaction stabilizes Frizzled receptors and their

co-receptors (like LRP5/6) which inhibiting the ubiquitin-mediated degradation driven by negative regulators such as RNF43 and ZNRF3. This promotes the stabilization and nuclear translocation of β-catenin, a key transcriptional co-activator, which regulates the expression of Wnt target genes. In its inactive state, β-catenin is continuously degraded by a destruction complex composed by APC, Axin, and GSK3β among others [24] (Figure 3). Interestingly, blocking Wnt ligands or genetic ablation of mesenchymal cells that provide Wnt source, result in reduction of ISC proliferation followed by crypt loss [25-27].

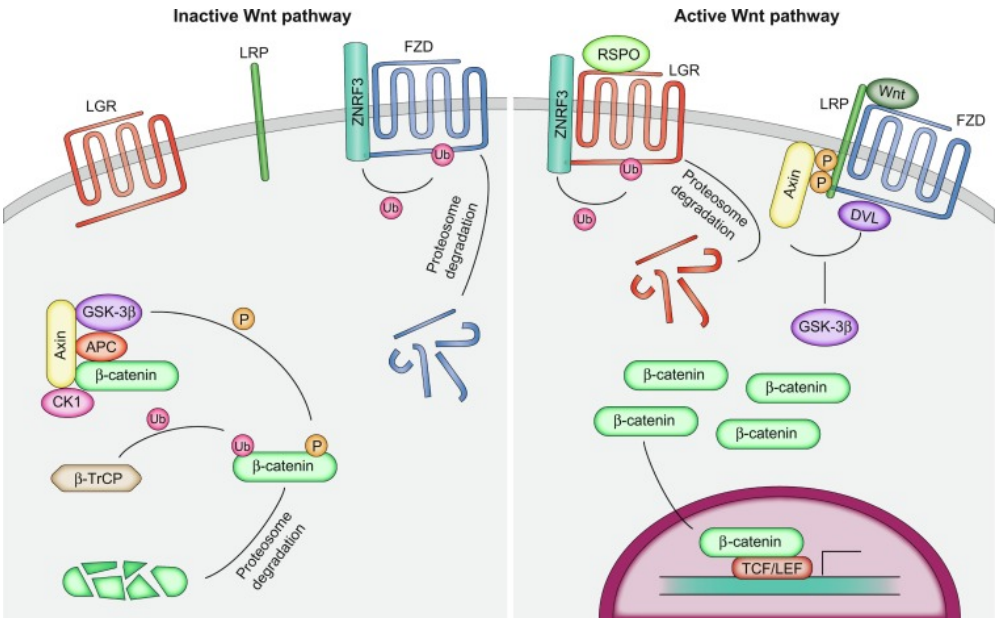

Figure 3: WNT signaling Cascade. In the absence of WNT ligand, the WNT pathway remains inactive, with ZNRF3 targeting FZD receptors for degradation and the β-catenin destruction complex promoting β-catenin degradation. This results in low FZD and β-catenin levels. When WNT is present, it binds to FZD, sequesters AXIN, and inhibits the destruction complex. As a result, β-catenin accumulates, enters the nucleus, and activates WNT target genes. RSPO

amplifies this process by binding to LGR, which recruits ZNRF3 away from FZD, increasing FZD receptor levels and enhancing cellular response to WNT. Adapted from the reference [28].

Notch signaling: Notch is essential for maintaining the pool of ISCs. The Notch signaling pathway in the small intestine involves interactions between Notch receptors (Notch1-4, with Notch-1 being the most prominent in the intestine) and their ligands, Delta-like ligands (Dll1, Dll3, Dll4) and Jagged ligands (Jag1, Jag2). Paneth cells have been identified as a source of Notch ligands from the delta-like family (Dll1/4), which activate Notch signaling in neighboring ISCs and support their maintenance [29-31]. Upon activation, the receptor undergoes cleavage by ADAM10 and γ-secretase, releasing the Notch intracellular domain (NICD). The NICD translocate to the nucleus, forming a transcriptional complex that upregulates genes like Hes1. Genes like Hes1 inhibit transcription factors necessary for secretory cell differentiation [32]. Therefore, this action promotes the differentiation of absorptive enterocytes while suppressing secretory lineages, maintaining intestinal epithelial balance (Figure 4). Inhibition of Notch leads to a reduction of the number and proliferation of Lgr5+ cells [33] and induced goblet cell differentiation [34]. Additionally, transgenic activation of Notch1 has been shown to increase ISC proliferation [35], while the combined deletion of Notch1 and Notch2 results in ISC loss and impairs regeneration after radiation [36].

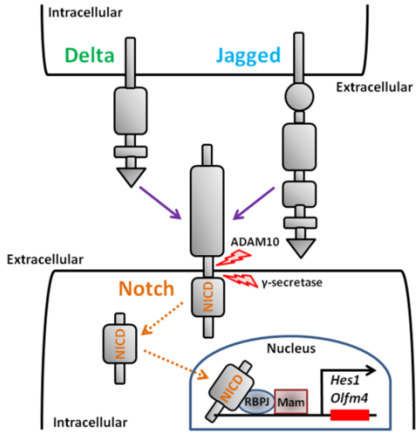

Figure 4: Notch signaling. Notch signaling requires interaction between two neighboring cells: one acting as the signal sender and the other as the receiver. The sender cell expresses ligands such as Delta and Jagged, which bind to Notch receptors on the receiving cell. This interaction triggers proteolytic cleavage of the receptor, releasing the Notch intracellular domain (NICD). The cleaved NICD translocate to the nucleus where it recruits a transcriptional coactivator complex that activates downstream transcription of Notch target genes such as Hes1. Adapted from the reference [32].

Bone morphogenetic protein (BMP) signaling: BMP signaling play a crucial role in the differentiation of epithelial cells and suppression of proliferation. BMP form an opposed gradient to Wnt signaling in the crypt-villus axis. Canonical BMP signaling is initiated when BMP ligands bind to a type II receptor, which then activates a type I receptor. This activation leads to the phosphorylation of SMAD1/5/8 proteins. The phosphorylated SMAD1/5/8 (pSMAD1/5/8) forms a complex with SMAD4, which translocates to the nucleus. This complex directly regulates the transcription of various target genes, such as Id2, which are crucial for cellular processes like differentiation. In addition to SMAD-mediated signaling activation, BMPs together with TGF-βs can also activate noncanonical signaling, which includes activation of the MAPK pathway [37] (Figure 5). BMP signaling activities can be modulated by several extracellular antagonists such as noggin and Grem1/2, which are secreted from mesenchyme [38, 39]. Inhibition of BMP signaling or transgenic expression of noggin or Grem1 in the villi results in ectopic crypt formation [40]. In addition, Noggin, inhibitor of Bmp and the agonist of Wnt,

R-Spondin1 are both important for the establishment of intestinal organoids cultures [41].

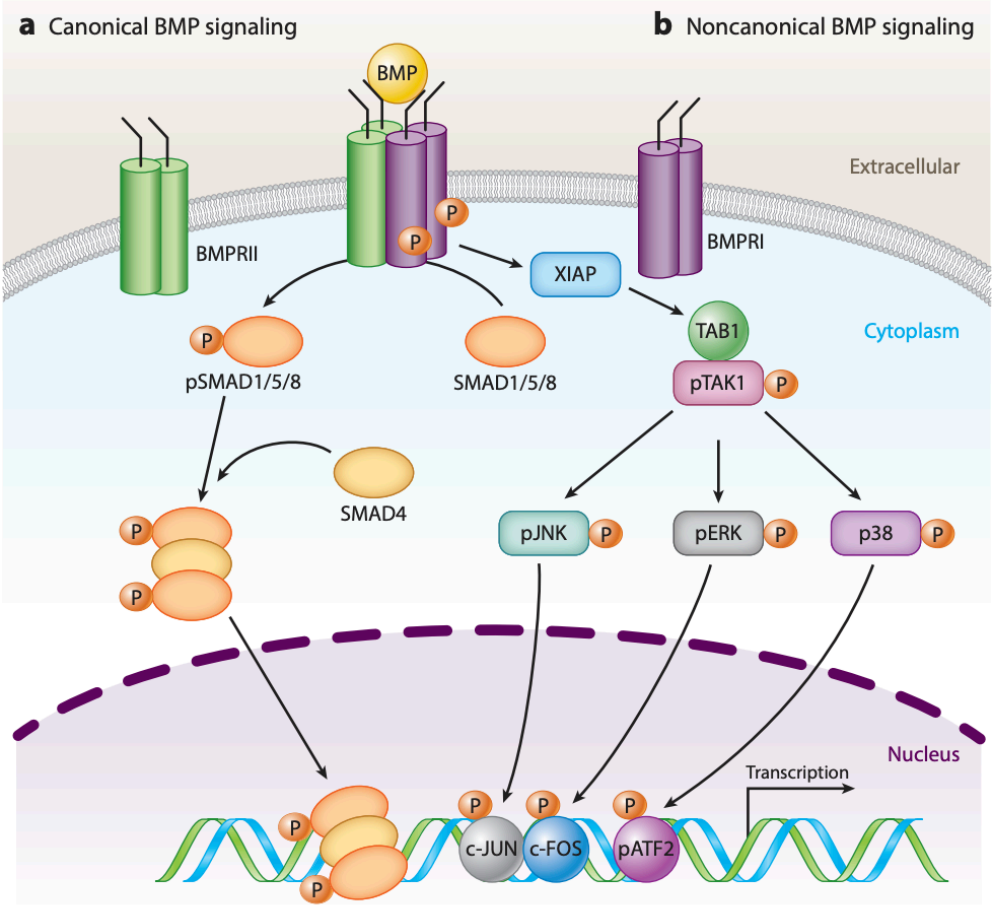

Figure 5: The BMP signaling pathway functions through canonical and noncanonical mechanisms. In canonical signaling, BMP ligands bind to a type II receptor, which phosphorylates the type I receptor, activating SMAD1/5/8. These SMADs form a complex with SMAD4 and regulate gene transcription in the nucleus. In noncanonical signaling, BMP receptors activate the TAK1-TAB1 complex, which triggers MAPKs (p38, ERK1/2, JNK). These kinases enter the nucleus, activating transcription factors like ATF2, c-JUN, and c-FOS, to control gene expression Adapted from the reference [37]

Hedgehog signaling: Hedgehog it's a very fascinating signaling, since the intestine, indirectly affects its own proliferation by secreting two Hedgehog ligands sonic hedgehog (Shh) and Indian hedgehog (Ihh). These two ligands regulate the secretion of the Bmp ligands from the surrounding fibroblasts, mesenchymal and muscle cells [42]. In the absence of Hh, Ptch inhibits Smoothened (Smo) from entering the cilium, while Sufu sequesters Gli proteins in the cytosol, leading to their phosphorylation and degradation into repressor forms (GliR). On the other hand, in presence of Hh, it is binding to Ptch, Smo enters the cilium, gets activated, and suppresses Sufu, stabilizing Gli activators (GliA). Hhip acts as a negative regulator by competing with Ptch for Hh binding, while other transmembrane proteins modulate Hh signaling [43, 44] (Figure 6). Suppression of Hedgehog signaling, induces crypt hyperproliferation and reduces differentiation [45].

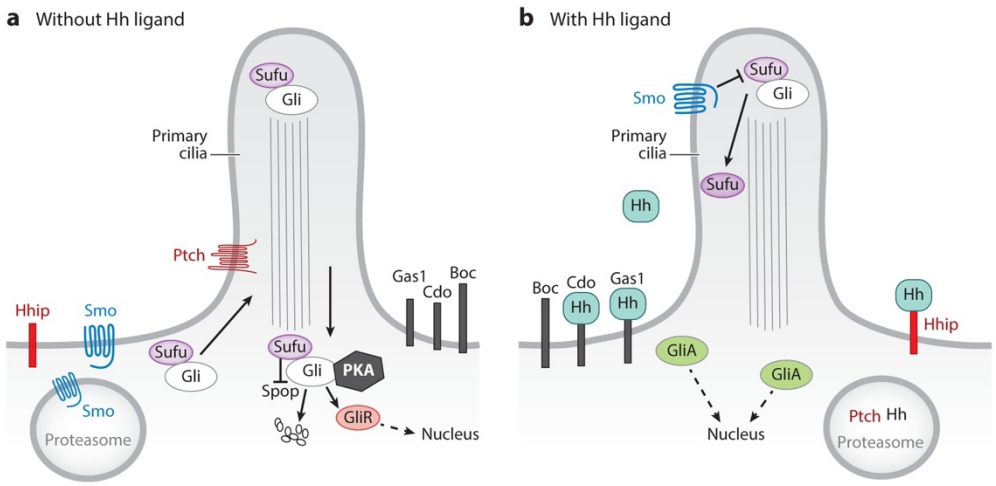

Figure 6: Hedgehog (Hh) ligands, secreted by epithelial cells, activate the pathway by binding to the Ptch receptor, allowing Smoothened (Smo) to enter the cilium and promote the stabilization of Gli activators (GliA). In the absence of Hh, Ptch prevents Smo entry, leading to the phosphorylation and degradation of Gli repressor forms (GliR). Hhip and other proteins like Cdo

modulate Hh signaling by interacting with Ptch or acting as coreceptors. Adapted from the reference [43].

Secretory cells lineage

1.1.2.2 Paneth cells

Paneth cells are located in the crypts of Lieberkühn adjacent to the intestinal stem cells. In contrary to the rest of differentiated cells, Paneth cells migrate towards the bottom of the crypt and their life span is around 2-4 weeks. Activation of Wnt/β-catenin pathway and inhibition of Notch results in differentiation of these cells [46]. Other important transcription factor for their differentiation is the Atoh1, which induces differentiation into a combined goblet/Paneth cell precursor cell lineage [47]. Paneth cells play a crucial role in maintaining intestinal homeostasis and host defense. They are characterized by their abundant secretory granules containing antimicrobial peptides such as defensins and lysozyme, to modulate microbiome which help to protect the intestinal epithelium from microbial invasion[48]. Additionally, Paneth cells as a part of the stem cell niche they are secreting proteins and peptides (Wnts, Notch and EGF ligands) to regulate the proliferation and differentiation of the ISCs [49], contributing to tissue repair and regeneration. However, multiple mouse models in which Paneth cell function is disrupted (for example, by loss of Paneth cells or disruption of their secretory activity) revealed profound alterations in bacterial colonization but not in the homeostatic renewal of the intestine [50, 51] suggesting that in their absence other cells can compensate their role as a ISC niche.

Representative markers of Paneth cells: Lyz, Defa4

1.1.2.3 Enteroendocrine cells (EECs)

Enteroendocrine cells produce a range of gut hormones that have key roles in the coordination of food digestion and absorption, insulin secretion and appetite [52]. They comprise only a small minority of the overall epithelial cells (<1%) [53]. Several transcriptional factors are required for the formation of enteroendocrine cells, with the most important the basic helix-loop-helix TF (NEUROG3)[54]. Interestingly, BMP signaling governs hormone expression dynamics in enteroendocrine cells along the intestinal crypt-to-villus axis which modulate their functional specialization and adaptability to gut environmental changes [55, 56]. Specifically, BMP signaling induces a switch in hormone profiles, with villus EECs expressing hormones like secretin (Sct) and peptide YY (Pyy), while crypt EECs predominantly express glucagon-like peptide 1 (GLP-1) [56]. Therefore, there are distinct subtypes of enteroendocrine cells in the gastrointestinal tract, and the hormones they secrete are highly dependent on their location reflecting their adaptability to different gut region's needs. In addition, enteroendocrine cells upon Paneth cell depletion, are able to provide Notch signals to ISCs [57].

Representative markers of Enteroendocrine cells: Chga, Chgb

1.1.2.4 Goblet cells

Goblet cells represent around the 10% of all IEC and secreting mucins and antimicrobial proteins (AMPs) which provides the first defense line against physical and chemical injury [58]. Differentiation of goblets cells is induced by both inactivation of Wnt and Notch signaling [59]. In patients with Crohn's disease, goblet cells show altered function and reduced mucus secretion,

which compromises the mucosal barrier and exacerbates intestinal inflammation [60]. In addition, goblet cells also interact with the immune system by presenting antigens and releasing cytokines, which play a role in modulating immune responses [61-63]. During colitis goblet cells upregulate RELM-β which promote the recruitment of CD4+ T-cells, increases interleukin-22 (IL-22) levels, and supports epithelial cell proliferation, resulting in reduction of mucosal injury [64]. Disruptions in this process are thought to contribute to irregular immune response and inflammatory environment. Interestingly, like enteroendocrine cells, goblet cells depend on their location in the crypt-villus axis display differences in expression of antimicrobial genes [65].

Representative markers of Goblet cells: Muc2, Tff3

1.1.2.5 Tuft cells

Tuft cells are a rare population of epithelial cells in the small intestine that play a critical role in sensing luminal stimuli and orchestrating immune responses. Although they derived from DLL+ secretory progenitors, their differentiation does not depend on secretory lineage transcriptional factors. Tuft cells are chemosensory and produce cytokines such as IL-25, which activate type 2 innate lymphoid cells (ILC2s), promoting immune responses against parasitic infections and regulating intestinal homeostasis [66]. Moreover, similar to enteroendocrine cells, upon Paneth cell ablation tuft cells are able to provide Notch signals to ISCs [57].

1.1.2.6 M cells

Microfold (M) cells are specialized epithelial cells located in the Peyer's patches in the small intestine. Their primary function is to transporting pathogens and particles from the lumen to immune cells to initiate mucosal immune responses [67]. They are essential for maintaining immune surveillance and promoting tolerance or defense against

ingested antigens and pathogens, making them important part of gut immunity. For the differentiation of M cells it requires the activation of nuclear factor-kB (RANK) by RANK ligands that are expressed from stromal cells covering the t Peyer's patches [68].

Absorptive cell lineage

1.1.2.7 Enterocytes

The majority of cells bordering the intestinal lumen are absorptive enterocytes. Enterocytes are columnar cells that play an important role in nutrient absorption and secreting immunoglobulins.

For the differentiation of enterocytes its necessary the WNT inhibition and Notch activation [59]. It is interesting that enterocytes are not characterized by one homogeneous population but rather a broad spatial heterogeneity in the crypt-villus axis [69]. At the lower part of the villus, enterocytes express an antimicrobial genetic program. Mid-villus enterocytes preferentially engage in the absorption of amino acids and carbohydrates, whereas villus tip cells are engaged in increased secretion of chylomicrons and are involved in anti-inflammatory pathways [69].

Representative markers of Enterocytes: Alpi, Ada

Although intestinal cell types are classified in these major groups each epithelial type consists of subpopulations with shared characteristics, but slightly distinct functions which influenced by their position along the villus-crypt axis and local signaling cues . This spatial specialization allows cells to respond dynamically to local signals, optimizing their roles in digestion,

nutrient absorption, immune function and to protect the host from infection and continuous exposure to potentially injury.

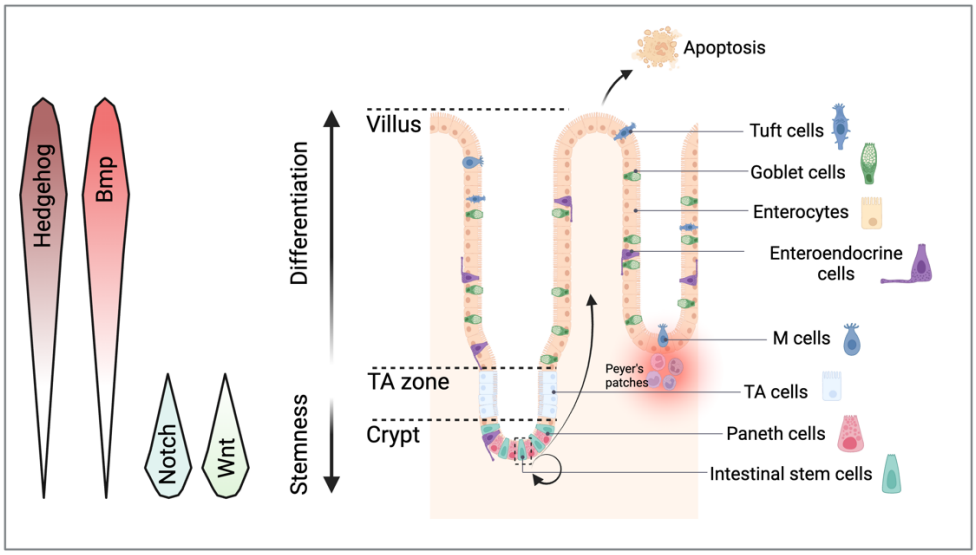

Figure 7: Organization of adult small intestine. The small-intestinal epithelium is structured into units called crypts and villi. Interspersed within the crypts are intestinal stem cells (ISCs), positioned alongside Paneth cells, which provide essential WNT and Notch ligands for maintaining stemness, as well as epidermal growth factor (EGF) to support proliferation. As stem cell daughter cells migrate upward from the crypt base, they encounter diminishing WNT signals and increasing bone morphogenetic protein (BMP) signals. BMPs negatively regulate stemness, and together with WNT and Notch signaling, they delineate the boundaries of the stem cell zone. The opposing gradients of WNT and BMP are established through differential expressions of agonists and antagonists along th9e crypt-villus axis. Additionally, the crypt houses transit-amplifying cells, which undergo multiple rounds of proliferation before maturing into functional secretory (enteroendocrine, goblet and tuft cells) and absorptive (enterocytes) cells and migrate to villi compartment. Eventually, cells are pushed from the villus tips at the end of their lifetime to undergo apoptosis. Illustration created using BioRender.

1.2 Radiation-induced enteritis and intestinal regeneration.

1.2.1 Radiation induced enteritis.

As radiation technology becomes more widely used, there is a high risk of accidental acute radiation. Exposure to ionizing radiation (IR) from radioactive sources can lead to total body irradiation (TBI), while radiotherapy as a treatment for abdominal cancer can increase the risk of whole abdominal irradiation (WAI) exposure. Radiotherapy has emerged as an efficient cancer treatment; with more than 12 million cancer survivors in Europe [70] and will likely keep growing. Approximately 50% of cancer patients undergo treatment with radiotherapy, with around half of them receiving radiation in the abdominal or pelvic cavity, typically as a treatment for cervical, prostate, colon, or pancreatic cancer. However, due to the close proximity of the GI tract to the pelvic organs and the high rate of crypt cell proliferation, the intestine is sensitive to damage by radiotherapy. Radiation damage to the intestine and consequential symptoms are classified as radiation-induced enteritis. Therefore, up to 90% of patients undergoing radiation therapy in the abdomen, pelvis, or rectum develop radiation-induced enteritis [71]. Initially, radiation triggers apoptosis of proliferative cells, this denudes the intestinal mucosa and in turn results in an inflammatory response. The symptomatology of radiation induced enteritis is characterized by bleeding, malabsorption, diarrhea, abdominal pain, nausea, and vomiting [71]. These effects are so dramatic that some patients are forced to interrupt their treatment, which can compromise the effectiveness of anticancer therapies. Unfortunately, treatments for the pathologies are only palliative because there is no medical cure [72]. Currently the most commonly adopted

approach is still a reduction in the delivered radiation dose [71, 73, 74], although this may lead to a decrease in treatment efficacy. In conclusion, the widespread use of radiotherapy in cancer treatment, coupled with the significant side effects that experienced cancers survivors, underscores the need to address this serious medical issue. Therefore, it is important to provide mechanistic insights into radiation-induced enteritis in order to develop treatment to boost intestinal regeneration and mitigate the side effects of radiation.

1.2.2 Radiation injury as model for studying intestinal regeneration.

The acute phase of radiation-induced enteritis occurs within days of exposure because of the loss of intestinal proliferative cells leading to loss of epithelial crypts and ulceration. The severity of the mucosal breakdown and the ability of the tissue to repair the damage and to achieve the restitution of the epithelium is strongly radiation dose dependent. Most radiation therapy regimens for humans are typically administered in fractions of 1.8 to 2 Gy per session delivered over the course of several weeks, this differs from the much higher doses of Gy that been used in mouse models. However, despite the difference in dosing, the histopathological effects observed in tissues such as villus shortening and degenerative crypts, are consistent across species, including mice, non-human primates, and humans [71, 75]. In mice lethal intestinal injury could be triggered by ≥6 Gy total body irradiation (TBI) and >15 Gy whole abdominal irradiation (WAI) [76]. The variances in survival rates between mice exposed to TBI and WAI can be attributed to hematological acute radiation syndrome. In TBI, even if mice successfully undergo intestinal

repair, they ultimately succumb to hematological acute radiation syndrome shortly afterward [77]. Conversely, in WAI if a fraction of bone marrow survives of radiation expose, may be sufficient to repopulate the hematopoietic system allowing long-term survival [78]. The first symptom in a mouse is weight loss. Weight loss increases as a result of dehydration during the diarrheal stage and if it fails to recover becomes necessary a human endpoint [78]. Histopathological, the structure of the small intestinal villi is destroyed and there is a vast reduction of crypts [78, 79] (figure 8).

However available information on TBI and WAI doses that cause intestinal damage among mice and the timepoints that the weight and the intestinal architecture is recovered are conflicting. This occurs due to the different irradiation techniques, radiators, age of mice and the genetic background of mice, resulting in different biological outcomes.

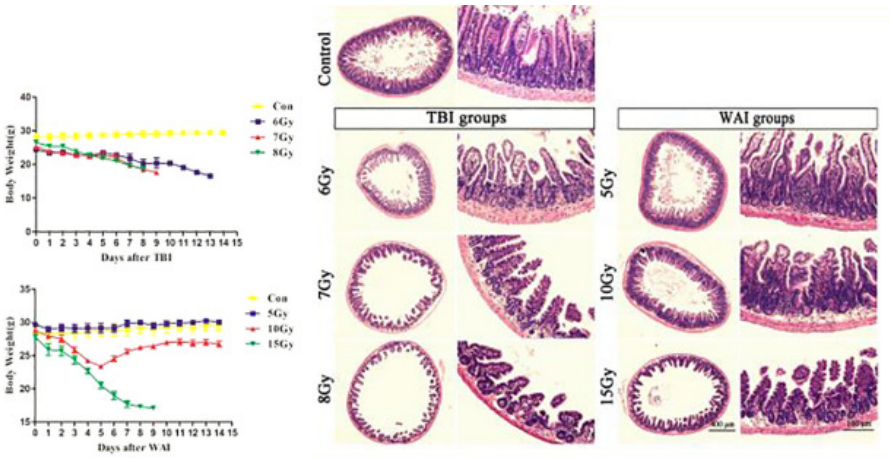

Figure 8: (A) The body weight of mice during different TBI and WAI doses. (B) H&E stained sections of the small intestine upon different radiation doses. The structures of the mucosa and submucosa were destroyed in the 6, 7, and 8 Gy TBI groups and in the 10 and 15 Gy WAI groups. Adapted from the reference [76].

1.2.3 Intestinal regeneration

The intestinal epithelium is normally replaced every 4–5 days and thus has one of the highest turnover rates in the human body, reflecting the impressive regenerative ability of this organ. The intestinal epithelium constantly faces various injuries and a plethora of therapies, including radiotherapy, chemotherapy and antibiotics can destroy the actively proliferating $Lgr5^{+}$ ISCs. Therefore, the integrity of the epithelial layer must be rapidly restored to prevent infections. To achieve this, the intestine is reprogrammed into a fetal-like primitive state. The epithelial restitution is achieved by the proliferation of active ISCs (Lgr5+) or via dedifferentiation of progenitors and committed cells that acquire a fetal-genetic program to *de novo* produce ISCs [80-84] (Figure 9). Upon injury, Dll1+ secretory progenitor cells revert to stem cells upon crypt damage [81]. Dll1+ secretory progenitors, a subset of Notch ligand-expressing cells derived from Lgr5+ intestinal stem cells, are primarily committed to generating secretory lineages, including goblet, Paneth, and enteroendocrine cells. However, under conditions of crypt damage, these cells can revert to a stem cell-like state, regaining their ability to sustain tissue regeneration. Another similar study, identifies the phosphorylation of ATOH1 as a key mechanism that governs the plasticity of secretory progenitor cells, enabling them to revert to a stem-like state [85]. Using lineage tracing, demonstrated that ATOH1+ cells can generate diverse intestinal cell lineages under both steady-state and regenerative conditions. However, a phosphomutant model (ATOH1(9S/T-A)) revealed that preventing ATOH1 phosphorylation biases these progenitors toward secretory differentiation, reducing their capacity for self-renewal and regenerative responses [85].

Also, absorptive progenitors are able to revert to a stem-like state. When Lgr5+ stem cells were ablated, Alpi+ cells dedifferentiated to produce long-lived crypt-villus "ribbons." These ribbons contained cells resembling both Paneth cells and functional proliferative stem cells [84]. In agreement with this, it was recently shown that isthmus cells (above +4 position), are able to give rise to Lgr5 ISCs [86]. Upon intestinal injury and loss of Lgr5+ stem cells, Lyz1+ Paneth cells proliferate and differentiate into villus epithelial cells [87]. RNA-seq revealed that Paneth cells sorted from irradiated mice acquired a stem cell-like transcriptome; when cultured *in vitro*, these individual Paneth cells formed organoids. Irradiation activated Notch signaling and forced expression of NICD in Paneth cells, but not Wnt/beta-catenin pathway activation, induced their dedifferentiation [87]. As mentioned previously Bmi1 was proposed as a quiescent stem cell marker[13] and later shown to be secretory progenitors. Bmi1+ upon injury can revert to Lgr5+ ISCs and regenerate the intestinal epithelium after ISC loss [88]. In addition, a subset of Dclk1+ tuft cells that are long-lived, retain the ability to dedifferentiate and regenerate the intestinal epithelium, or form tumors in loss of APC function upon injury [89].

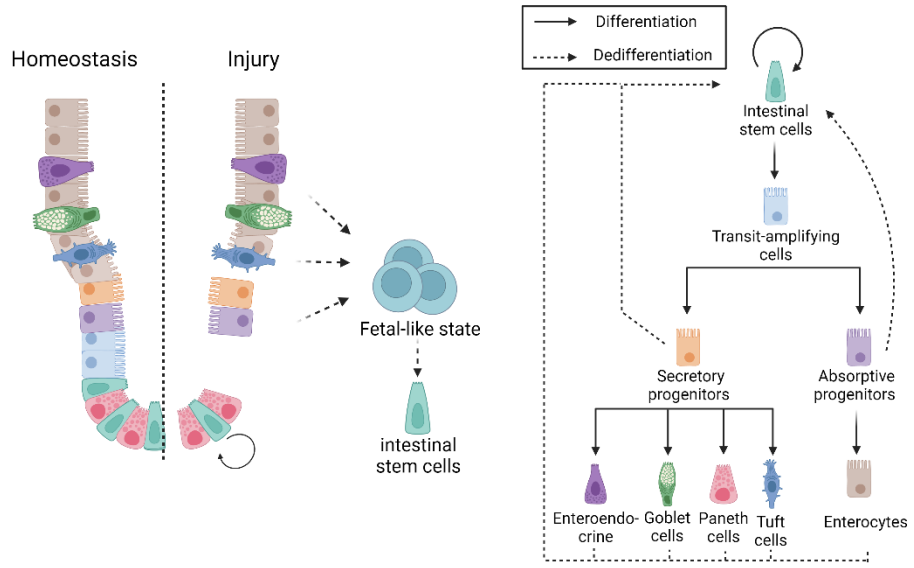

Figure 9: Schematic of repair mechanisms in adult small intestine in response to injury. Upon radiation injury, there is a significant loss of intestinal stem and proliferating cells. This damage triggers a regenerative response in which differentiated cells and progenitors undergo dedifferentiation, acquiring a fetal-like state. This enables them to repopulate the depleted stem cell pool, facilitating the restitution of the intestinal epithelium. Moreover, the intestinal stem cells that survived the radiation injury play a crucial role in the regeneration process by proliferating and differentiating to restore normal intestinal function. The interplay between dedifferentiated cells and surviving stem cells ensures a robust and efficient recovery of the intestine, highlighting the remarkable plasticity and resilience of the intestinal epithelium in response to injury. Illustration created using BioRender.

Epigenetic modifications, such as DNA methylation, play crucial roles in the differentiation of the intestinal epithelium [90]. However, studies have shown that the differences in DNA methylation profiles between ISCs and differentiated cells are not vast [91, 92], indicating that the epigenetic state of the intestinal epithelial cells is not hard-wired. This adaptable epigenetic state of intestinal epithelial cells makes them susceptible to the exposure of

factors that support the stem cell fate and allows them to de-differentiate and to acquire stem cells properties. Therefore, it appears that most intestinal epithelial cells, whether progenitors or differentiated, retain a degree of plasticity that allows them to dedifferentiate and regain stem cell properties. This strongly influenced probably by their location within the crypt-villus axis and their access to signals and factors that promote stem cell fate.

As expected, signaling networks such as Wnt and Notch pathway that play a pivotal role in the proliferation and self-renewal of ISCs, they have been reported to be involve also in the intestinal repair following injury [36, 93-95]. For instance, Rspo3 restore the intestinal epithelial barrier by promoting the reprogramming of differentiated cells into stem-like states [95]. Specifically, Rspo3 drives recovery by inducing Lgr4-dependent signaling in differentiated cells such as Krt20+ enterocytes, enabling them to regain stem cell properties [36]. Furthermore, after radiation in Notch1- and Notch2-deleted intestine the crypt regeneration was impaired, suggesting that higher Notch activity is required post-injury. In addition, activation of Notch supported epithelial regeneration by suppressing goblet cell differentiation, but it also promoted cell proliferation [93]. Another key player that is considered a hallmark of regeneration is the Hippo pathway and its downstream effectors, the transcriptional coactivators Yes-associated protein (YAP) and transcriptional coactivator with PDZ-binding motif (TAZ)[82, 83, 96]. The cellular localization of YAP/TAZ is particularly essential for their activation. Upon injury, YAP/TAZ undergo translocation from the cytoplasm to the nucleus, where they become activated and modulate gene expression programs associated with proliferation, survival, and tissue remodeling. In addition, YAP/TAZ activation can suppress components of the Wnt pathway, creating a regulatory balance

between proliferation and differentiation. YAP overexpression has been observed to elevate markers associated with the fetal epithelium while reducing markers linked to adult stem cells and differentiated lineages [83]. Its absence/inhibition resulting in increased levels of epithelial apoptosis, less proliferation, and decreased mice survival during intestinal injury [83, 96, 97]. On the other hand, hyperactivation of YAP may associated with cancer development [98] (Figure 10)

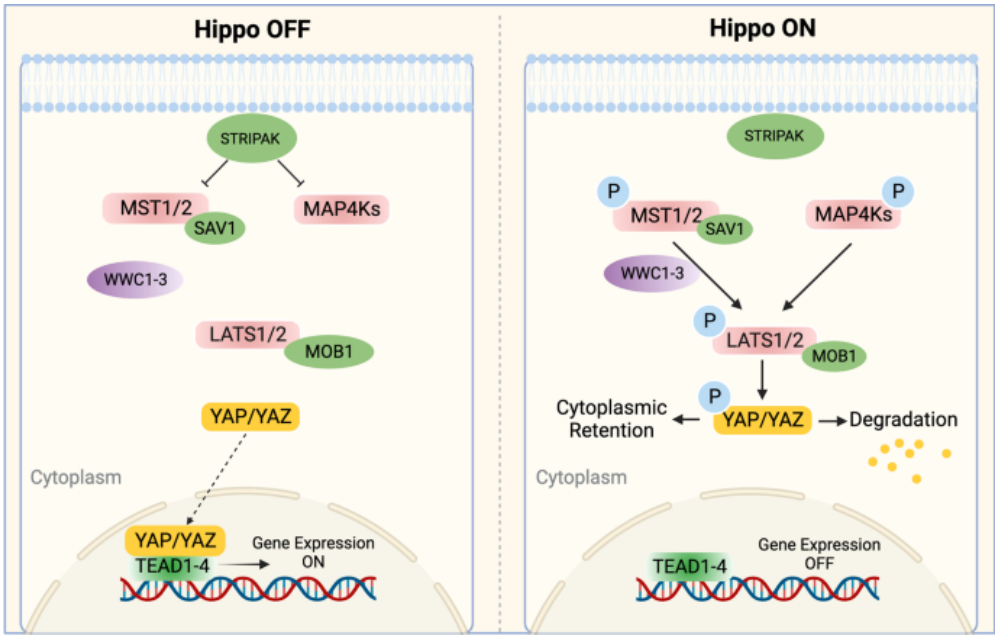

Figure 10: The core Hippo pathway is regulated by the STRIPAK complex, which controls MST1/2 and MAP4Ks. These kinases, with the help of scaffolds like SAV1 and WWC1–3, activate LATS1/2. Phosphorylated MOB1 enhances LATS1/2 activation, leading to the phosphorylation and inactivation of YAP/TAZ. This process prevents YAP/TAZ from entering the nucleus and binding to TEAD transcription factors. Adapted from the reference [99].

1.2.4 Fetal-like transcriptional program

The contribution of YAP/TAZ in intestinal regeneration have been study extensively. Additionally, there other signaling networks that coordinate cellular plasticity of intestinal epithelium in response to damage. For instance, several groups have identified the presence of fetal-like transcriptional program in response to intestinal damage which characterize by the expression of stem cell antigen-1 (Sca1) marker [82, 83, 100]. YAP and TAZ are required for the repair process after DSS-induced injury and are closely associated with driving the formation of the Sca1-expressing repaired epithelium [83]. In that case intestinal epithelial cells acquire a fetal-like/regenerative signature to promote repair. The last years with the advance of single cell RNA sequencing have been identified several fetal-like markers including Clu, Anxa1, Anxa3, Anxa5, Sppr1a among others [82, 101]. In fact, all epithelial cells irrespective of their location and pattern of LGR5 and differentiation markers expression in the fetal gut contribute actively to the adult intestinal stem cell pool [80], indicating that cellular plasticity is physiological during development. If this tremendous plasticity of intestinal epithelial cells is exclusively intrinsically regulated or instead requires modulation from their cell niche remains poorly characterized.

1.3 Macrophages: scavengers or architects?

1.3.1 Intestinal macrophages

In the intestine, regeneration of the intestinal epithelium relies on complex crosstalk between epithelial cells and surrounding niche cells that include endothelial, mesenchymal, neuron and immune cells [102][103-107]. The last decade macrophages have garnered significant attention due to their multifaceted functions.

In the gut, macrophages are present directly beneath the intestinal epithelial cell layer in the lamina propria [108] and also reside in deeper layers in the

intestine, including the submucosa and the muscularis externa. In the intestine there is the biggest accumulation of macrophages [108, 109]. Macrophages form a dense network of cells along the GI tract and ontogenically can be distinguished toward two main subtypes: i) tissue-resident macrophages which are proliferate locally and are long-lived during steady-state adulthood [110, 111] and ii) monocyte-derived macrophages that can have different life cycles and either become long-lived or shorter-lived and constantly be replenished from bone-marrow HSCs [110]. Gut resident macrophages are characterized by the expression of CD4 and Tim-4 markers among others [112]. However, there is currently no definitive marker specific to intestinal macrophages. Nevertheless, some widely used pan-macrophage markers include CD11b, F4/80, and CD68 among others. Traditionally, macrophages have been described as phenotypically either pro-inflammatory (M1) or anti-inflammatory (M2) as an over-simplification [113]. *In vitro* the polarization of macrophages towards these phenotypes is very well characterized. However, *in vivo* there is a grater complexity that includes a gradation of phenotypes between pro- and anti-inflammatory macrophages [114, 115]. This high heterogeneity that macrophages present also reflect their ability to regulate different cellular process such as inflammation, repair, remodeling, development and regeneration in numerous tissues including the small intestine [116, 117].

1.3.2 Homeostatic functions of intestinal macrophages

Macrophages are master regulators of the innate immune system and are needed to maintain tissue homeostasis (Figure 11). It's very well characterized their role in defense against invading pathogens via phagocytosis or uptake of bacterial antigens, crosstalk to other immune cells,

and promote or inhibit inflammation [118]. Since the intestine harbors the greatest bacterial load in the human body [119] intestinal macrophages play an important role in preventing bacterial dysbiosis [120] and maintaining tissue homeostasis. In line with their function, intestinal macrophages exhibit elevated expression of genes linked to phagocytosis, including Mertk, Cd206, Gas6, Axl, Cd36, Itgav, and Itgb5 [121, 122]. Itgb5 deficiency results in increased susceptibility to DSS-induced colitis [122], highlighting a particularly important role of macrophages in the process of repair. Besides their immune function macrophages involved in the regulation of gastrointestinal motility. Muscularis macrophages engage in bidirectional communication with neurons, with macrophage-derived bone morphogenic protein 2 (BMP2) acting on BMP receptors (BMPR) expressed by enteric neurons. This interaction plays a role in regulating smooth muscle contractions, thereby controlling peristalsis [123].

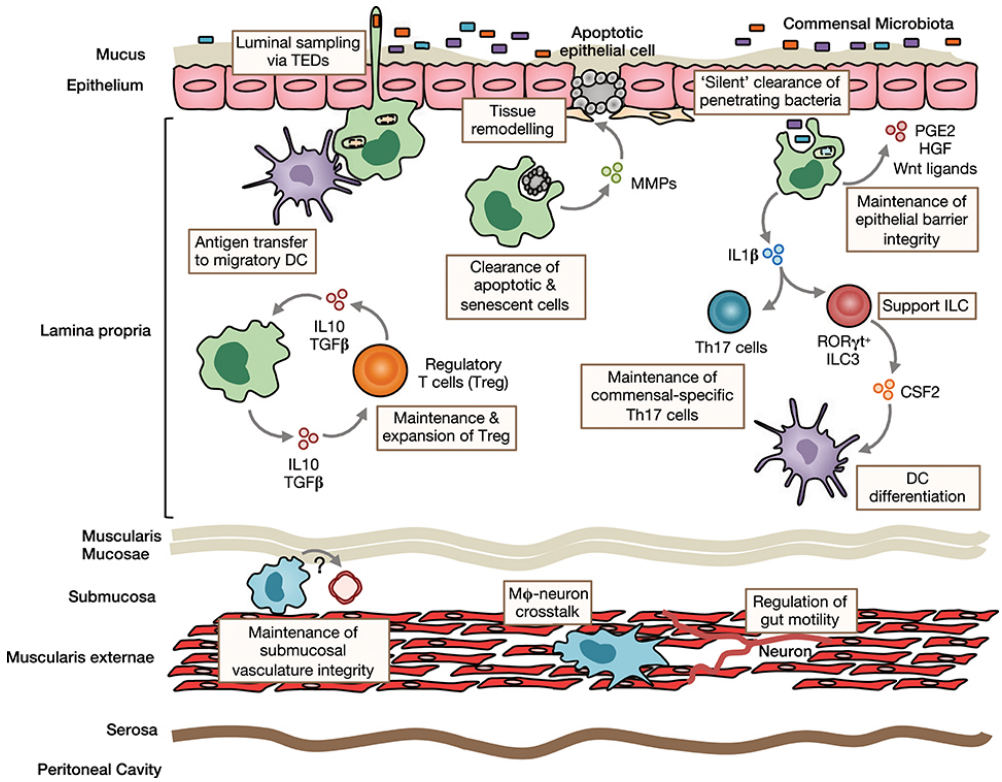

Figure 11: Macrophages function during intestinal homeostasis. Macrophages locate in district compartment through the small intestine and based on their interaction with surrounding cells presents different functions. In lamina propria, macrophages crosstalk with other immune cells, Dendritic cells, T-cells to promote their differentiation or activation. In addition, they perform clearance of bacteria, apoptotic and senescent cells, and contribute to the tissue remodeling and epithelial barrier maintenance through the secretion of metalloproteins and growth factors. In the submucosa/muscularis, macrophages involved in the maintenance of submucosal vasculature integrity, crosstalk with neuron cells and regulate the gut motility. Adapted from the reference [118]

1.3.3 Macrophages and intestinal regeneration

Damage to the intestine often triggers infection or inflammation, leading to activation of the immune system. Upon activation or recruitment, immune cells, such as macrophages, play a crucial role in intestinal regeneration by participating in various processes such as tissue repair, immune regulation, angiogenesis, clearance of cellular debris and extracellular matrix remodeling.

Tissue repair: Intestinal macrophages secrete growth factors and cytokines that promote the proliferation of epithelial cells necessary for tissue repair. Upon irradiation macrophages secrete extracellular vesicles-packaged WNTs to rescue ISCs from radiation lethality [107]. Depletion of extracellular vesicles from macrophages increases intestinal damage upon radiation [107]. Moreover, macrophages secreting growth factors like TGFB1 that promote intestinal regeneration by inducing a fetal-like regenerative state in the epithelium upon radiation injury [101, 124]. These studies, among others, demonstrate the directed involvement of macrophages in intestinal regeneration.

Immune regulation: Macrophages help regulate the immune response during tissue repair by balancing pro- and anti-inflammatory signals [125]. In addition, macrophages also have the ability to crosstalk to other immune cells. Several studies have shown the essential role of intestinal macrophages and their secreting cytokines for regulating T-cell responses in gut [126-128]. Moreover, lamina propria macrophages initiate a Th2-driven immune response to ensure protective responses by production of IL-4 and IL-13.

Angiogenesis: Macrophages contribute to the formation of new blood vessels (angiogenesis) by releasing pro-angiogenic factors like VEGF-A [129, 130]. This enhanced blood supply facilitates nutrient and oxygen delivery to regenerating tissues, promoting their growth and repair.

Extracellular matrix remodeling: Fibrosis is an essential part of the healing process. During intestinal damage, there is an accumulation and proliferation of fibroblast and myofibroblast at the wound bed in the epithelium regeneration process. These cells express smooth muscle actin (SMA) and produce abundant collagen to initiate mucosal repair [131, 132]. This collagen-rich matrix replaces the damaged matrix, and fibroblasts and myofibroblasts migrate into the wound sites to remodel the extracellular matrix (ECM) [131]. YAP/TAZ, as mentioned before, is key player in intestinal regeneration and were recognized as primary sensors of the cellular microenvironment [133]. They are central players in mechanotransduction [134] and can be activated by increased ECM stiffness, mechanical stress and growth factors. In line with these, macrophages are master regulators to intestinal fibrosis and fibrolisis [135]. Macrophages secrete pro-fibrotic cytokines or mediators to activate the myofibroblast during injury and synthesize enzymes that inhibit collagen degradation [135]. On the other hand, they are involved as well in the resolution of fibrosis and can negatively regulate this process through the production of matrix metalloproteinases (MMPs). MMPs can degrade ECM and also suppress intestinal myofibroblasts resulting in a reduction of ECM deposition [136] Therefore, macrophages upon intestinal injury, indirectly may involve in intestinal regeneration by regulating the ECM and therefore the activation of YAP/TAZ.

Macrophages play a crucial role in the regeneration of various tissues, including the heart, muscle, lung, and skin, by coordinating repair processes through their dynamic functional states. In the heart, macrophages promote angiogenesis and cardiomyocyte proliferation following injury[137]. In skeletal muscle, they aid regeneration by clearing debris and secreting factors like insulin-like growth factor 1 (IGF-1) to activate satellite cells [138]. In the lung, macrophages help restore epithelial integrity and resolve inflammation during alveolar repair [139]. Similarly, in skin, macrophages orchestrate wound healing by modulating fibroblast activity, promoting re-epithelialization, and secreting extracellular matrix components [140, 141]. While the role of macrophages in regeneration is better understood in other tissues, our understanding of their involvement in intestinal regeneration has only recently begun to emerge. Nevertheless, we lack a comprehensive framework that outlines how macrophages coordinate the process of regeneration at cellular and molecular levels, their potential role in the acquisition of fetal-like reprogramming, and ultimately whether these processes are conserved or not in humans.

1.4 Functional characterization of Intestinal Stem Cells

Functional characterization of intestinal stem cells (ISCs) involves assessing their ability to maintain homeostasis and regenerate the epithelium under physiological and injury conditions. ISCs are typically identified by specific markers such as Lgr5, located at the crypt base, and their capacity for self-renewal and differentiation into various intestinal lineages. Therefore, techniques like lineage tracing, three-dimensional intestinal organoids, single cell RNA sequencing provide insights into ISC behavior during epithelial repair

and their interaction with surrounding cells, such as macrophages, in the intestinal microenvironment.

1.4.1 Lineage tracing

Lineage tracing is a powerful technique used to study the behavior, fate, and dynamics of intestinal stem cells (ISCs) and their progeny *in vivo [142, 143]*. This approach allows to track specific cell populations over time to understand their role in tissue homeostasis, repair, and regeneration. Most lineage tracing studies rely on Cre-loxP recombination systems [144]. A tissue-specific or marker-specific promoter (such as Lgr5, Krt20, Bmi1, and Tert target specific ISC or progenitor populations) [95, 145], drives the expression of Cre recombinase, ensuring activation in the targeted cell population (e.g., Lgr5-CreERT2 for ISCs) [145]. A reporter allele, such as Rosa26-LoxP-STOP-LoxP-tdTomato, is activated upon Cre-mediated recombination, leading to permanent expression of a fluorescent protein in the target cells and their progeny. The addition of a tamoxifen-inducible Cre system (CreERT2) provides precise temporal control [146]. Tamoxifen administration activates Cre, initiating recombination and marking the lineage at specific time points (Figure 12). Thus, fluorescent proteins (e.g., GFP, tdTomato) allow visualization of marked cells under fluorescence microscopy or flow cytometry. This helps track the proliferation, migration, and dedifferentiation patterns of intestinal epithelial cells.

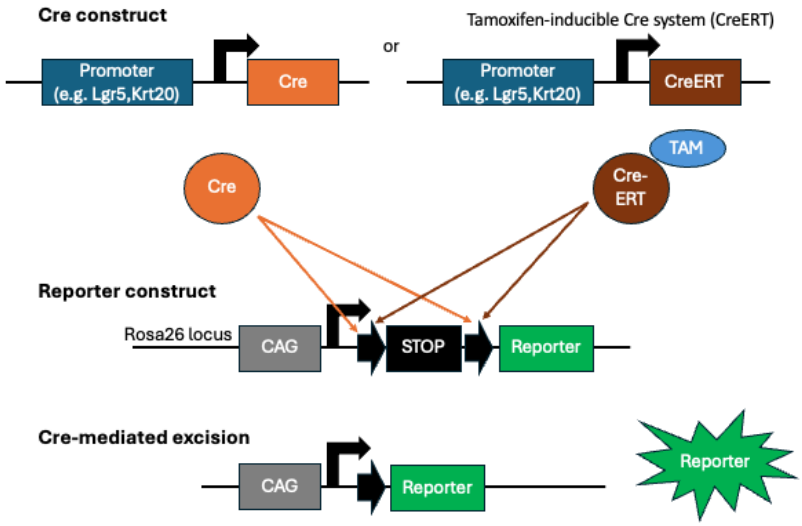

Figure 12: Genetic lineage tracing strategies. A. Schematic representation of the CRE-Lox system consisting of two main elements: a construct in which the gene for CRE or a tamoxifen-inducible Cre system (e.g. CreERT) is placed under the control of an appropriate cis-regulatory element (promoter e.g., Lgr5,Krt20) to gain lineage specific expression; a reporter construct from which the expression of a marker protein (e.g., GFP, Tdtomato) occurs after CRE-mediated excision of a "STOP" cassette flanked by two LoxP sites. Without CRE, the STOP cassette inhibits expression of the marker. Adapted from the reference [147], Illustration created using ppt.

1.4.2 Single-Cell RNA Sequencing (scRNA-seq)

Single-cell RNA sequencing (scRNA-seq) allows to analyze gene expression at the resolution of individual cells. This technique has revolutionized the study of intestinal stem cells (ISCs) by uncovering cellular heterogeneity, identifying rare cell populations, and mapping dynamic changes during homeostasis, injury, and regeneration. Tools like RNA velocity and CellRank can predict cell trajectories and dedifferentiation processes, providing insights into intestinal epithelial cell dynamics [148, 149]. Furthermore, gene ontology and differential gene expression analysis identifies marker genes and

activation/suppression of pathways for specific cell types or states. Therefore, this technology can reveal the cellular heterogeneity of the intestinal epithelium, distinguishing ISCs, transit-amplifying progenitors, and specialized cell types [150]. It has illuminated the plasticity of the epithelium, inferring how progenitor or differentiated cells dedifferentiate into ISCs following injury, thereby contributing to regeneration [83, 86, 96, 101]. By analyzing niche interactions, receptor-ligand analysis may identify key interactions between ISCs and their niche, Paneth cells, and immune cells like macrophages, that regulate ISC function [151, 152]. Additionally, in disease models, it highlights stress responses and inflammation-driven pathways, offering targets for therapeutic intervention [153]. In cancer research, scRNA-seq maps the transformation of ISCs into tumor-initiating cells, providing insights into oncogenic pathways [154, 155].

scRNA-seq can be integrated with other technics like ATAC-seq (chromatin accessibility) [156] or proteomics to link gene expression with regulatory mechanisms and protein activity or with Spatial transcriptomics providing information about cell location in the tissue [157].

Single-cell RNA sequencing has become an indispensable tool for unraveling the complexity of ISC biology, providing unprecedented resolution to study the cellular and molecular processes underlying intestinal homeostasis and regeneration.

1.4.3 Intestinal organoids

Organoids are self-organized three-dimensional tissue cultures that are derived from stem cells and differentiated into multiple organ-specific cell types [41]. Intestinal organoids (IOs) recapitulate many properties of the intestine, including the heterogeneity of the cellular composition, appropriate physiology, region-specific features of the intestine, and self-renewal dynamics [41]. Moreover, IOs culture can also be considered a regeneration model, as it involves activation of defined signaling pathways critical for tissue regeneration, including transient activation of YAP [97, 158]. Of note, fetal intestines give rise to spherical organoids (Figure 13A) On the other hand, adult small intestines give rise to budding organoids with villus- and crypt-like domains (Figure 13B). However, when the regenerative program is activated for instance by activation of YAP signaling, adult organoids acquire a fetal-like spherical shape [97] (Figure 13C). Thus, the circularity of organoids might be used as a proxy for regeneration *in vitro*. Although this is not unequivocal because organoids with overactivation of Wnt signaling pathway are also spherical [159, 160]. Therefore, these self-organized three-dimensional structures provide us with a powerful tool to study mouse and particularly human intestinal biology [161], opening new horizons for organoid transplantation therapy.

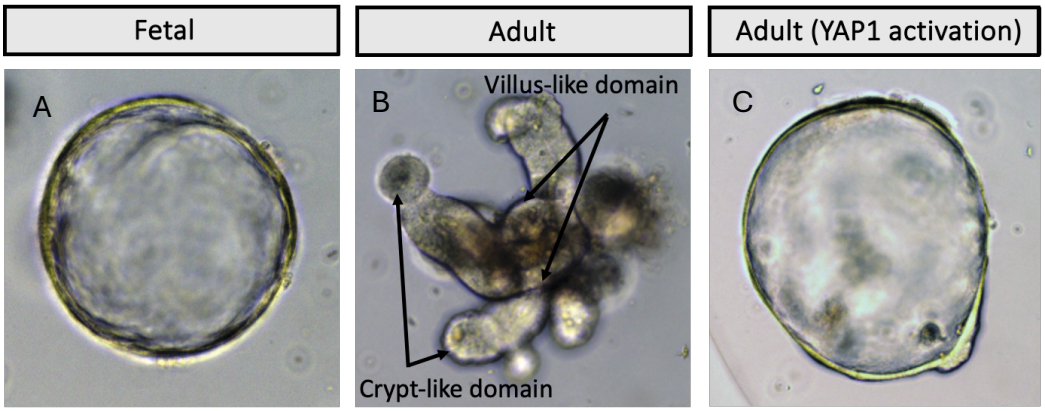

Figure 13: *Murine intestinal organoid. A) A fetal intestinal organoid with spherical characteristic shape. B) an adult intestinal organoid with budding shape, forming crypt- and villus-like domain. C) an adult intestinal organoid upon YAP1 activation that acquires a fetal-like spherical shape. Image generated in Jordi Guiu´s group.*

1.4.4 Immune cell–intestinal organoid interactions, a tool for understanding intestinal regeneration and beyond.

The traditional perception of immune cells, including macrophages, has been associated primarily with inflammation and pathogen clearance. However, it is now recognized that they perform a myriad of functions. These functions occur deep within tissues that are often inaccessible and subject to environmental variations, particularly in humans. Intestinal organoids offer a promising solution to some of these limitations. While recent advancements in organoid co-cultures with immune cells have primarily focused on lymphocytes [106, 162, 163], the importance of myeloid cells, such as macrophages has been the subject of extensive research the last years for studying their non-immune function [164, 165]. Consequently, organoid co-cultures are increasingly recognized as a crucial model for exploring the bi-directional interactions between immune and epithelial cells (Box 1),

expanding beyond the traditional context of immune-mediated pathogen clearance.

However, it's important to acknowledge that co-culturing organoids with immune cells also presents limitations. For instance, the culture components necessary for the differentiation or maintenance of one cell type may inadvertently impact the other. Additionally, the composition of media used in these cultures may induce phenotypes that are not observed *in vivo*. Therefore, it is important to validate any proposed mechanisms based on *in vitro* observations through *in vivo* experimentation.

Box 1: organoids as a tool for understanding the interactions between epithelial and immune cells.

Various strategies have been used or could potentially be explored in the future, to co-culture immune cells or their products (growth factors, cytokines, extracellular proteins) with organoids for studying immune-epithelial cells interactions in the context of development, differentiation and regeneration.

- Organoid culture media can be supplemented with recombinant cytokines to mimic immune-derived stimuli [106, 166, 167].
- Immune cells can be isolate from primary tissues and resuspend in the same extracellular matrix bubble with intestinal organoids, allowing the interactions between immune and epithelial cells [166, 168].
- Transwell experiments and ''organ on a chip'' approaches allow the separation of the epithelial from immune cells or epithelial and immune cells from microbial components for the development of more complex disease models and drug development [169, 170]
- With 3D bioprinting technology it may be possible to include immune cell into macro-scale in vitro models (mini guts) [171].

The mammalian immune cells that are used in those co-culture experiments can be derived either directly from adult or fetal tissue or differentiated first from hematopoietic stem cells or iPSCs.

2 Aim

Several studies over the past decade have demonstrated that macrophages play a crucial role in regulating homeostasis and promoting the regeneration of various tissues, including the heart, liver, skin, kidney, muscle, and nerves. However, their involvement in intestinal regeneration remains poorly characterized.

The aim of this study is to uncover the mechanisms by which macrophages coordinate intestinal regeneration, focusing on their role at the cellular and molecular levels, their contribution to fetal-like reprogramming, and the conservation of these processes in humans.

Specific subaims:

1. Identify if macrophages directly crosstalk with epithelial cells.

2. Determine if macrophages are necessary for intestinal regeneration.

3. Assess the impact on the intestinal regenerative program when macrophages are ablated following injury.

4. Elucidate the mechanisms by which macrophages promote intestinal regeneration.

5. Evaluate whether the function of macrophages in enhancing intestinal regeneration is conserved in humans.

3 Methodology

3.1 Mice and treatment

All in vivo experiments were performed in accordance with relevant guidelines and regulations under the terms of local regulations and supervision of suitable agencies. The National animal ethics committees in Catalonia reviewed and approved all animal experiments. Rosa-CAG-LSL-Tdtomato (Jax stock number 007905), Krt20-T2A-Cre-ERT2 (Jax stock number: 030600) and Lgr5-eGFP-IRES-CreERT2 (Jax stock number 008875) were kindly provided by Dr. Kim B. Jensen. ITGAX-DTR-eGFP and B6.129S6(Cg)-Spp1tm1Blh/J (SPP1 KO) mice was imported from Jackson laboratory (Jax stock number: #004509, #004936), wild-type C57BL/6j mice were imported from Charles River and bred inhouse (Table 2). Mice were used for experiments at 8-20 weeks old. Animals were maintained under a 12/12-hour light/dark cycle at a temperature of 20oC, with free access to food and water.

To study the involvement of macrophages in the intestinal regeneration upon injury, wild-type C57BL/6 mice and the transgenic murine lines that were mentioned above were challenged with 14 Gy abdominal irradiation, as detailed in the next section. Experiments were analyzed within groups exposed to the same irradiator treatment.

3.1.1 Conditional macrophages ablation

ITGAX-DTR-eGFP and Krt20-T2A-Cre-ERT2:R26-Flox-STOP-Flox-Tdtomato;ITGAX-DTR-eGFP mice were injected intraperitoneally with one dose of 25ng/g diphtheria toxin (DT) (Sigma-Aldrich, Cat# D0564). Upon injury, mice were injected with DT immediately following irradiation.

3.1.2 Lineage tracing experiments

Krt20-T2A-Cre-ERT2:R26-Flox-STOP-Flox-Tdtomato and Krt20-T2A-Cre-ERT2:R26-Flox-STOP-Flox-Tdtomato;ITGAX-DTR-eGFP mice were injected intraperitoneally with 200 µl 4-hydroxytamoxifen in corn oil at 10 mg ml-1. Upon injury, mice were injected with 4-hydroxytamoxifen, 1h before irradiation.

3.1.3 Edu labeling

mice were injected intraperitoneally with a single dose of 150 µg Edu (Click-iT, Invitrogen #C10340), 1h before the small intestine collection.

3.1.4 SPP1 and NRG1 *in vivo* treatment

For SPP1 or NRG1 treatment, ITGAX-DTR-eGFP mice were injected intraperitoneally on day 2-, 3- and 4-post irradiation with 15µg/mL per mouse of NRG1-beta 1 Protein (Medchemexpress, # HY-P7365) or with 15µg/mL per mouse of Osteopontin (SPP1) Protein (Medchemexpress, # HY-P70499).

3.2 Radiation injury protocol

An irradiation protocol to deliver 14 Gy to the abdominal cavity of the mice was designed. The bottom half of the mice bodies were placed in bolus, a flexible tissue equivalent material, to attain a full scatter geometry. Two PMMA layers of 1 cm width were placed in top and bottom positions to account for the build-up region of the photon beams and reach electronic equilibrium in the mice tissue. To avoid irradiation to mice upper body, mice were placed in the field edge, leaving only the bottom half inside the

irradiation beams. Irradiation was carried out in a Varian Clinac Truebeam Medical Linear Accelerator. Photon energy selection was 6 MV. Radiation isocenter was placed at half depth of the mice body. Irradiation geometry consisted of two isocentric coplanar plane-parallel opposing beams, each delivering a total absorbed dose of 7 Gy to the isocenter. Dose heterogeneity in the whole abdominal cavity is less than 5%.

3.3 Organoid culture and treatments

Murine small intestinal tubes were dissected out and flushed with cold PBS to remove feces. Small intestinal tissues were opened longitudinally, scraped with a glass coverslip to remove villi, cut into 5-mm pieces, and incubated in 2 mM EDTA-PBS solution for 45 minutes at 4°C with agitation. After incubation, tissue was washed with cold PBS two times. The tissue was then vigorously shaken to release the epithelium, and crypts passed through a 70-µm cell strainer in cold 1% BSA-PBS. Intestinal crypts were centrifuged three times at 300g for 3 min at 4°C (with washing with 1% BSA-PBS every time). Freshly isolated crypts were then mixed with 25 µl of Matrigel and seeded in prewarmed 48-well plate and incubated at 37°C for 20-30 minutes. After the incubation, 250 µl of culture medium (Advanced DMEM/F12, Life Technologies, #12634010) was added, supplemented with penicillin/streptomycin (Merck Life Science, #P0781), glutamax (Life Technologies, #35050-038), 10 mM HEPES (Thermofisher, #15630080), 50 ng/mL hEGF (Peprotech, # AF-100-15), 100 ng/mL Noggin (Stemcell Technologies, #78061) and 250 ng/mL R-spondin 1 (Stemcell Technologies, #78213.1). Intestinal organoids

were maintained in a 370C humidified atmosphere under 5% CO2 and medium was replaced every 2 days.

3.3.1 Organoids treatment with NRG1 and SPP1

Small intestinal organoids derived from three wildtype C57BL/6 mice were mechanically passaged and cultured in ENR (EGF, Noggin, R-spondin 1) medium supplemented with 100 ng/mL NRG1 (BIO-TECHNE R&D Systems, #396-HB-050/CF) or 6µg/mL-1 SPP1 (Merck Life Science, #SRP3131) or with NRG1 and SPP1 together. After 2 days, the medium was replaced with fresh complete culture medium containing fresh factors. On day 4, organoids were collected for RNA extraction, using the RNeasy micro kit (Qiagen, Cat# 74004) according to manufacturer's instructions for Bulk RNA sequencing.

3.3.2 Murine co culture of intestinal organoids and macrophages

3.3.2.1 Macrophage isolation

Femur and tibia bones were isolated from 6–8-week-old mice, hair was rinsed off and the bone was cut open. Bone-marrow cell precursors were isolated by flushing out the marrow 4 times from the femur with ice-cold PBS, using a 10 mL syringe and a 21G needle. Flush medium was collected into a sterile 15 mL conical tube containing 5-6 mL cold PBS and sample was centrifuged at 500g for 5 min at 4°C. Cell pellet was resuspended in 1 mL of Red Blood Cell lysis buffer (Biolegend, #420301),

to remove the red blood cells followed by 10 min incubation at room temperature, protected from light with occasional agitation. After incubation, the sample was centrifuged at 500g for 5 min at 40C and the cell pellet was resuspended in 10 mL of culture medium Advanced DMEM/F12, (Life Technologies, #12634010), supplemented with penicillin/streptomycin (Merck Life Science, #P0781), GlutaMAX (Life Technologies, #35050-038), 10 mM HEPES (Thermofisher, #15630080), 10% FBS and 10 ng/mL of recombinant murine M-CSF (Prospec, Cat# CYT-439) at a concentration of 1,4x105 cells/mL. 2 mL cell suspension was seeded in a 6-well plate and incubated for 7 days at 37 °C. On day 3 and 5, medium was replaced. On day 5-7, formation of mature bone marrow-derived macrophages (BMDM) was evaluated using flow cytometry analysis and fluorophore-conjugated antibodies, to detect cells expressing CD11b and F4/80. For polarization of BMDM toward to pro-inflammatory like-phenotype (IFN-γ/LPS-induced) or anti-inflammatory like-phenotype (IL4-induced) macrophages, medium was replaced on day 7 with Advanced DMEM/F12 medium supplemented with 10% FBS, 100 ng/mL LPS (Ibian Technologies, S.L, Cat# TLRL-3PELPS) and 50 ng/mL IFNγ (BIO-TECHNE R&D Systems, Cat# 485-MI-100), or with Advanced DMEM/F12 medium supplemented with 10% FBS, and 10 ng/ml IL-4 (Bionova, Cat# 214-14) respectively. After one day, the expression of genes characteristic of activated IFN-γ/LPS-induced and IL4-induced macrophages, including il-1β, tnf-α and il-6 (IFN-γ/LPS-induced) or arg1 and pparγ (IL4-induced) were determined by using qRT-PCR.

To set up a co-culture system, pre-grown (5-7 days) intestinal organoids were mechanically passaged, mixed with BMDM or activated macrophages (IFN-γ/LPS-induced or IL4-induced) at a final ratio 1:2 (intestinal cells:macrophages), resuspended in 25 µl of Matrigel and seeded in a prewarmed 48-well plate and incubated at 370C for 20-30 minutes. 250 µl of ENR medium was then added in each well. The co-culture was cultivated for 48h at 37oC. On day 3, 200 µL/well cell recovery solution was added (Corning, #354253) for 30 min at 4°C. Then, cells were centrifuged at 500g for 5 min at 4°C. Harvested cells were incubated with 1 mL of 0.05% trypsin for 10 min at 37°C, followed by vigorous agitation every two minutes for dissociation to single-cell level. After the incubation, trypsin was blocked with basal medium and 10% FBS, centrifuged at 500g for 5 min at 4°C and the pellet was resuspended with 100 µL of 1% BSA-PBS for staining. For identifying intestinal cells and macrophages, cells were incubated for 15 min with Anti-CD236-APC (BD Bioscience, Cat# 563478, 1:100) and Anti-CD45- FITC (BD Bioscience, Cat# 561088, 1:200) antibodies, respectively. PI- CD45- EpCAM+ cells were sorted for RNA extraction using the RNeasy micro kit (Qiagen, Cat# 74004) according to manufacturer's instructions for bulk RNA sequencing.

3.3.3 Human co-culture of intestinal organoids and macrophages

To culture human intestinal organoids, ileum samples from four healthy patients were provided by the Biobank HUB-ICO-IDIBELL, funded by

Instituto de Salud Carlos III (PT20/00171) and by Xarxa de Bancs de Tumors de Catalunya sponsored by Pla Director d'Oncologia de Catalunya (XBTC). Human intestinal organoids were cultured in Intesticult organoid Growth medium (Stem Cell Technologies, #6010) and subsequently multiplexed in the same culture. Human Peripheral Blood CD14+ Monocytes (Lonza, #2W-400C) were seeded in a 6-well culture plate at a concentration 1x106 /well in 2 mL RPMI medium (Life technologies, #31870-074) containing 10mM, 1mM sodium pyruvate, GlutaMAX, penicillin/streptomycin and 10% FBS supplemented with 50 ng/mL GM-CSF (Peprotech, #300-03-20UG) or 50 ng/mL M-CSF (Peprotech, # 300-25) for IFN-γ/LPS-induced and IL4-induced macrophage polarization, respectively and finally incubated at 37oC and 5% CO2. Medium was replaced every 2 days and necessary factors were added every day. On day 6, to fully polarize and mature macrophages to IFN-γ/LPS-induced or IL4-induced, the medium was replaced with RPMI complete medium supplemented with 50 ng/mL IFN-γ (BIO-TECHNE R&D Systems, Cat# 485-MI-100) and 10 ng/mL LPS (Invitrogen, Cat# TLRL-3PELPS) for IFN-γ/LPS-induced and 20 ng/mL IL-4 (Peprotech, # 200-04) for IL4-induced. Both were incubated for 1 day. On day 7, IFN-γ/LPS-induced and IL4-induced polarized macrophages were co-cultured with human intestinal organoids. To set up a co-culture system, pre-grown (5-7 days) intestinal organoids were mechanically passaged, mixed with activated macrophages (IFN-γ/LPS-induced or IL4-induced) at final ratio of 1:3 (intestinal cells:macrophages), resuspended in 25 µl of Matrigel, seeded in a prewarmed 48-well plate and incubated at 37oC for 20-30 minutes. After this 250 µl of Intesticult DEM medium was added. The co-

culture was cultivated for 48h at 37oC. On day 3, 300 µL/well cell recovery solution was added (Corning, #354253) for 30 min at 4°C. Organoids were then collected, and centrifuged at 500g for 5 min at 4°C. Harvested cells were incubated with 1 mL of TrypLE (Life Technologies S.A., #12604-013) for 10 min at 37°C, followed by vigorous agitation every 5 minutes to dissociate organoids to single cells. Next, TrypLE was neutralized by addition of basal medium. The suspension was then centrifuged at 500g for 5 min at 4°C and the pellet was resuspended with 200 µL of 0,1% BSA-PBS. Cells were then passed through a 70 µm cell strainer, transferred into appropriate FACS tubes and propidium iodide (PI) was added to a concentration of 2 mg/mL. PI- cells were sorted out in 0.1% BSA/PBS. Cells were then centrifuged at 2.500 RPM for 5 min at 4oC, resuspended in 0.01% BSA/PBS and encapsulated in a NADIA instrument (Dolomite Bio, #3200590) as described in the transcriptome analysis section for the single cell RNA sequencing of intestinal epithelial cells. The same procedure used for irradiating murine organoids was applied to human organoids.

3.4 Protein quantification

Human NRG1-b1 and Human SSP1 (Osteopontin) ELISA kits (ThermoFisher Scientific™, #EHNRG, #EHSPP1) were used to measure NRG1-β1 and SPP1 levels in vitro according to the manufacturer's protocol. Prior to ELISA, cell culture media from non-irradiated and irradiated organoids alone or co-cultured with macrophages were collected 3 days after irradiation. One-hundred microliters of cell culture supernatant, standard NRG1-β1 (0 pg/mL-20,000 pg/mL) or standard SPP1 (0 pg/mL-18,000 pg/mL) was added to the wells in duplicate. Assay

diluent B was used to prepare standards and served as the zero standards (0 pg/mL). Absorbance at 450 nm was measured on an Infinite M Nano microplate reader (TECAN). A standard curve ($r^2 \geq 0.99$) for each assay was generated with a four-parameter logistic curve fit in GraphPad Prism by plotting the absorbance vs. the corresponding NRG1-β1 or SPP1 concentration. The concentration of NRG1-β1 and SPP1 in the cell culture supernatants were obtained by interpolating the absorbance values using the standard curves in GraphPad Prism.

3.5 Quantitative RT-PCR

Total RNA extraction was performed using the QIAGEN RNeasy micro kit (#74004) and complementary DNA (cDNA) was synthesized using the Transcriptor First Strand cDNA Synthesis Kit (Roche, Cat# 04897030001), using the manufacturer's instructions. Real-time quantitative PCR (RT-qPCR) was performed using PowerUPTM SYBR Green Master Mix (Applied Biosystems, Cat# A25742) and samples were analyzed on a LightCycler 480 machine (Roche Diagnostics). Gene expression levels were calculated using the 2-ΔCt method using the geometric mean of housekeeping gene β-actin. Primers are listed in Table 1.

3.6 Imaging and histology

3.6.1 Tissue fixation

Tissues from the medial part of the mouse small intestine were flushed with cold PBS to remove feces and opened longitudinally. Fragments were fixed from 4h to overnight at 4°C with 4% paraformaldehyde or 10%

formalin and then washed three times with cold PBS. For paraffin embedding, tissues were then dehydrated through ascending alcohols and processed with xylene prior to embedding. For cryo-embedding, tissues were processed with 30% sucrose until tissues sunk prior to freezing in OCT compound. 5 µm-thick paraffin sections and 10 µm-thick cryosections were used for immunohistochemistry and immunofluorescence.

3.6.2 Immunohistochemistry and immunofluorescence on paraffin embedded tissues

Sections were rehydrated before antigen retrieval. Slides were then blocked with 70% methanol, 30% distilled water and 2% hydrogen peroxide for 5 min and blocking buffer (1X TBS, 0.5% triton X-100 and 6% donkey serum) for 1h at room temperature before overnight incubation at 4°C with primary antibody Anti-Ki-67 (Dako # M7249). Slides were washed with TBS and detected using the Envision dual link kit (Dako #K5007). Sections were counterstained with hematoxylin, dehydrated, cleared with xylene, and mounted with Dibutylphthalate Polystyrene Xylene (DPX).

3.6.3 Immunofluorescent on cryo-embedded tissue

sections were washed first with PBS two times. Then, blocking and permeabilization was performed in 10% fetal bovine serum, 0.3% Triton X-100, 5 % milk in PBS for 2-4h at 4°C. Primary antibodies (indicated in

Table S2) were incubated overnight in 10% fetal bovine serum, 5 % milk in PBS at 4°C. slides were washed twice with PBS and were incubated with secondary antibodies (indicated in table S1) in 0.5% bovine serum albumin, 10% fetal bovine serum in PBS 1h at room temperature.

EdU was detected using the cell proliferation assay (Click-iT; Invitrogen #C10340) according to manufacturer's instructions.

3.6.4 Immunofluorescence on organoids

Organoids were incubated with 200 µL/well cell recovery solution (Corning, #354253) for 30 min at 4°C. organoids were then collected, and wells were washed with 0.1% BSA-PBS. The organoids were then centrifuged at 300g for 3 min at 4°C, followed by washing with 0.1%BSA-PBS. Cell pellets were resuspended in 0.1% BSA-PBS. To deposit organoids on slides we used a Cytospin 4 centrifuge 8 (Thermo Scientific # TH-CYTO4). 80 µL of sample was loaded into the cytofunnel, spun down at 600rpm for 2 min and then slides were dried, fixed with 4% paraformaldehyde for 15 min, washed with PBS and stored in 100% methanol at -20oC. We performed immunofluorescence as described above for immunofluorescent on cryo-embedded tissue.

For immunofluorescence, Diamidino-2-phenylindole dihydrochloride (DAPI, 1 µM, Invitrogen, #D21490) was used to counterstain nuclei in the indicated experiments. Fluorescent images were acquired using a Leica SP5-1 inverted confocal and a Zeiss LSM 980 Airyscan2 microscope.

Immunohistochemistry samples were imaged using Leica DM6000B vertical fluorescence microscope. All images were subsequently analyzed in the Imaris cell imaging software and Fiji.

3.6.5 Whole-mount immunostaining

We performed whole-mount immunostaining in small intestine fragments as previously described (Guiu et al., 2019). Briefly, the proximal half of the small intestine was fixed with 10% formalin from 4 h to overnight at 4 °C, following dehydration in methanol. Samples were then stored in methanol at -20°C. Next, tissue was rehydrated in a series of washes with PBS and blocked/permeabilized in blocking solution (1% BSA, 0,5% Triton X-100 in PBS), overnight at 4°C with gentle agitation. The tissue was then washed six times with 0,5% triton X-100 in PBS and incubated two days at 4°C with primary antibodies (indicated in table S1) in blocking solution (1% BSA, 0,5% triton X-100 in PBS). Diamidino-2-phenylindole dihydrochloride (DAPI, 1 µM, Invitrogen, #D21490) was used to counterstain nuclei. Subsequently, tissue was washed 6 times with 0,5% triton X-100 in PBS, followed by incubation with secondary antibodies (antibodies indicated in the table S1) for two days at 4°C. Samples were then washed six times with 0,5% triton in PBS, dehydrated in methanol and kept at -20°C. Samples were cleared with a solution 50% of benzyl alcohol:benzyl benzoate (BABB) (Merck, #108006, #B6630) and mounted within a Fast Well (FW20-FastWells, 20-mm diameter × 1.0-mm depth). Z-stack images were acquired using laser-scanning confocal microscopy (Zeiss LSM 980 Airyscan2). Three-dimensional

reconstructions and clone volume were performed using Imaris cell imaging software. For the three-dimensional reconstruction shown in (Figure 1D), Imaris cell imaging software was used to generate surfaces for each channel. These surfaces were used to mask the intensity, reflecting the structure of the tissue. Since macrophages are located within the villi compartment, different masks were applied to the E-cadherin and DAPI channels to enhance the visibility of the interior of the villi. Finally, the volume data from each channel was removed, retaining only the surface structures for the final visualization.

3.7 Single molecule RNA in situ hybridization (ISH)

ISH was carried out on fresh frozen tissue samples fixed in 10% neutral buffered formalin overnight at 4°C. RNA probe for NRG1 (bio-techne, #418181) and RNAscope 2.5 HD assay – Red kit (bio-techne, #322360) was used according to the manufacturer's instructions (user manual 323900-USM). Tissue sections were not counter stained with hematoxylin. Slides were mounted with glycerol medium and photographed using zeiss axio observer z1 inverted fluorescence microscope.

3.8 Isolation of stem and progenitor from Femur and Humerus bones samples.

The femur and Humerus bones were isolated from 8-10-week-old mice, hair was rinsed off and the bone was cut open. Bone-marrow cell precursors were isolated by flushing out the marrow 4 times from the femur with ice-cold PBS, using a 10 mL syringe and a 21G needle. Flush

medium was collected into a sterile 15 mL conical tube containing 5-6 mL cold PBS and sample was centrifuged at 500g for 5 min at 4°C. Cell pellet was resuspended in 1 mL of Red Blood Cell lysis buffer (Biolegend, #420301), to remove the red blood cells followed by 10 min incubation at room temperature, protected from light with occasional agitation. After incubation, the sample was centrifuged at 500g for 5 min at 4°C and the cell pellet was resuspended in 10 mL cold PBS. Sample was centrifuged at 500g for 5 min at 4°C and the cell pellet was resuspended in 200µL of 1% BSA with lineage cocktail antibodies (Anti-CD8a (Cat# 13-0081-82), Anti-CD45R (Cat#13-0452-82), Anti-TER-119 (Cat#13-5921-82), Anti-CD11b (Cat# 13-0112-82), Anti-Ly6g (Cat# 13-9668-82) and Anti-CD5 (Cat# 13-0051-82)) followed by 15 min incubation at room temperature. Cells were washed with cold 1mL PBS, centrifuged at 500g for 5 min at 4°C and resuspended in a final volume of 200µL cold 1% BSA with the Anti-c-kit (Invitrogen, Cat# 17-1172-82, 1:200) Anti-Sca-1 (Invitrogen, Cat# 25-5981-82, 1:200), Anti-FCgRII/III (CD16/32) (BioLegend, Cat#553145, 1:200), Anti-CD34 (Invitrogen, Cat#11-0341-82, 1:200) and Anti-Lin-SA (Invitrogen, cat#48-4317-82, 1:200). followed by 15 min incubation at room temperature. Cells were washed twice with cold PBS, centrifuged at 500g for 5 min at 4°C and resuspended in a final volume of 0.5 ml cold PBS. Cells were then passed through a 100 µm cell strainer, transferred into appropriate FACS tubes and propidium iodide (PI) was added to a concentration of 2 mg/mL. Flow cytometry analysis was carried out in Beckman coulter Gallios analyzer.

3.9 FACS isolation of intestinal epithelial cells and macrophages

Tissues from the medial part of the mouse small intestine were flushed with cold PBS to remove feces, opened longitudinally, and 3 cm pieces of tissue were cut into 1 mm pieces. Fragments were resuspended in digestion buffer containing prewarmed 0.1% BSA/PBS and 375 µg/mL collagenase (Merck Life Science, Cat# C9407-500MG) for 45 min at 37°C with gentle agitation, followed by pipetting with 10ml pipette every 5 min. Next, the tissue was washed with cold 0.1% BSA/PBS followed by centrifugation at 400 g for 5 min at 4°C. Fragments were passed through a 100 µm cell strainer and centrifuged at 400 g for 5 min at 4°C. Antibody labeling was performed in 1% BSA/PBS. Cells were incubated with Anti-CD45- FITC (BD Bioscience, Cat# 561088, 1:200), Anti-CD11b-PE-Cy7 (BD Bioscience, Cat# 561098, 1:200), Anti-F4/80-PE (BD Bioscience, Cat# 565410, 1:200) and Anti-CD236-APC (BD Bioscience, Cat# 563478, 1:100) or Anti-CD236-BV510 (BD Bioscience, Cat# 747748 1:100) antibodies in 400 µl volume for 30 min at 4°C. Cells were washed twice with cold 0.1% BSA/PBS, centrifuged at 400g for 5 min at 4°C and resuspended in a final volume of 1 ml cold 0.1% BSA/PBS. Cells were then passed through a 100 µm cell strainer, transferred into appropriate FACS tubes and propidium iodide (PI) was added to a concentration of 2 mg/mL. Flow cytometry analysis and cell sorting was carried out in Beckman coulter Gallios analyzer and Beckman coulter CytoFLEX SRT benchtop cell sorter respectively. The sorting strategy is described in detail in the extended figure S1E.

3.10 Transcriptome analysis

3.10.1 Single cell RNA sequencing of intestinal macrophages

Cells were isolated from a pool of 3 proximal small intestines (3 cm in length of 3 fragments each) from 6 dpi or unirradiated mice, using collagenase treatment and cell sorting as described in the previous section. DAPI−CD45+ CD11b+ F4/80+ cells (113,000 cells from 6 dpi mice and 78,000 cells from unirradiated control mice) were processed using Chromium Next GEM Chip G (scRNA-Seq 3') following 10x Genomics Chromium protocols in the single cell facility at Josep Carreras Leukemia Research Institute.

3.10.2 Single cell RNA sequencing of intestinal epithelial cells

Cells were isolated from a pool of 3 proximal small intestines (3 cm in length of 3 fragments each) from non-irradiated mice, irradiated mice and irradiated mice with CD11c cells ablated using collagenase treatment and cell sorting as described in the previous section. DAPI-CD45- EpCAM+ cells (75,000 cells each sample) were encapsulated in a NADIA instrument (Dolomite Bio, #3200590), following the protocol provided by the company (scRNA-Seq on the Nadia Instrument v2.0). Briefly, 75.000 cells were loaded in a volume of 250 µl of 0.01% BSA/PBS and 150.000 Macosko oligodT beads (ChemGenes Corporation,

#Macosko-2011-10 (V +)) in 250 µl lysis buffer (6% w/v Ficoll PM-400, 0.2% v/v Sarkosyl, 0.02 M EDTA, 0.2 M Tris pH 7.5 and 0.05 M DTT in nuclease-free water). Cells and beads co-flowed in the microfluidic chip of the device with a capture efficiency of 5–7%. Immediately after the droplet emulsion breakage, the RNAs captured by the oligodT were reverse transcribed (maxima H RT Master Mix, Thermo, #EP0751). Then, the excess bead primers that did not capture an RNA molecule were removed by the incubation of the beads with Exonuclease I (New England Biolabs, #174M0293L) for 45 min at 37 °C. Collected single-cell transcriptomes attached to microparticles (STAMPS) were counted and resuspended in nuclease-free water at 400 beads µl−1 and amplified for 11 PCR cycles. After cDNA purification with 0.6:1 AMPure XP Beads (Agencourt, #A63881), samples were quantified with Qubit dsDNA HS Assay (Thermo, #Q32851) and fragment size check-up was performed using a 4200 TapeStation System (Agilent, #G2991BA). Nextera XT DNA Library Prep Kit (Illumina, #FC-131-1096) was used for the tagmentation of 600 pg of cDNA. The size of Nextera libraries after being purified with 0.6:1 AMPure XP Beads was determined using a 4200 TapeStation System and quantified with quantitative RT-PCR. 1.8 pM of pooled libraries was sequenced on an Illumina NextSeq 550 sequencer, using Nextseq 550 High Output v2 kit (75 cycles) (Illumina, #20024906) in paired-end mode; 20 bp for Read 1 using the custom primer Read1CustSeqB37 (cell barcode and UMI) and 64 bp for Read 2, and 8 bp for i7 index.

3.11 Bioinformatics

3.11.1 RNA analysis

The raw RNA sequencing data were aligned to the mouse genome (GRCm38) using the rnaseq pipeline (https://github.com/nf-core/rnaseq) deposited in the nf-core framework [172]. The version of the pipelines used in the analysis were 3.4 for the RNA-seq of murine intestinal organoids co-cultured with pro-inflammatory (IFN-γ/LPS-induced), anti-inflammatory (IL4-induced) and non-polarized (naive) macrophages (murine co-culture of intestinal organoids-macrophages) and 3.12.0 for the RNA-seq of murine intestinal organoids after treated with the factors NRG1, SPP1 or a combination of both (murine organoids treatment with NRG1 and SPP1). The resulting gene expression matrices were further analyzed to find differentially expressed genes with the R library DESeq2 (version 1.30.1) with R 4.0.2 for murine co-culture intestinal organoids-macrophages and version 1.36.0 with R 4.2.0 for murine intestinal organoids treatment with NRG1 and SPP1 [173]. In these figures the gray dots represent those genes that have not been considered for multiple test correction. DESeq2 discarded these genes in the FDR process. Black dots represent genes whose FDR is not significant (p>= 0.05) and whose fold change is between -1 and 1.

GSEA Analysis

Gene set enrichment analysis was computed using the GSEA software (version 4.3.2) [174].

3.11.2 scRNA-seq Analysis

The raw RNA single cell sequencing data of macrophages sorted from unirradiated (control) and irradiated (6dpi) were aligned to the mouse genome (mm10) using Cell Ranger (version 7.1.0) (https://www.10xgenomics.com/support/software/cell-ranger). The mouse reference dataset (version refdata-gex-mm10-2020-A) was obtained from the website of 10x genomics (https://cf.10xgenomics.com/supp/cell-exp/refdata-gex-mm10-2020-A.tar.gz).

The raw RNA single cell sequencing data of human intestinal organoids after co-culture with pro-inflammatory (IFN-γ/LPS-induced) or anti-inflammatory (IL4-induced) macrophages and the raw RNA single cell sequencing data of intestinal $EpCAM^+$ sorted cells from unirradiated, irradiated and irradiated with macrophages ablation mice were aligned to the human genome (GRCh38) and mouse genome (mm10) respectively using Drop-seq_tools (v2.4.0) (https://github.com/broadinstitute/Drop-seq/) and STAR (v2.7.8a) [175]. All the resulting expression measurements were further analyzed with the R library Seurat (version 4.1.1 with R 4.2.0) to identify clusters of cells and markers genes. For the expression of genes in UMAP plots used the FeaturePlot function from the Seurat package. By default, Seurat normalizes

and scales gene expression data. Normalization is performed by dividing the expression of each gene by the total gene expression within the cell and then multiplying by a scaling factor of 10,000. The resulting values are log-transformed (natural log), helping to manage a broad range of expression values and reducing the influence of highly expressed outlier genes. The normalization formula is: Normalized Value = $\log_e$((Expression of Gene i in Cell j / Total Expression in Cell j) × scaling factor + 1), where +1 is added to avoid taking the logarithm of zero.

ScRNA-seq analysis of co-culture of human organoids with polarized pro-inflammatory (IFN-γ/LPS-induced) or anti-inflammatory (IL4-induced) macrophages.

The aligned sequences were demultiplexed to recover the information of the four donors using the software cellsnp-lite (version 1.2.2) [176] and vireo (version 0.5.7) [177]. The combined matrices of control (only organoids), IFN-γ/LPS-induced and IL4-induced were first filtered (we removed cells with a mithocondrial content > 5%, cells with less than 200 genes, and cells with more than 15968 counts) and then were analyzed with Seurat. The analysis revealed 6 clusters of cells (resolution 0.2). The analysis was repeated by removing macrophages and successively cells that showed a stress signature. To assess changes in cell composition we used scCODA (version 0.1.9) [178]. We chose cluster 2 (proliferative stem cells) as a reference cell type as this cluster had a good number of cells and a very low amount of dispersion (expressed as differences between groups). To ensure the results were consistent and reproducible, scCODA

was run 10 times using the Hamiltonian Monte Carlo (HMC) sampling method.

Analysis of scRNA-seq of Epcam+ sorted cells from unirradiated (control), irradiated (5dpi) and irradiated with macrophages ablation (5dpi + macrophages ablation).

The combined matrices of Control, 5dpi, and 5dpi + macrophages ablation were first filtered (we removed cells with a mithocondrial content > 5%, cells with less than 200 genes, and cells with more than 21470 counts) and then integrated with SCTransform using Canonical Correlation Analysis (CCA). Initially, we attempted to analyze the data by simply combining the samples; however, we observed that the resulting clusters were predominantly defined by the different experiments. This indicated a strong batch effect that masked the underlying biological variation. As a result, we decided to integrate the data and correct for the batch effect using canonical correlation analysis (CCA). It is important to mention that, unlike the other single-cell experiments in the manuscript—conducted simultaneously using a multi-way cartridge for cell encapsulation—the scRNA-seq experiment presented in Figure 3 was performed on separate days due to technical limitations. This likely contributed to the observed batch effect. The Seurat analysis revealed 6 clusters of cells (resolution 0.3).

Analysis of macrophages sorted from unirradiated (control) and irradiated mice (6dpi).

The combined matrices of Control and 6dpi were filtered removing cells with a mithocondrial content > 20%, cells with less than 206 genes, and cells with more than 64001 counts. The Seurat analysis identified 10 clusters of cells (resolution 0.2). To isolate macrophages, we repeated the analysis after removing epitelial cells, B-cells, T-cells, neutrophiles and dendritic cells. We filtered cells with a mithocondrial content > 20%, cells with less than 205 genes, and cells with more than 65143 counts. This second analysis resulted in 5 clusters (resolution 0.2). Marker genes were identified using Seurat's FindAllMarkers function, which applies the Wilcoxon Rank Sum test to detect differential gene expression between cell groups. We restricted the analysis to genes with a minimum average log-fold change of 0.25 between the two cell populations and tested only those expressed in at least 25% of cells in either group. Finally, the results were filtered to include only genes with an adjusted p-value< 0.01.

The plots of classically activated and alternatively activated signature were generated using Seurat's AddModuleScore function to calculate gene set activity. This function compares the expression of a specified gene set to that of control genes with similar expression levels, as described by [179]. In practice, genes are first binned based on their average expression across all cells. For each gene in the input set, a number of control genes are randomly selected from the same expression bin, and the gene's expression is adjusted by subtracting the average expression of these control genes. This process is repeated for all genes in the set, and the results are averaged to calculate the gene set activity (or module score). Essentially, this score represents the log-fold-change of the gene set compared to expression-matched control genes.

3.11.3 RNA velocity

Loom files containing spliced and unspliced reads data matrices were generated from BAM files using velocyto (version 0.17.15). Metadata from the Seurat-processed object was combined with the loom file, including the gene expression count matrix, UMAP embeddings, cell and cluster IDs into an annotated data (AnnData) object, using anndata (version 0.8.0). RNA velocity was performed on the AnnData object, using unitvelo (v0.2.4.1) according to default settings (Gao et al., 2022). For the mouse data, the number of neighbors were expanded to 150 in the unitvelo configuration file to amplify the lower splicing dynamics, compared to the organoid data where default settings were used. Finally, estimated velocity vectors were projected and visualized as stream on the previously calculated UMAP embeddings, using scvelo (version 0.2.5).

For Cellrank and PAGA: cellrank (v1.5.1) was used according to default settings, using cr.tl.terminal_states with n=2. PAGA was plotted after Cellrank calculations, using scv.tl.paga from scvelo, with groups = clusters, root_key = initial_states_probs, end_key = terminal_states_probs and use_time_prior = velocity_pseudotime.

3.12 Statistical analysis

Statistical significance ($p<0.05$) was determined using the Mantel–Cox, one-way ANOVA, or Unpaired/Paired Student t-test in GraphPad Prism (version 7.03) depending on experimental design and according to the

figure legends. The circularity of intestinal organoids was determined using the circularity shape parameter of Fiji software (version 2.1.0) and the formula: 4pi (Area/Perimeter^2). A value of 1.0 indicates a perfect circle

Table 1: List of primers used in this study.

Gene	**Forward primer**	**Reverse primer**
IL-1B (Mouse)	TGCCACCTTTTGACAGTGATG	TGATGTGCTGCTGCGAGATT
PPARg (Mouse)	GTCACACTCTGACAGGAGCC	CACCGCTTCTTTCAAATCTTGT
Arginase (Mouse)	GTAGACCCTGGGGAACACTAT	ATCACCTTGCCAATCCCCAG
IL-6 (Mouse)	ACAAGTCCGGAGAGGAGACT	GAATTGCCATTGCACAACTCT
TNF-a (Mouse)	CAGGCGGTGCCTATGTCTC	CGATCACCCCGAAGTTCAGTAG
β-actin (Mouse)	CACTGTCGAGTCGCGTCCA	CATCCATGGCGAACTGGTGG
IL-6 (Human)	TAGTGAGGAACAAGCCAGAGC	TGGGTCAGGGGTGGTTATTG
IL-1B (Human)	AACAGGCTGCTCTGGGATTC	AGTCATCCTCATTGCCACTGT
TNF-a (Human)	TGCACTTTGGAGTGATCGGC	GCTTGAGGGTTTGCTACAACA
KLF4 (Human)	ATCTTTCTCCACGTTCGCGT	CTCCCGCCAGCGGTTATTC

GAPDH (Human)	GCACCGTCAAGGCTGAGAAC	AGGGATCTCGCTCCTGGAA
Cre	GCCTGCATTACCGGTCGATGC AACGA	GTGGCAGATGGCGCGGCAACA CCATT
Tdtomato wt	AAGGGAGCTGCAGTGGAGTA	CCGAAAATCTGTGGGAAGTC
Tdtomato mutant	CTGTTCCTGTACGGCATGG	GGCATTAAAGCAGCGTATCC
Itgax Common	ACAACAGAAATCACCCTGGA	
Itgax wt		TGGCAGTGTTAAAATGCAGA
Itgax mutant		CGAGAGGACCTCAGACTGCT

Table 2: Experimental Models: Organisms/lines

Mouse: ITGAX-DTR-eGFP	The Jackson laboratory	RRID:IMSR_JAX:004509
Mouse: Lgr5-eGFP-IRES CreERT2	The Jackson laboratory	RRID:IMSR_JAX:008875
Mouse: Krt20-T2A-Cre-ERT2	The Jackson laboratory	RRID:IMSR_JAX: 030600
Mouse: R26-Flox-STOP-Flox-Tdtomato	The Jackson laboratory	RRID:IMSR_JAX: 007905
Mouse: B6.129S6(Cg)-*Spp1*^{tm1Blh}/J	The Jackson laboratory	RRID:IMSR_JAX:004936

4 Results

4.1 Macrophages are recruited around the hyperplastic regenerative crypts upon radiation injury.

4.1.1 Radiation as an injury model for studying regeneration

Whole body irradiation of mice at doses above 8 Gy induces systemic effects including hematopoietic stem cell injury and death. To overcome this limitation, we developed a system to irradiate mice exclusively in the abdominopelvic cavity at 14 Gy (Figure 14). That allowed us to investigate tissue repair, following radiation-induced damage without impairing the survival of mice. Moreover, analysis of hematopoietic stem cells and progenitors from non-irradiated and irradiated humerus and femur bones of mice shows that the hematopoiesis is not impaired in non-irradiated bones (Figure 15).

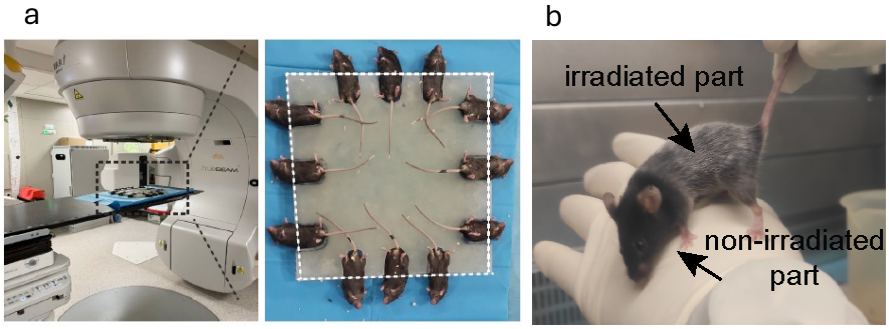

Figure 14: ***a****) Abdominal radiation of mice using the same radiator for patients. Mice irradiated with a single dose of 14Gy.* ***b****) 2.5 months post irradiation showing the part of the mouse that been irradiated (grey fur).*

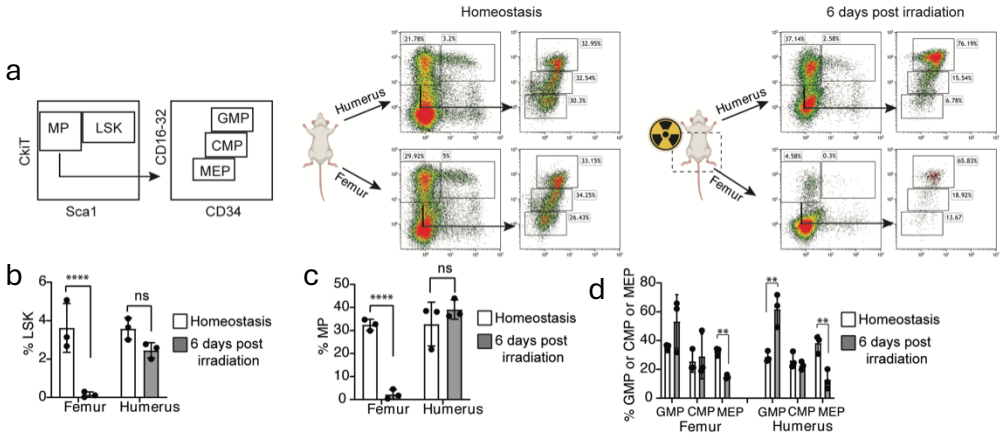

*Figure 15: **a**) strategy for isolation of myeloid progenitor (MP), hematopoietic stem cells, Lin⁻ Sca-1⁺ c-Kit⁺ (LSK), granulocyte-monocyte progenitor (GMP), common myeloid progenitor (CMP) and megakaryocyte-erythroid progenitor (MEP) from non-irradiated and 6 days post irradiated femur and humerus. Aggregates, debris, PI+ and lineage-specific markers (Lin) events were first depleted. **b**) Quantification of the % of hematopoietic stem cells (LSK) from non-irradiated and 6 days post irradiated femur and humerus. **c**) Quantification of the % of myeloid progenitor (MP) from non-irradiated and 6 days post irradiated femur and humerus. **d**) Quantification of the % of monocyte progenitor (GMP), common myeloid progenitor (CMP) and megakaryocyte-erythroid progenitor (MEP) deriving from myeloid progenitor cells from non-irradiated and 6 days post irradiated femur and humerus. (n=3 mice; unpaired t test; ∗∗p < 0.01, ∗∗∗∗p < 0.0001).*

4.1.2 Hyperproliferative and regenerative crypts detected at 6 days post irradiation

Upon radiation injury, mice showed a reduction of their body weight, peaking at 6-7 days post irradiation (dpi) which normalized 2-weeks post irradiation (Figure 16a). To study the dynamics of proliferation, regeneration, and recovery in mice following radiation exposure, we analyzed the mice at various time points: 3-, 6-, 14-, and 30-days post-irradiation (dpi) (Figure 16b). Radiation led to a severe disruption of the intestinal architecture. At 3dpi, the loss of mKI67+ proliferative intestinal epithelial crypts were widespread (Figure 16c). This was followed by enlargement of hyperplastic and hyperproliferative crypts by 6dpi and similar to the weight loss tissue,

architecture was restored by 14dpi (Figure 16c). To assess the activation of the regenerative cellular program in the epithelium qualitatively, we used Sca1 marker, which has been shown to be expressed upon epithelial damage [82, 83]. Immunofluorescence time course analysis of Sca1 revealed increased levels at 3dpi from the stomal cells and at 6dpi from the repairing epithelium (Figure 16d).

Taken together, this data indicates that following 14 Gy abdominal irradiation, the intestinal epithelium at 6dpi is under a proliferative and regenerative state with the re-emergence of mKI67+ cell populations and increased levels of Sca1.

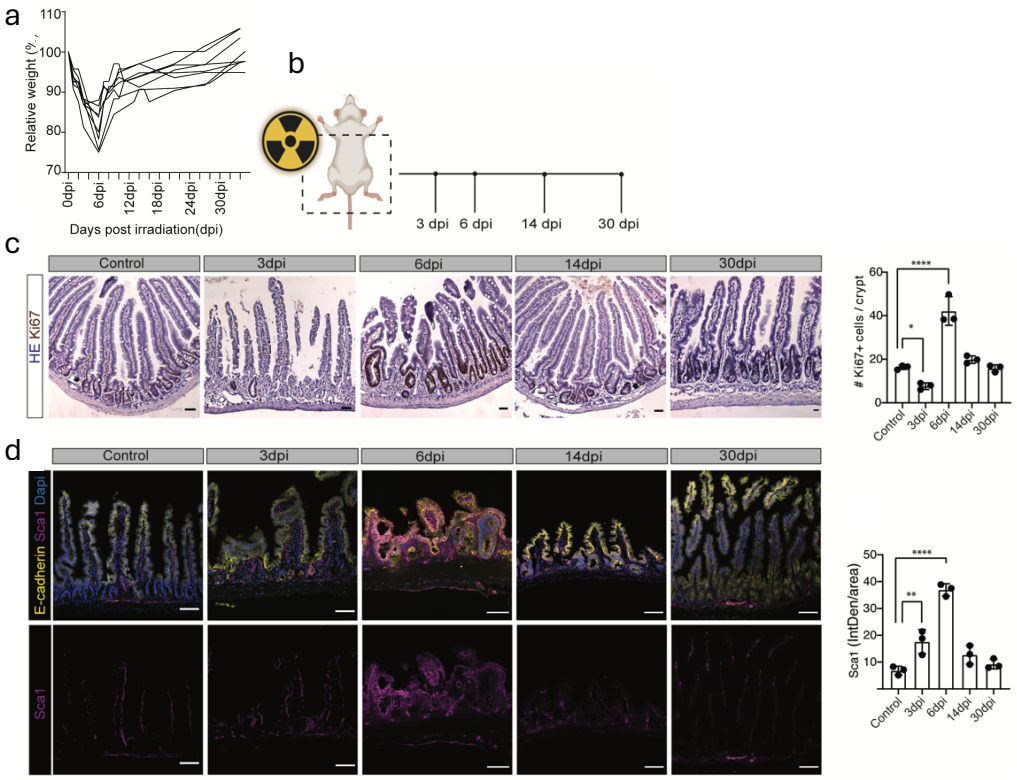

Figure 16: Hyproliferative and regenerative crypts at 6dpi. ***a****) Body weight curves after abdominal radiation injury. Acute enteritis induces body weight reduction, a cohort of 8 mice is shown as an example.* ***b****) The small intestine of WT mice after 14 Gy posterior half irradiation was analyzed in a time course (0, 3, 6, 14 and 30 dpi).* ***c****) Immunohistochemistry staining of mKi67 proliferative marker (brown color) and hematoxylin (blue) reveals that at 3dpi epithelial crypt cells are lost and subsequently restored at 6dpi, when highly proliferative*

*regenerative clusters of cells expand. From 14dpi the architecture and morphology of the small intestine is comparable to the non-irradiated control. Scale bar, 50 µm. Quantification of Ki67+ cells per crypt compartment at indicated timepoints (n=3 mice; one-way ANOVA; *p < 0.05, **** p < 0.0001).* ***d****) Immunofluorescence of Sca1 regenerative marker (magenta) revealed that the initial elevated levels in the stroma at 3dpi and subsequently increase in the repairing epithelium at 6dpi, from 14dpi Sca1 expression is comparable to the non-irradiated control. Scale bar, 100 µm. Quantification of Integrated Density (IntDen)/area of Sca1 at indicated timepoints. (n = 3; one-way ANOVA; ** p < 0.01, **** p<0.0001)*

4.1.3 Macrophages are recruited around the intestinal crypts following injury and anti-correlate with the ISCs

To characterize the dynamics of macrophages (F4/80+) during intestinal regeneration following radiation injury, we performed 3-dimensional imaging of the small intestine to define their location. During homeostasis, macrophages are mainly located in the villi underneath the differentiated epithelium (Figure 17).

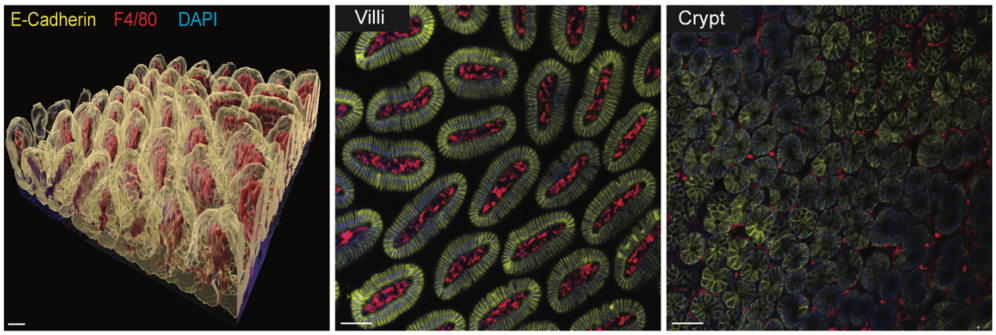

Figure 17: 3D imaging of the small intestine. Detection of E-Cadherin (epithelium, yellow), F4/80 (macrophages, red) and DAPI (blue) in tissue whole mounts from the small intestine, showing that during homeostasis the main location of macrophages is in the villi compartment. Scale bar = 50 µm.

Upon radiation injury, macrophages were massively recruited in the small intestine, emerging around the hyperplastic regenerative crypts at 6dpi (Figure 18a) where they were closely contact to the epithelium (Figure 18b).

From 30dpi onwards, the proportion and the localization are normalized (Figure 18 a and c). Of note, macrophage recruitment followed a similar dynamic as the regenerative marker Sca1.

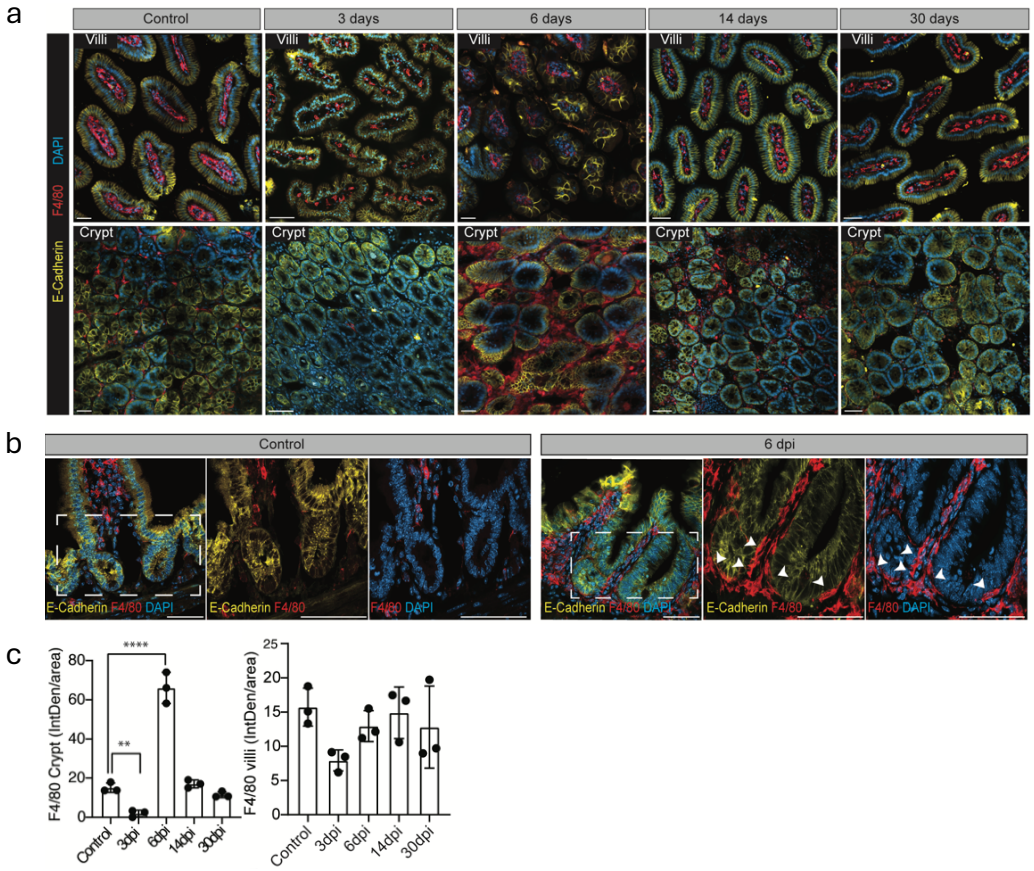

*Figure 18: Massive recruitment of macrophages upon injury. **a**) Detection of E-Cadherin (epithelium, yellow), F4/80 (macrophages, red) and DAPI (blue) in tissue whole mounts from the small intestine during homeostasis and following radiation, showing the recruitment of macrophages around the hyperplastic regenerative crypts at 6 dpi and the restoration of their location at 30 dpi. **b**) Direct interaction between macrophages and intestinal crypt cells at 6 days post irradiation when compared to steady state. **c**) Quantification of Integrated Density (IntDen)/area of F4/80 staining in villi and crypt compartment (n = 3; one-way ANOVA; ** p < 0.01, **** p<0.0001) Scale bar = 50 µm. Representative images of n=3 mice at indicated timepoint.*

To gain a deeper understanding of the correlation between macrophages and ISCs, we employed Lgr5-eGFP-ires-creERT2 transgenic mice [145] to track the

ISCs, using Lgr5-eGFP as a reporter. At 6dpi, there was a notable decrease in the number of EpCAM^{+} Lgr5^{+} ISCs and on the other hand increased numbers of macrophages (Figure 19a and 19b). This was concomitant with a significant increase of macrophages around the hyperplastic regenerative crypts (Figures 18a and 19a). At 14- and 30 dpi, the numbers of ISCs and macrophages were not significantly changed compared to control (Figure 19b).

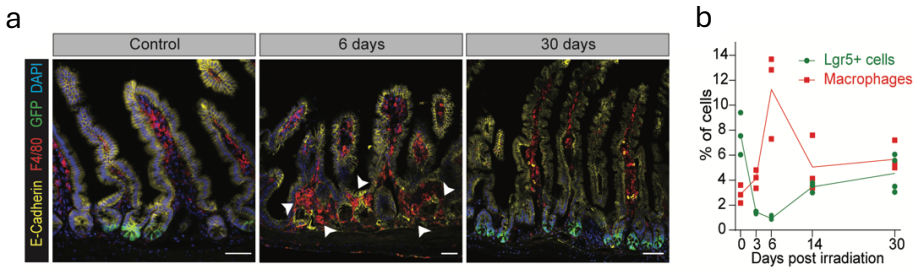

Figure 19: Macrophages anticorrelate with ISCs upon injury ***a****) Tissue section from Lgr5-eGFP-ires-creERT2 mice at the indicated time points. Arrows indicate the location of macrophages around the hyperplastic crypt at 6dpi. Scale bar = 50 µm. (Representative image of n=3).* ***b****) Flow cytometric analysis of macrophages (CD326-/CD11b+/F4/80+) and ISCs (CD326+/ Lgr5-GFP+) at 0 dpi (non-irradiated) (n=3), 3 dpi (n=3), 6 dpi (n=3), 14 dpi (n=3) and 30 dpi (n=4) from Lgr5-eGFP-ires-creERT2 mice. Lgr5+ cells show a significant decrease in percentage at days 3 (estimate = -6.21, p < 0.001), 6 (estimate = -6.73, p < 0.001), 14 (estimate = -4.2, p = 0.004), and 30 (estimate = -3.47, p = 0.015) compared to baseline. In contrast, macrophages increase significantly at each corresponding time point compared to baseline, with increases at day 3 (estimate = 7.46, p = 0.001), day 6 (estimate = 15.14, p < 0.001), day 14 (estimate = 6.38, p = 0.002), and day 30 (estimate = 6.43, p = 0.002). Negative correlation (t=-0,648; p-value 0.0159) between percentage of Lgr5+ cells and Macrophages from day 0 to day 6 (Kendall's Tau analysis).*

Considering that i) macrophages were located around the hyperproliferative regenerative crypts; ii) macrophage recruitment correlated with the epithelial overexpression of the regenerative marker Sca1 and iii) the numbers of macrophages were inversely correlated with ISCs; we hypothesize that macrophages may crosstalk with intestinal cells to regulate the process of intestinal regeneration.

4.2 Polarized macrophages crosstalk with intestinal epithelial cells and induce the regenerative program *in vitro*.

To model the putative interaction of macrophages and intestinal cells we developed an *in vitro* primary intestinal organoid and macrophage co-culture system. Of note, adult intestines give rise to budding organoids, but in contrast, when the regenerative program is activated, organoids acquire a spherical shape [97, 159, 180, 181]. Thus, organoid shape might be used as a proxy of an activated regenerative reprogramming, although this is not unequivocal because organoids with overactivation of Wnt signaling pathway are also spherical [159, 160]. To investigate whether macrophages can induce this process, we isolated bone marrow cells that were i) differentiated towards non-polarized macrophages (naïve) using M-CSF, ii) polarized towards pro-inflammatory-like phenotype (IFNγ and LPS-induced) using IFNγ and LPS, and iii) polarized towards anti-inflammatory-like phenotype (IL-4-induced) using IL-4 (Figure 20 a,b,c and d). After macrophages activation, they were subsequently embedded into Matrigel together with murine organoids for 2 days. On day 3, intestinal organoids were collected from the cocultures for morphological characterization and bulk RNA sequencing (Figure 21).

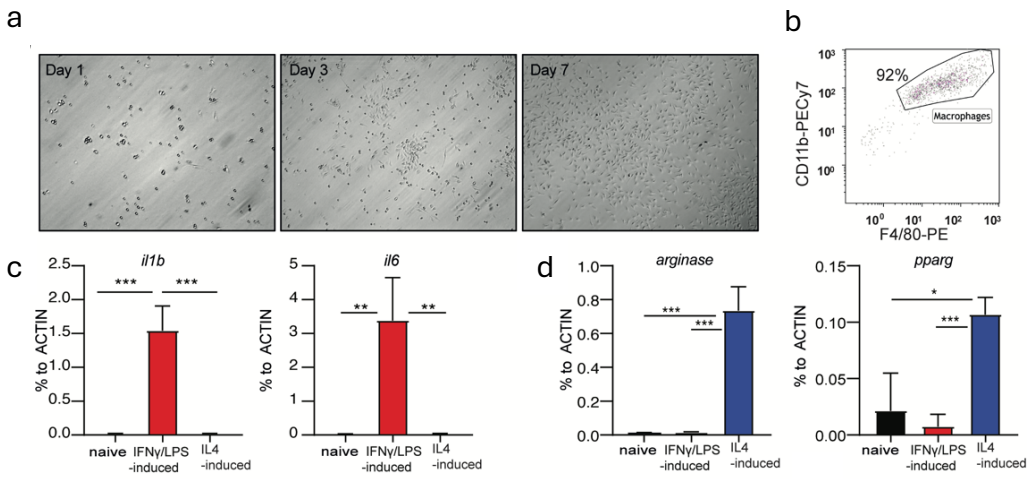

Figure 20: Characterization of polarized macrophages. ***a****) Representative images of hematopoietic cells treated with M-CSF on day 1, 3 and 7.* ***b****) Flow cytometry analysis of bone marrow derived macrophages after 7 days treated with M-CSF show the majority of the cells (92%) express macrophage markers F4/80 and CD11b.* ***c****) qRT-PCR analysis of pro-inflammatory genes (il-1b and il-6) after the formation of mature bone marrow derived macrophages naive and their activation toward to IFN-γ/LPS-induced and IL4-induced.* ***d****) qRT-PCR analysis of anti-inflammatory genes (arg1 and pparγ) after the formation of mature bone marrow derived macrophages naive and their activation to IFN-γ/LPS-induced and IL4-induced. qRT-PCR analysis of n=3 biologically independent samples (n=3, unpaired t test; ****p < 0.0001)*

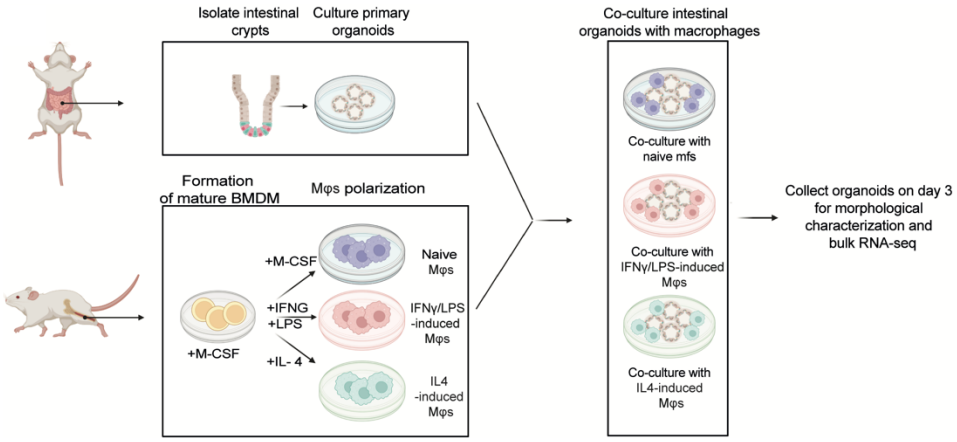

Figure 21: Schematic of experimental design of organoids-macrophages co-cultures. Isolated hematopoietic cells from bone marrow of mice were pre-treated with M-CSF for 7 days for formation of mature bone marrow-derived macrophages (BMDM) and then were treated with LPS and IFNγ for IFN-γ/LPS-

induced macrophages or with IL-4 for IL4-induced macrophages for 1 day. Intestinal organoids were mechanically passaged and mixed with bone marrow derived macrophages naive or activated macrophages (IFN-γ/LPS-induced or IL4-induced) and were cultured for 2 days. On day 3, intestinal organoids were collected for morphological characterization and bulk RNA-seq.

Non-polarized naïve macrophages did not promote a significant change in organoid shape when compared to control. In contrast, IFNγ/LPS-induced and IL4-induced macrophages induced a spherical shape in adult intestinal organoids, which is characteristic of regeneration for murine organoids [97, 159, 180, 181] (Figures 22a and b).

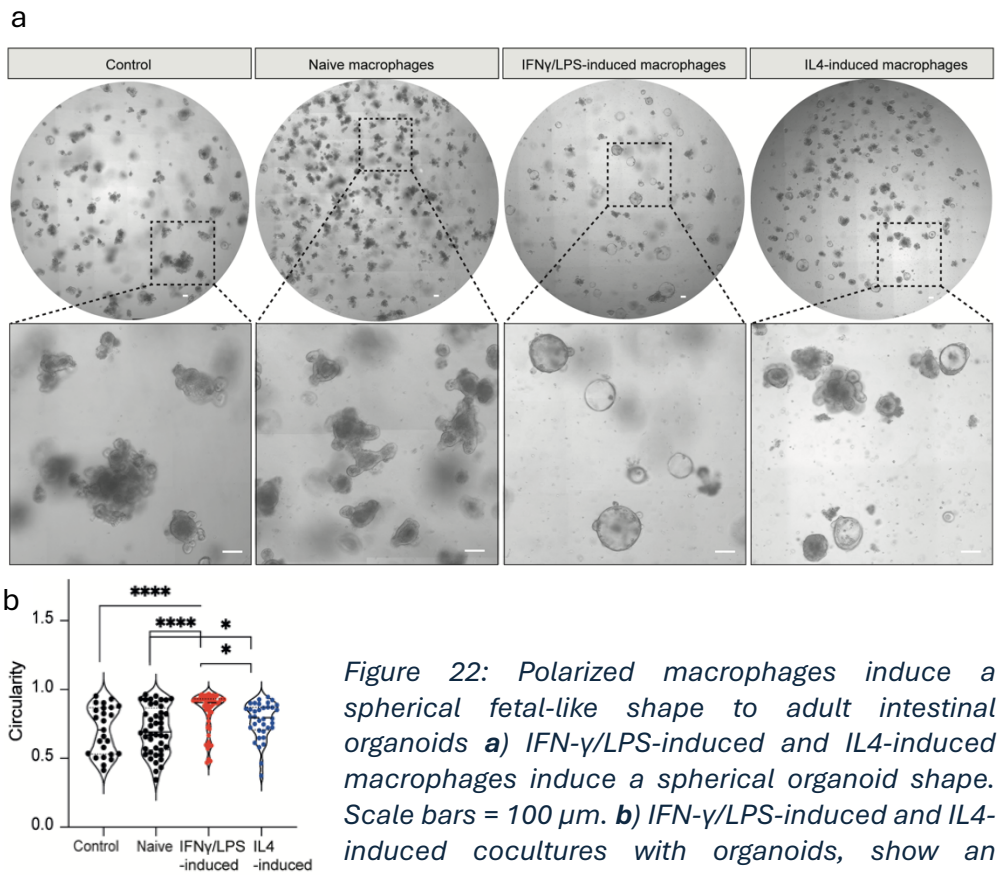

*Figure 22: Polarized macrophages induce a spherical fetal-like shape to adult intestinal organoids **a**) IFN-γ/LPS-induced and IL4-induced macrophages induce a spherical organoid shape. Scale bars = 100 µm. **b**) IFN-γ/LPS-induced and IL4-induced cocultures with organoids, show an increase in organoids circularity compared to naïve or control (Control n=25, naive n= 44, IFN-γ/LPS-induced n=53, IL4-induced n=36; Unpaired t test *p < 0.05 ***p < 0.0001).*

To understand whether those morphological changes correlated with the changes in gene expression, we performed RNA-seq of sorted murine intestinal organoids from the co-cultures with naïve macrophages, IFNγ/LPS-induced and IL4-induced macrophages. Differential gene expression analysis revealed 70 significant differentially expressed genes (DEGs) in the Naïve/control, 392 DEGs in the IFNγ/LPS-induced / control, and 154 DEGs in the IL4-induced/control (Figure 23). These changes combined with the observed organoid ´s shape suggested that polarized macrophages are able to induce prominent changes in the intestinal epithelial cells.

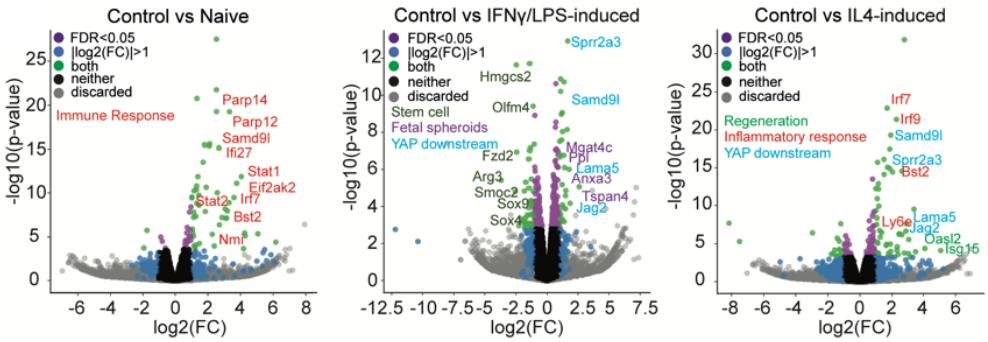

Figure 23: Differential expressed genes of cocultures. Volcano plots of differential expressed genes of epithelial cells from co-cultures. Previously described fetal-, stem cells-, regeneration -, YAP downstream -, immune- and inflammatory-specific genes are labeled in the plot.

To characterize these genetic regulatory programs triggered by polarized macrophages, we performed gene set enrichment analysis (GSEA) [174], which revealed a highly significant enrichment in the gene signatures for fetal enterospheres [181], intestinal regeneration [82] and YAP1 downstream genes [22] (Figure 24). The nuclear activation of the YAP1 was subsequently validated by immunofluorescence and quantification (Figure 24).

Collectively, this data demonstrates that both IFNγ/LPS-induced and IL4-induced macrophages can lead to the activation of a transcriptional program characteristic of the regenerative epithelium. Although

macrophages can be in vitro polarized towards pro- and anti-inflammatory profiles [182], it is well established that this is simplification of the *in vivo* cell behavior because macrophage heterogeneity is also dictated by their niche [183].

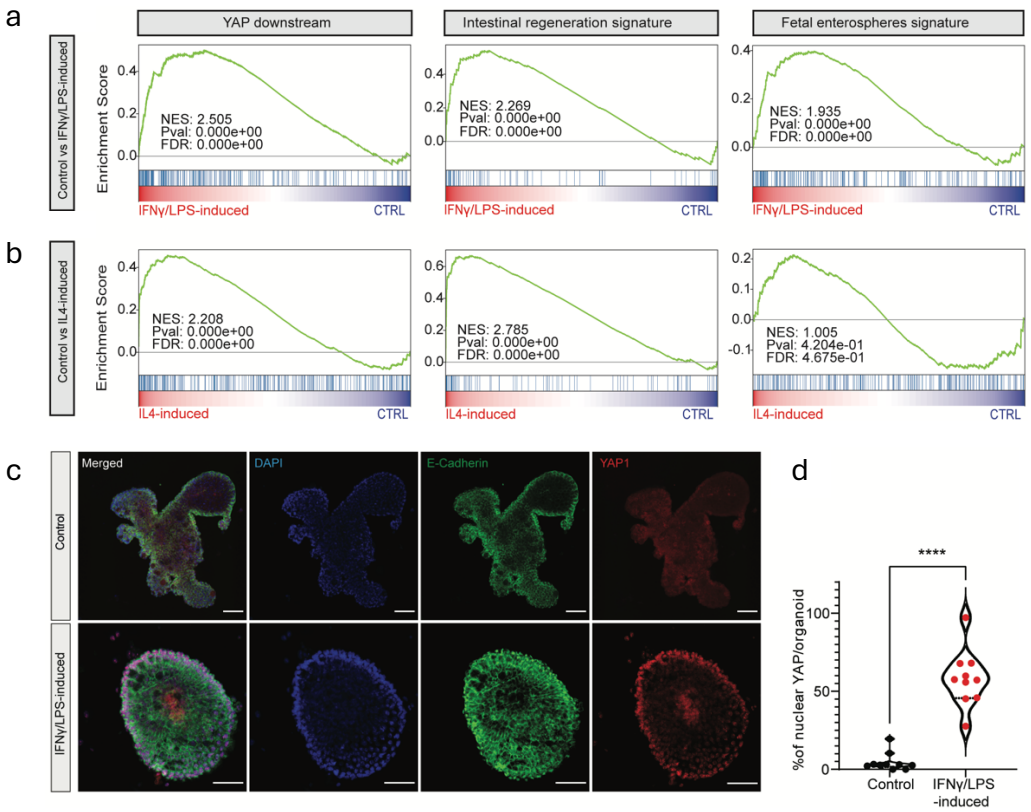

*Figure 24: Polarized macrophages induce the regenerative signature in organoids. **a**) Bulk RNA-seq of intestinal organoids co-cultured with IFN-γ/LPS-induced macrophages show strong correlation with published gene signatures associated with intestinal regeneration, fetal spheroid and YAP signaling, as measured by GSEA. **b**) Bulk RNA-seq of intestinal organoids co-cultured with IL4-induced macrophages, shows strong correlation with published gene signatures associated with intestinal regeneration and YAP signaling. For fetal spheroid signature there was no statistical significance compared to control as measured by GSEA (n=3 independent organoid cultures). **c**) Detection of E-Cadherin (epithelium, green), DAPI (blue) and active nuclear translocation of YAP1 (red) in intestinal organoids after co-culture with IFN-γ/LPS-induced macrophages. Scale bar = 50 µm. Representative images of n=3 biologically*

independent samples. ***d****) Quantification of the total nuclear YAP per organoid (n=10 orgnoids per condition; unpaired t test; ∗∗∗∗p < 0.0001)*

4.3 Macrophages are indispensable to drive intestinal regeneration *in vivo*.

4.3.1 Conditional macrophage ablation using CD11c-DTR-eGFP mouse model

The acquisition of the regenerative state induced by YAP is required for tissue regeneration [83]. Therefore, if macrophages can induce a regenerative program *in vitro* is tempting to speculate that the absence of macrophage upon intestinal injury may impair the process of intestinal regeneration. In order to test this hypothesis, we took advantage of the CD11c-DTR-eGFP mouse model [184]. CD11c is a marker of macrophages and dendritic cells [185]. Importantly, 85% of CD11c+ cells in the intestine are F4/80^{+} CD11b^{+} macrophages and on the other hand the >90% of macrophages are CD11c^{+} as shown by flow cytometry (Figure 25 a, b and c) and immunofluorescence (Figure 26 a). Consequently, CD11c-DTR-eGFP mice were injected with one dose of diphtheria toxin (DT) 25ng/g and flow cytometry and immunofluorescent validate the ablation of the majority of macrophages in the small intestine (Figure 26 a and b).

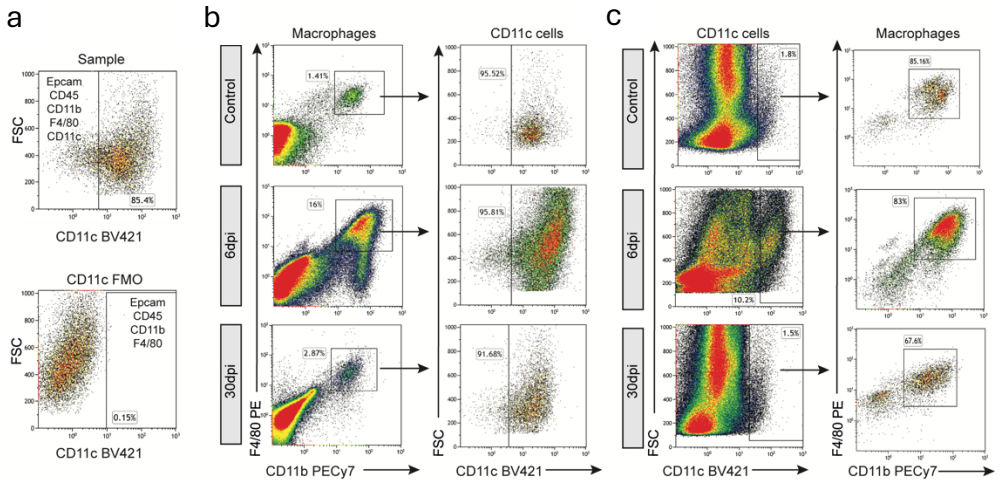

Figure 25: The majority of the CD11c+ cells in the intestine are macrophages. ***a****) Fluorescence minus one (FMO) control for the CD11c antibody.* ***b****) Representative flow cytometry plot showing most mac ages (F4/80+ and CD11b+) are expressing CD11c marker in unirradiated nice (control) and irradiated mice exposed to abdominal radiation (14Gy) after 6- and 30-dpi.* ***c****) Representative flow cytometry plot showing the majority of CD11c+ cells are expressing macrophages markers (F4/80+ and CD11b+) in unirradiated mice (control) and irradiated mice exposed to abdominal irradiation (14Gy) after 6dpi and 30dpi.*

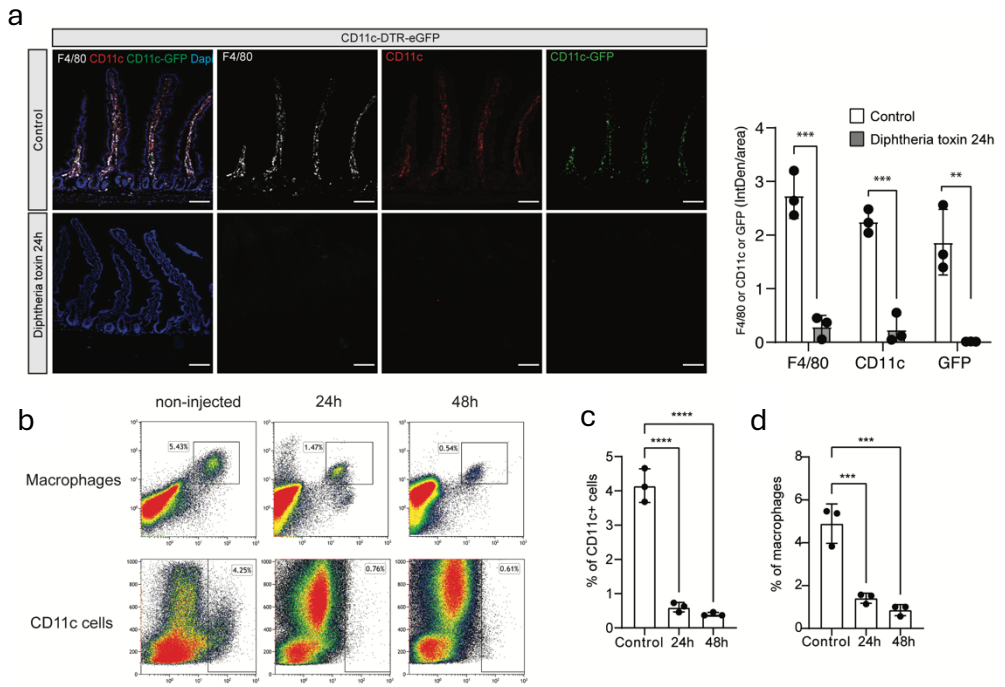

Figure 26: Conditional macrophage ablation. ***a****) Detection of F4/80 (white), CD11c (red), CD11c-GFP (green) and DAPI (blue) in tissue section from small intestine from ITGAX-DTR-eGFP mice 24 hours after being injected (or not) with one dose of DT. Scale bar 100 µm. Quantification of the intensity of F4/80, CD11c and GFP staining per area (n=3 mice; unpaired t test; **p < 0.01, ***p < 0.001).* ***b****) Representative flow cytometry plots of macrophages and CD11+ cells in non-injected, 24h and 48h injected mice with DT.* ***c****) Graph showing the reduction of the percentage of CD11c+ cells from single alive cells, 24h and 48h after DT injection in ITGAX-DTR-eGFP mice compared with uninjected ITGAX-DTR-eGFP mice (control), quantified by flow cytometry analysis. (n=3 mice per group; each dot represents a mouse at the indicated group; unpaired Student's t test; ****p <0.0001).* ***d****) Graph shows the reduction of the percentage of macrophages (F4/80+ and CD11b+) from single alive cells, 24h and 48h after DT injection in ITGAX-DTR-eGFP mice compared with uninjected ITGAX-DTR-eGFP mice (control), quantified by flow cytometry analysis. (n=3 mice per group; each dot represents a mouse at the indicated group; unpaired Student's t test; ***p < 0.001).*

To understand if macrophages play a role in the process of regeneration, a cohort of 7 mice were irradiated in the abdominal cavity and subsequently injected with DT to ablate macrophages *in vivo*. Upon macrophage ablation, mice must be sacrificed at 5-6dpi as they reach the humane endpoint due to severe weight loss (Figure 27), also some of the non-irradiated mice died likely due to a previously described myocarditis [186].

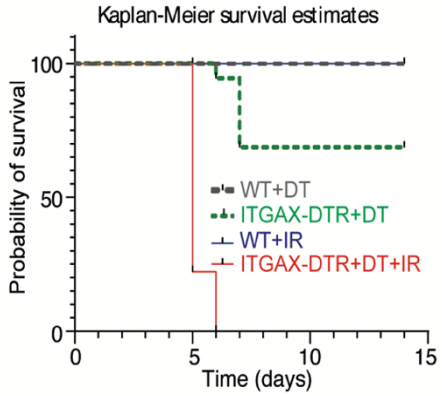

*Figure 27: Macrophages are important for the survival of mice upon injury. Kaplan–Meier survival analysis. ITGAX-DTR-eGFP mice injected with DT have reduced survival against abdominal radiation (14Gy) compared with irradiated WT mice. (***P<0.0001, Mantel–Cox test; n= 7 mice per group).*

4.3.2 Single cell RNA sequencing of epithelial cells following radiation injury and macrophage ablation

To comprehend how macrophage ablation impacts the regenerative program at a transcriptomic resolution, we performed scRNA-seq of intestinal epithelial cells from non-irradiated mice, irradiated mice (5dpi) and irradiated mice (5dpi) with CD11c cells ablated (Figure 28a). Following visualization using Uniform Manifold Approximation and Projection (UMAP), we identified 6 different clusters represented in the different conditions (Figure 28 b) corresponding to ISCs/transit amplifying (TA) (smoc2+, olfm4+, mki67+) [12], progenitors (mki67low), enterocytes

(alpi+) [84], distal enterocytes (alpi+, ada+) [69], goblet cells (muc2+,tff3+) [58] and enteroendocrine cells (chgA+, chgB+) [56] (Figure 28 c, d, e, and g)

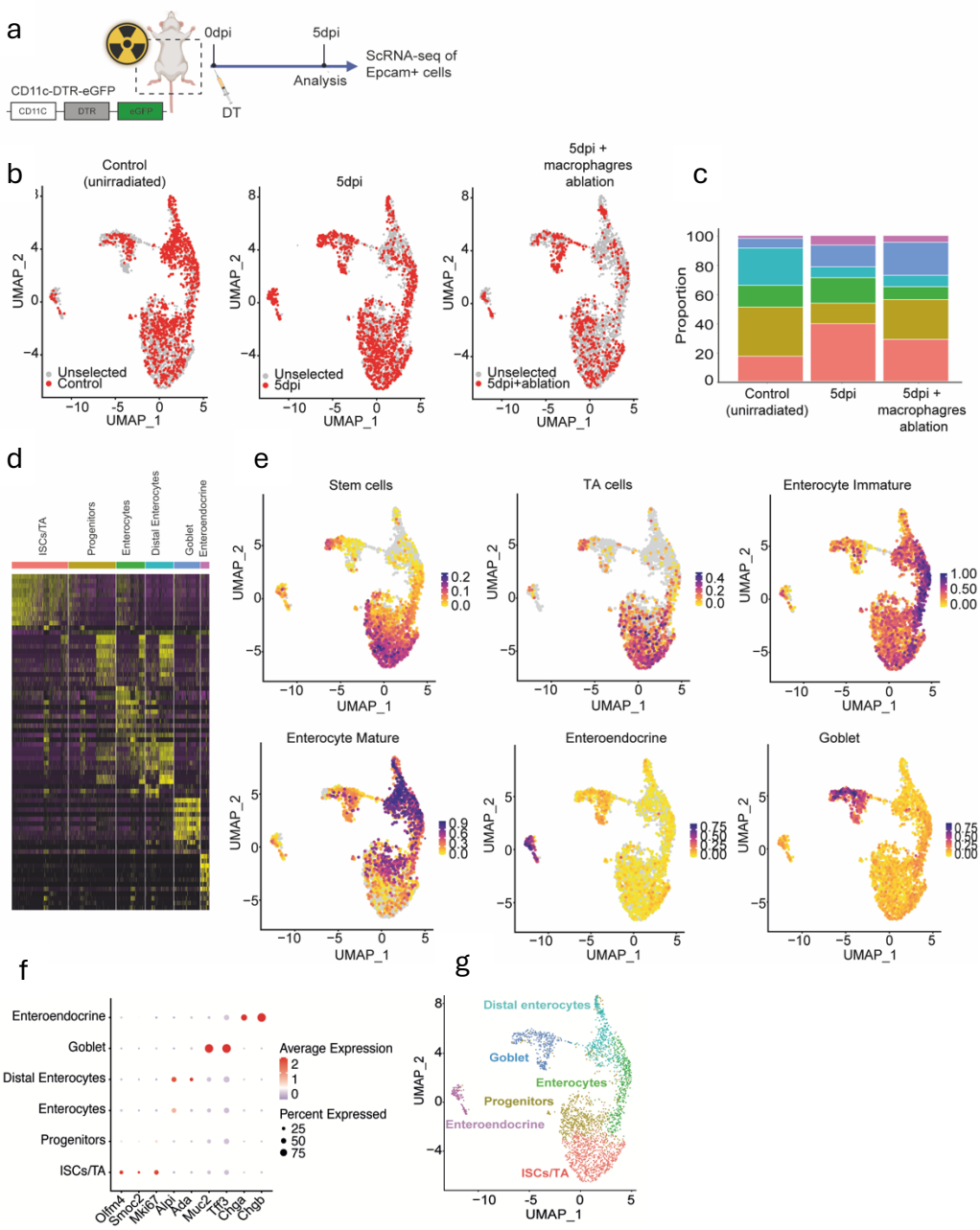

Figure 28: Characterization of the scRNA-seq of epithelial cells. ***a****) Induction protocol for deletion of CD11c+ cells followed by radiation injury. Mice were*

irradiated and subsequently injected with DT to ablate macrophages. At 5dpi, small intestines were collected for encapsulation of EpCAM+ cells for scRNA-seq ***b****) Number of cells assigned to each condition.* ***c****) ScCODA analysis showing the proportion of clusters in different conditions.* ***d****) Heatmap of scRNA-seq data shows differences in gene expression between the clusters.* ***e****) UMAP of scRNA-seq of the epithelial cells show the expression of published gene signatures associated with intestinal stem cell, transit amplifying (TA) cells, immature and mature enterocytes, enteroendocryne and goblet cells. Resulted in the identification of six cell clusters, stem cells /TA cells, proliferative stem cells, progenitors and differentiated cells.* ***f****) Bubble plot showing expression of known marker genes to distinguish ISCs/ transit amplifying cells (TA) (Olfm4, Smoc2 and Mki67), progenitors (mki67), enterocytes (alpi), distal enterocytes (alpi and dada), goblet cells (muc2 and tff3) and enteroendocrine cells (chga and chgb) to identify different cell-type clusters. Dot plot shows the fraction of expressing cells (size of the dot) and mean expression levels (dot color). Number of cells after filtering in each condition is; 1026 cells in control; 1122 cells at 5dpi and 555 cells at 5dpi with macrophages ablation.* ***g****) UMAP projection of all conditions (non-irradiated mice, irradiated mice and irradiated mice with CD11c cells ablated) results in the identification of 6 clusters.*

It has been previously reported that intestinal regeneration is driven by the dedifferentiation of progenitor and committed cells [13, 81, 84, 87, 187]. RNA velocity trajectory inference [148] predicted that in non-irradiated mice, ISCs as expected are at the apex of the cellular hierarchy, giving rise to the other intestinal lineages (Figure 29). However, upon injury, there was change in directionality of the arrows indicate that the origin of the clusters are the progenitors and committed cells, representing the process of the dedifferentiation (Figure 29). However when macrophages are ablated these patterns are more similar to control (unirradiated condition) indicate interruption of the regeneration (Figure 29).

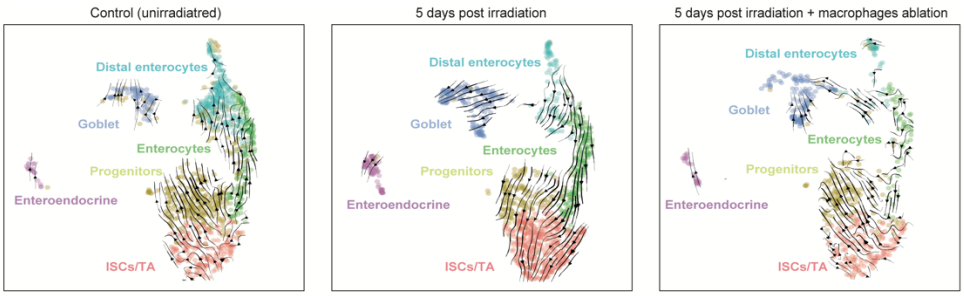

Figure 29: Macrophage ablation impairs the cell trajectory upon injury. RNA velocity cell trajectory analysis for each condition (non-irradiated mice, irradiated mice and irradiated mice with macrophages ablated) identifies that upon injury in irradiated mice there is inversion of cell trajectory because of cell dedifferentiation. However, in irradiated mice when macrophages are ablated the process of dedifferentiation is impaired and ISCs are in the apex of cellular hierarchy similar to unirradiated mice.

4.3.3 Lineage tracing of KRT20 cells and EdU proliferative assay upon homeostasis and radiation injury

In order to test this prediction, we took advantage of a Krt20-driven tamoxifen-inducible Cre system mouse model combined with a Rosa26-loxP-STOP-loxP-Tdtomato reporter to perform lineage tracing of KRT20^{+} cells. KRT20 is a marker of differentiated intestinal villi cells and upper crypt progenitor cells [80, 188] (Figure 30a). Therefore, upon 4-hydroxytamoxifen (4-OH TAM) injection into these mice, villi cells were labeled with a Tdtomato fluorescent mark that overlaps with KRT20 expression (Figure 30b). During homeostasis and due to fast turnover of the intestine, at 3 days post 4-OH TAM there are Tdtomato^{+} cells in the upper part of the villi compartment, resulting to a completely wash out after seven days because of full replacement of the intestinal epithelium (Figure 30c, d, e and f). However, when mice were irradiated, Krt20 labeled cells were able to replenish the crypt compartment at 7dpi and persist long term even 3 weeks post irradiation (Figure 30g and h).

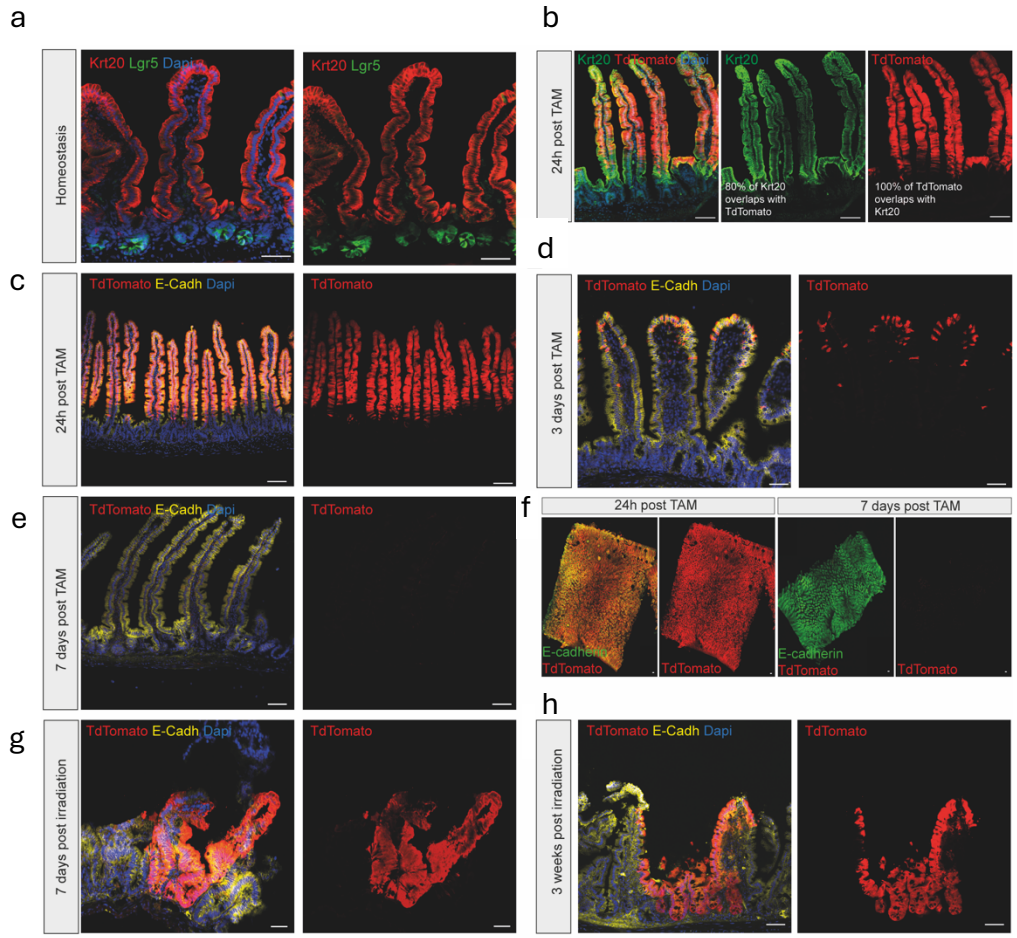

Figure 30: lineage tracing of Krt20+ cells. ***a****) Detection of KRT20 (red), Lgr5-EGFP (green) and DAPI (blue) in tissue section from small intestine from Lgr5-eGFP-ires-creERT2 mouse demonstrate the location of KRT20+ in the villi compartment.* ***b****) Detection of Tdtomato (red), KRT20 (green) and DAPI (blue) in tissue section from small intestine from Krt20-T2A-Cre-ERT2;R26-Flox-STOP-Flox-Tdtomato mice shows the overlapping of Tdtomato + and KRT20+ cells at 24h following by the administration of 4-OHT.* ***c****) Detection of Tdtomato (red), E-cadherin (yellow) and DAPI (blue) in tissue section from small intestine from Krt20-T2A-Cre-ERT2;R26-Flox-STOP-Flox-Tdtomato mice shows the Tdtomato + cells in the villi compartment at 24h following by the administration of 4-OHT.* ***d****) Detection of Tdtomato (red), E-cadherin (yellow) and DAPI (blue) in tissue section from small intestine from Krt20-T2A-Cre-ERT2;R26-Flox-STOP-Flox-Tdtomato mice shows the location of Tdtomato + cells in the upper part of the villi 3 days following by the administration of 4-OHT.* ***e****) Detection of Tdtomato (red), E-cadherin (yellow) and DAPI (blue) in tissue section from small intestine from Krt20-T2A-Cre-ERT2;R26-Flox-STOP-Flox-Tdtomato mice shows the complete washout of Tdtomato + cells 7 days following by the administration of*

*4-OHT. (**f**) Detection of E-cadherin and Tdtomato in tissue whole mount, isolated from Krt20-T2A-Cre-ERT2; R26-Flox-STOP-Flox-Tdtomato; mice at 24h and 7 days post 4-hydroxytamoxifen (4-OHT) injection. **g**) Detection of Tdtomato (red), E-cadherin (yellow) and DAPI (blue) in tissue section from small intestine from Krt20-T2A-Cre-ERT2;R26-Flox-STOP-Flox-Tdtomato mice shows a whole part of villus-crypt axis to be Tdtomato+ 7 days following by the administration of 4-OHT and radiation injury indicating the de-differentiation of KRT20+ cells. **h**) Detection of Tdtomato (red), E-cadherin (yellow) and DAPI (blue) in tissue section from small intestine from Krt20-T2A-Cre-ERT2;R26-Flox-STOP-Flox-Tdtomato mice shows the long-term persistence of a Tdtomato clone 3 weeks following by the administration of 4-OHT and radiation injury.*

Interestingly, when macrophages are ablated, the dedifferentiation process is impaired (Figure 31a) and Tdtomato^{+} cells are significantly reduced (Figure 31b). Thus, these results experimentally support that cells expressing differentiation markers contribute to tissue regeneration following tissue damage and that macrophages are required to orchestrate this process.

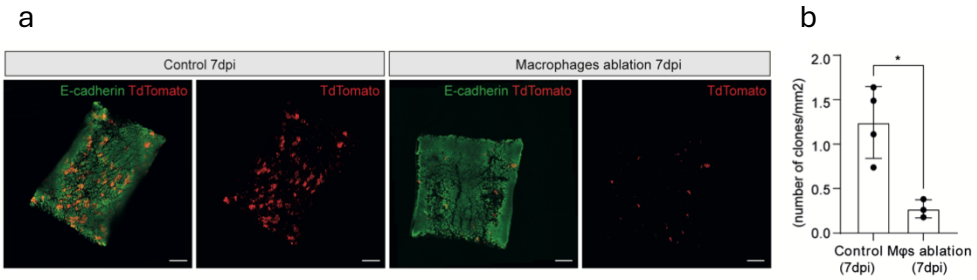

*Figure 31: Macrophage ablation impairs the process of dedifferentiation upon injury. **a**) Detection of E-cadherin (green) and Tdtomato (red) in tissue whole mounts from proximal small intestine isolated from Krt20-T2A-Cre-ERT2; R26-Flox-STOP-Flox-Tdtomato; ITGAX-DTR-eGFP mice at 7dpi (n=3 mice) and from Krt20-T2A-Cre-ERT2; R26-Flox-STOP-Flox-Tdtomato mice at 7dpi (n=4 mice). Mice were injected with 4-hydroxytamoxifen (4-OHT) on the same day with abdominal irradiation and with DT at 4- and 5-dpi shows the interruption of the process of de-differentiation upon irradiation and macrophage ablation. Scale bar 1000 μm. **b**)Relative number of clones per mm2 is shown. Macrophage (Mϕs) ablation results in the reduction of the number of surviving clones in irradiated mice. Each dot represents a mouse at the indicated group. (unpaired Student's t test; $* p < 0.05$).*

To elucidate why the regenerative process is impaired in the absence of macrophages, we focused on the proliferative potential of the intestinal epithelium. Using a previously reported intestinal proliferative gene signature [189], our data reveals that the average gene expression levels characteristic of proliferation are significantly activated upon injury (Control versus 5 dpi, p-value<0.0001) , but this activation is significantly impaired when macrophages are ablated (5 dpi versus 5 dpi with macrophage ablation, p-value<0.0001) (Figure 32a). To functionally assess if the proliferative regenerative potential is affected by macrophage ablation, we injected 5-Ethynyl-2'-deoxyuridine (EdU) into irradiated mice. In the absence of macrophages, the number of hyperplastic EdU positive crypts, as well as the total number of EdU positive cells, was significantly reduced (Figures32b, c and d).

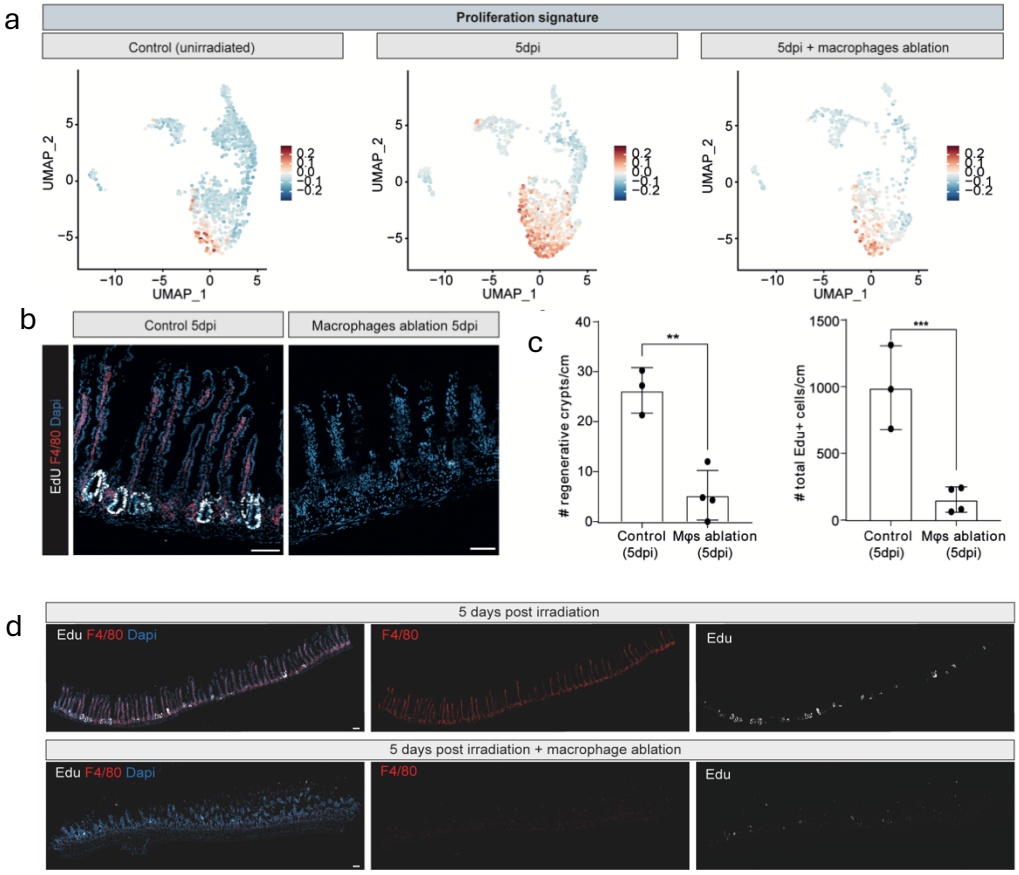

Figure 32: Macrophage ablation impairs the intestinal proliferation upon injury. ***a****) UMAP of scRNA-seq of EpCAM+ cells show that the proliferative gene signature is significantly different in ISCs/TA and progenitor cluster between the following comparisons: Control vs. 5 dpi (p-val <0.0001), Control vs. 5 dpi with macrophage ablation (p-val <0.0001), and 5 dpi vs. 5 dpi with macrophage ablation (p-val <0.0001) (Wilcoxon test).* ***b****) Detection of EdU, F4/80 and DAPI in tissue section from small intestine showing the interruption of proliferation upon irradiation and macrophages ablation. scale bar 100 µm.* ***c****) Quantification of the number of EdU+ crypts per cm or the total number of EdU+ cells per cm, 1 h after EdU labeling. (Each dot represents a mouse at the indicated group; unpaired t test; **p < 0.01 and ***p <0.001).* ***d****)Detection of EdU, F4/80 and DAPI in tissue section from a strip of a small intestine.*

Collectively, these findings demonstrate that macrophages are indispensable for triggering the tissue regeneration process, characterized by the presence of hyperplastic proliferative crypts and epithelial cell dedifferentiation.

4.4 Macrophages secrete NRG1 and SPP1

4.4.1 Single cell RNA sequencing of macrophages upon homeostasis and radiation injury

To elucidate how macrophages are able to orchestrate intestinal regeneration in response to radiation injury we performed scRNA-seq of macrophages during homeostasis and upon radiation injury. Although macrophages were sorted using flow cytometry (CD45+, CD11b+, F4/80+ and EpCAM- cells) (Figure 33a), we could detect small clusters of T-cells, B-cells, epithelial cells, dendritic cells and neutrophiles, alongside two major clusters of macrophages (Figure 33b-e). Of note, T-cells, B-cells, epithelial cells, dendritic cells and neutrophiles clustered together irrespective of whether they were coming from irradiated or non-irradiated mice (Figure 33c). in addition, macrophages clusters were enriched in macrophage specific markers with low and negligible expression of eosinophil markers (Figure 33f). Of note, although we observed enrichment of gene signatures of pro- and anti-inflammatory macrophages [190] these did not overlap with the identified clusters (Figure 33g). This suggests, in line with previous studies (reviewed in [191]), that macrophage complexity in vivo is greater than the observed *in vitro*. Furthermore, it indicates that pro- and anti-inflammatory transcriptional features may not be the primary determinants of macrophage cluster identity. In addition, UMAP visualization of the expression of *Timd4* and *Cd4* which define intestinal tissue resident macrophages [112] indicating that the majority of macrophages upon

injury are not tissue resident (Figure 33h). Of note, the two samples were processed for scRNA-seq in parallel at the same day. Comparable results were obtained integrating the scRNAseq datasets (data not shown).

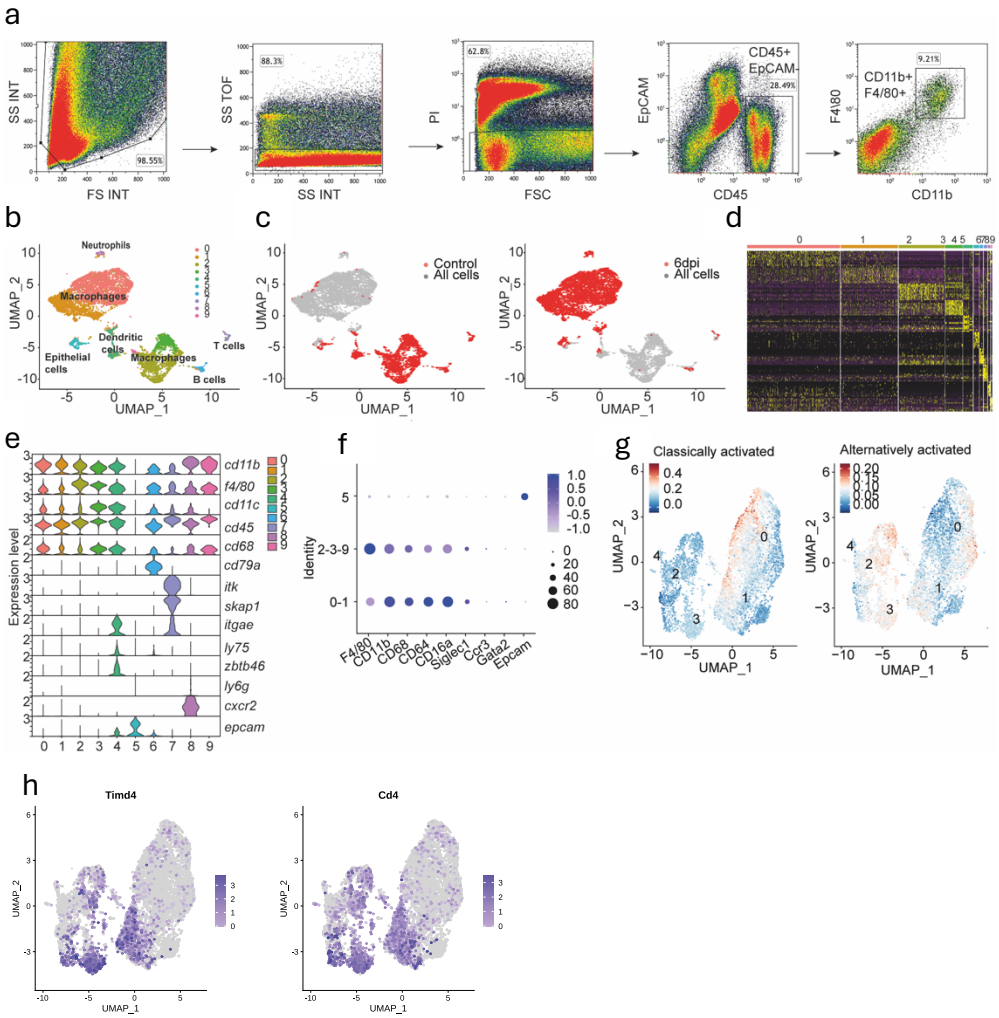

*Figure 33: Characterization of scRNA-seq of macrophages in homeostasis and post irradiation. **a**) Fluorescence-activated cell analysis strategy for sorting of macrophages. Aggregates, debris, PI+ and EpCAM+ events were first depleted. Live single cells were then stratified into CD45+ CD11b+ F4/80+ macrophages and sorted for scRNA-seq. **b**) UMAP of scRNA-seq of all sorted cells from small intestine of non-irradiated and 6dpi mice showing the different cell-type clusters. Macrophages, T-cells, B-cells, neutrophils, dendritic and epithelial cells. **c**) T cells, B cells, epithelial cells, dendritic cells, neutrophile cells*

clustered together irrespective of whether they were coming from non-irradiated mice or irradiated mice. Macrophages generated two isolated clusters belonging to control and irradiated intestines. ***d****) Heatmap of scRNA-seq data shows differences in gene expression between the clusters.* ***e****) Violin plot showing expression of known marker genes for macrophages (Itgam, Adgre1, Itgax, ptprc, cd68), T-cells (cd79a) B-cells, itk, skap1), dendritic cells (itgae, ly75, zbtb46), neutrophils (ly6g, cxcr2) and epithelial cells (epcam) to distinguish the different cell type clusters.* ***f****) Bubble plot showing expression of known marker genes to distinguish macrophages (F4/80, CD11b, CD68, CD64, CD16a) and eosinophils (Siglec1, Ccr3, Gata2) and epithelial cells (Epcam). Dot plot shows the fraction of expressing cells (size of the dot) and mean expression levels (dot color).* ***g****) UMAP of scRNA-seq after subclustering the macrophages from the small intestine of non-irradiated and 6 dpi mice shows the expression of published gene signatures associated with classically activated (pro-inflammatory) or alternatively activated (anti-inflammatory) macrophages [190].* ***h****) UMAP of scRNA-seq of macrophages showing the expression of Timd4 and Cd4 indicating the presence of tissue resident macrophages.*

Following sub-clustering of the macrophages, we identified 5 clusters (Figure 34a) representing the cells derived from control and 6 dpi (Figure 34b). DEG analysis revealed that during the process of regeneration, macrophages significantly upregulate Neuregulin 1 (*nrg1*) and Osteopontin also known as spp1 (secreted phosphoprotein 1) (Figure 34c and d). The differential expression of nrg1 and spp1 between control and 6dpi was also significant in pseudo bulk comparison (Nrg1 Control vs 6days post irradiation avg_log2FC=0.89, padj<0.0001; Spp1 Control vs 6dpi avg_log2FC=1.2, padj<0.0001). Comparable results were obtained when integrating with CCD the scRNAseq dataset (data not shown). NRG1 is one of four members in the neuregulin family that act on the Epidermal growth factor receptor, a critical pathway that is a major driver of intestinal epithelial proliferation [124, 192]. Furthermore, NRG1 has been implicated as a key driver of regeneration in a variety of tissues [193-195]. Osteopontin is a matricellular protein, that is expressed by various cell types, including immune cells, in different tissues and is associated with various signaling pathways including the WNT, integrin, PI3K/AKT, MAPK, and NF-κB signaling pathways [196-198].

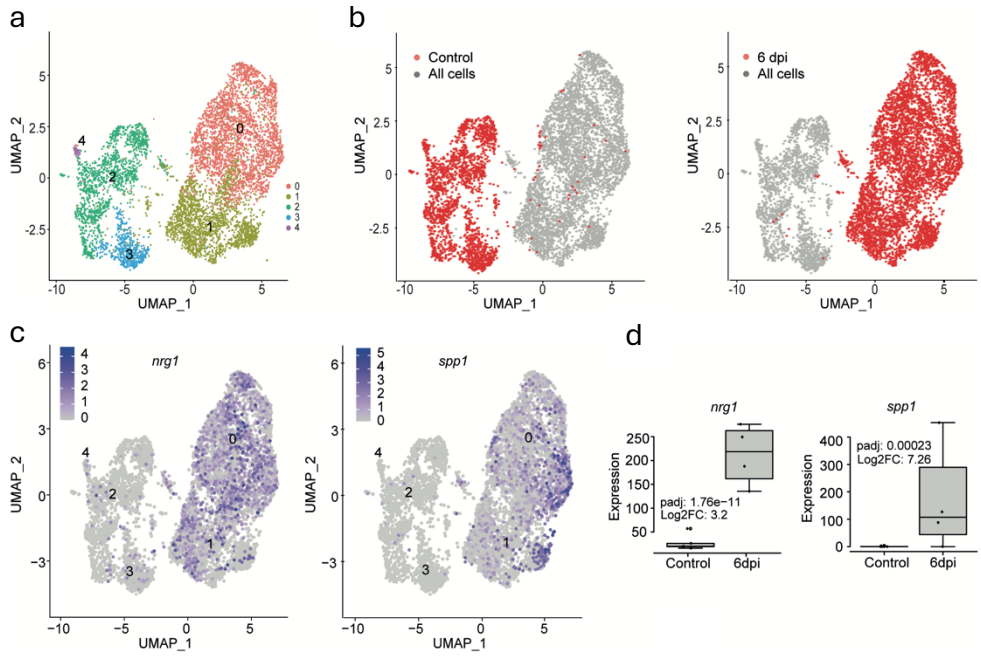

Figure 34: Macrophages upon injury express nrg1 and spp1. ***a****) UMAP of scRNA-seq of macrophages from the small intestine of non-irradiated and 6dpi mice showing five different clusters of macrophages. (Number of cells after filtering in each condition is Control: 2085; 6 days post irradiation: 4834).* ***b****) UMAP analysis of scRNA-seq of macrophages reveals distinct macrophage populations originating from either the control group or the group exposed 6dpi.* ***c****) UMAP of scRNA-seq of macrophages from the small intestine showing that Nrg1 (p-value= 3.46e-138, cluster 0) and Spp1 (p-value= 3.05e-12, cluster 0) are significantly expressed (Wilcoxon test).* ***d****) Pseudo-bulk comparison of Spp1 and Nrg1 expression across clusters in control macrophages and macrophages post-irradiation. The results demonstrate significant upregulation of Spp1 (log2FC = 7.26, padj = 0.000233) and Nrg1 (log2FC = 3.2, padj = 1.76e-11) in macrophages after irradiation (Wilcoxon test).*

Immunofluorescence of SPP1 and *in situ* hybridization of nrg1 revealed its upregulation in the intestinal crypt compartment during intestinal regeneration (Figure 35a and b) and its downregulation when macrophages were ablated (Figure 35c and d). Stromal secreted NRG1 was previously shown [124] to contribute to intestinal regeneration, however the contribution of SPP1 is unknown.

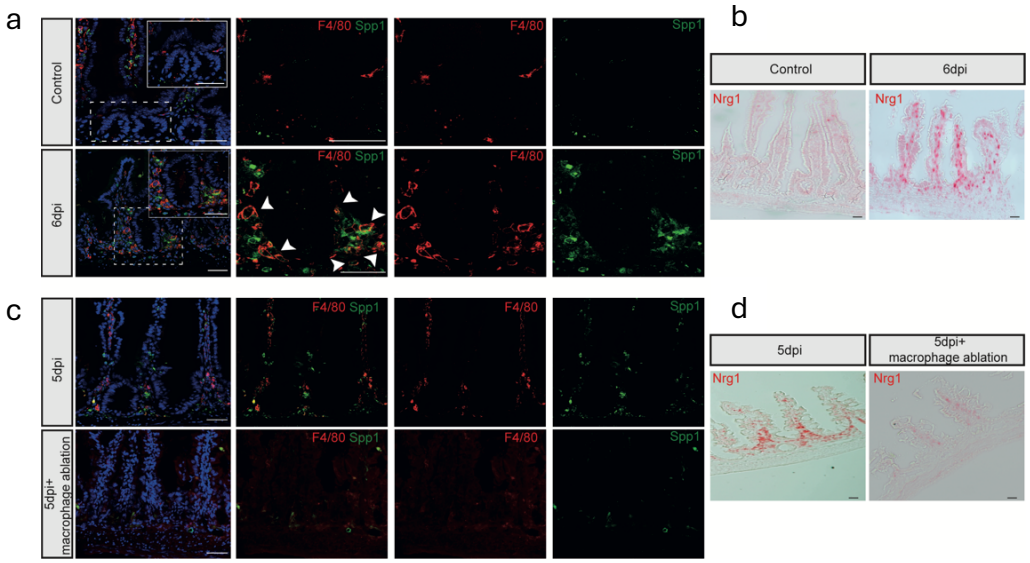

Figure 35: Increase expression of Nrg1 and Spp1 upon injury. ***a****) Detection of SPP1, F4/80 and DAPI in tissue section from small intestine from WT mice showing the increased expression of SPP1 around the hyperplastic crypts at 6dpi. Arrows indicate the expression of SPP1 either inside or around the macrophages.* ***b****) In situ hybridization of NRG1 in tissue section from small intestine from WT mice showing the increased expression of NRG1 at 6dpi.* ***c****) Detection of SPP1, F4/80 and DAPI in tissue section from small intestine from ITGAX-DTR-eGFP mice showing reduced expression of SPP1 at 5dpi.* ***d****) In situ hybridization of NRG1 in tissue section from small intestine from control and ITGAX-DTR-eGFP mice injected with DT show reduced expression of NRG1 at 5dpi when CD11c cells are ablated. scale bar 50 µm.*

4.4.2 NRG1 and SPP1 induce the regenerative genetic program and promote stem cell fate

In order to test the effect of SPP1, NRG1 and combination of the two we treated murine organoids. This was followed by bulk RNA sequencing of intestinal organoids to assess their potential to induce a regenerative program in vitro (Figure 36a). Analysis of differential gene expression unveiled 44 DEGs in the SPP1/control group and 3084 DEGs in the NRG1/Control group. Remarkably, the combined SPP1 and NRG1 treatment increased the number to 5949 DEGs in the SPP1+NRG1/control group (Figure 36b-d), suggesting a synergistic effect of the combined treatment. Of note, the number of differentially expressed genes (DEGs) identified. (e.g. 7000) is remarkably high. However, this finding is consistent with previous publications involving organoids [159]. This is likely due to the high reproducibility of replicates using organoids.

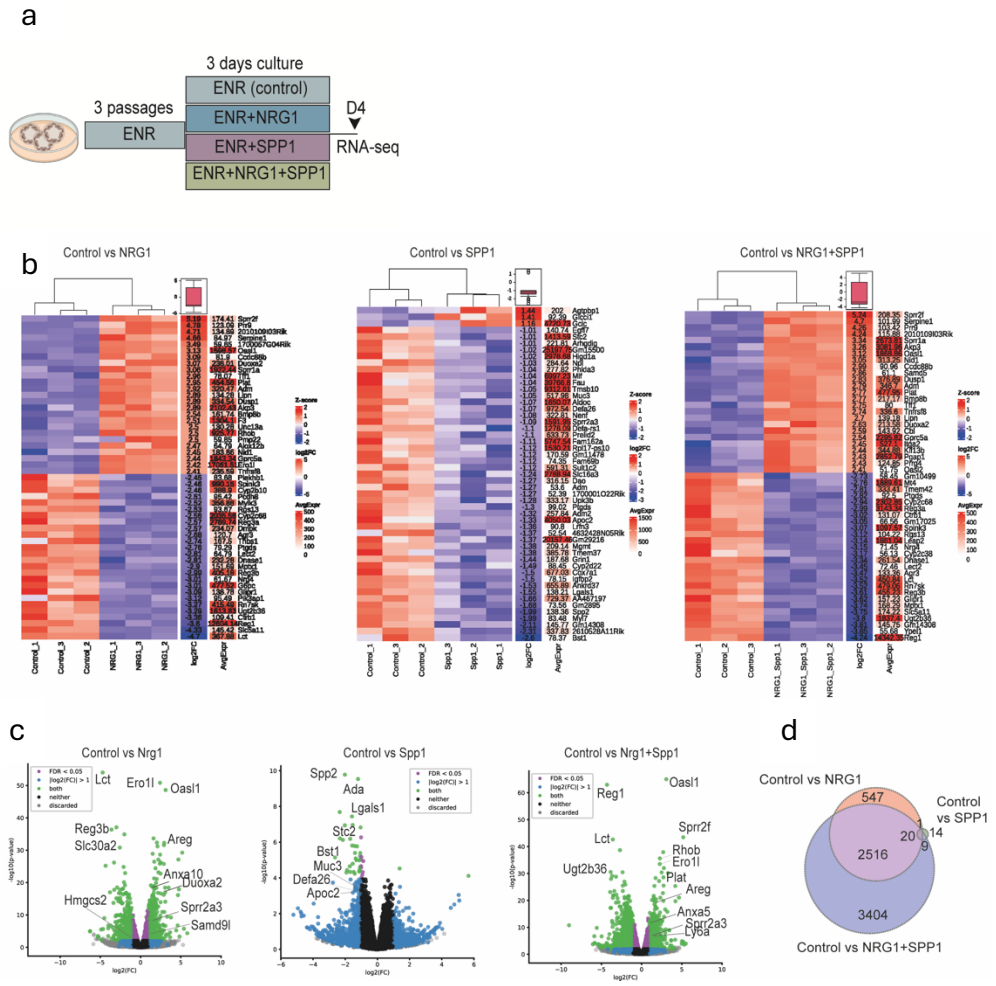

Figure 36: RNA-seq of intestinal organoids treated with Nrg1 and Spp1. ***a****) Experimental design of pre-grown organoids treatment for 3 days with NRG1, SPP1 or a combination of both. Organoids were collected for bulk RNA-seq on day 4. For all conditions, EGF, R-spondin 1 and Noggin (ENR) were added. Heatmap of bulk RNA-seq data indicating every replicate of each condition.* ***b****) Heatmap of bulk RNA-seq data indicating every replicate of each condition.* ***c****) Volcanos plot of differential gene expression analysis unveiled 3084 genes differentially expressed in the Nrg1/control group, 44 genes differentially expressed in the Spp1/control group and 5949 genes differentially expressed in the Spp1 + Nrg1/control group. Top differentially expressed genes are indicated in the plots.* ***d****) Venn diagram plot represents the overlapping of differentially expressed genes in different conditions.*

In the presence of NRG1, we observed significantly elevated levels of genes associated with fetal/regenerative/YAP signaling signatures [82, 96, 181] (Figure 37a), consistent with a previous report [199]. GSEA analysis for SPP1 treatment showed significant enrichment in the Lgr5 stem cell signature [12] (Figure 37b) but lacked enrichment in signatures related to regeneration [82] or transcripts associated with a fetal signature [181]. Similar patterns were observed in organoids treated with both NRG1 and SPP1 (Figure 37c). Of note when we compared the NRG1/SPP1-treated group with the NRG1-treated organoids, the stem cell [12] and WNT signaling signatures [200] were upregulated (Figure 37d). This is noteworthy, as the WNT pathway is a key regulator of stem cell fate [201].

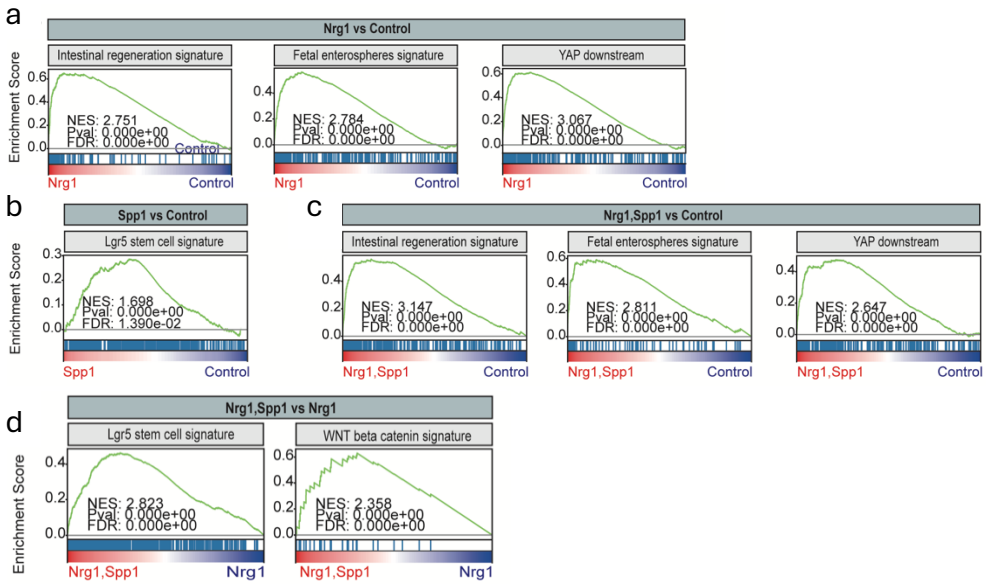

Figure 37: Nrg1 and Spp1 activate different pathways in epithelial cells. ***a****) GSEA of NRG1 treatment shows upregulation of published gene signatures associated with intestinal regeneration, fetal spheroid and YAP signaling [82, 181] (n=3).* ***b****)GSEA of SPP1 treatment, shows upregulation of Lgr5 stem cell signature [12] (n=3).* ***c****)GSEA of NRG1+SPP1 shows upregulation of published gene signatures associated with intestinal regeneration [82], fetal spheroid [181], YAP [96] (n=3).* ***d****)GSEA of NRG1+SPP1 show upregulation of published gene signatures*

associated with Lgr5 stem cell [12] signature and WNT beta catenin signaling [200] compared to Nrg1 treated organoids. (n=3).

Since it was difficult to know if this was due to differences in cell heterogeneity response or to global changes, we performed scRNA-seq on organoids treated with NRG1 and SPP1 (Figure 38a). Following visualization using Uniform Manifold Approximation and Projection (UMAP), we identified 6 different clusters represented in the different conditions (Figure 38b), corresponding to ISCs/transit amplifying (TA) (smoc2+, olfm4+, mki67+), progenitors (mki67low), enterocytes (alpi+), distal enterocytes (alpi+, ada+)goblet cells (muc2+,tff3+)and enteroendocrine cells (chgA+, chgB+) (Figure 38c-h).

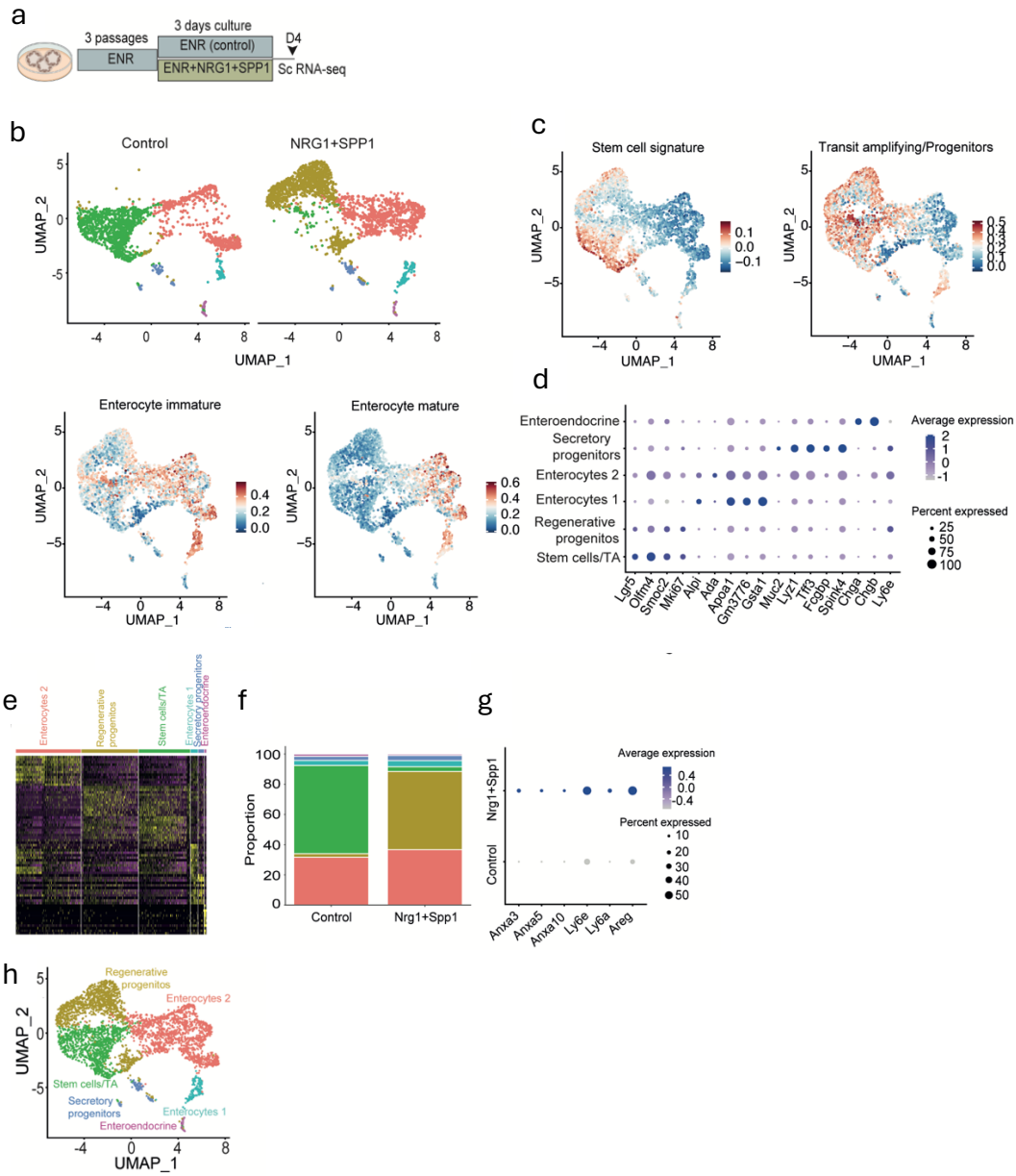

*Figure 38: Characterization of the scRNA-seq of organoids treated with Nrg1 and Spp1. **a**) Experimental design of pre-grown organoids treatment for 3 days with NRG1+SPP1. Organoids were collected for scRNA-seq on day 4. For all conditions, EGF, R-spondin 1 and Noggin (ENR) were added. **b**)UMAP of scRNA-seq of cells deriving from untreated or treated organoids culture with NRG1+SPP1. **c**) UMAP of scRNA-seq of organoids show the expression of published gene signatures associated with intestinal stem cell, transit amplifying cells and immature and mature enterocytes [150]. **d**) Bubble plot*

showing expression of known marker genes to distinguish stem cells (Lgr5, Olfm4, Smoc2, Mki67), Enterocytes (Alpi, Ada, Apoa1, Gm3776, Gsta1) goblet/secretory progenitors (Muc2, Lyz1, Tff3, Fcgbp, Spink4), enteroendocrine cells (Chga, Chgb) and regenerative state cells (Ly6e). Dot plot shows the fraction of expressing cells (size of the dot) and mean expression levels (dot color). ***e****) Heatmap of scRNA-seq data shows differences in gene expression between the clusters.* ***f****) ScCODA analysis showing the proportion of clusters in different conditions.* ***g****) Bubble plot showing expression of known marker genes that related with intestinal regeneration (Anxa3, Anxa5, Anxa10, Ly6a, Ly6e, Areg) in control and treated condition. Dot plot shows the fraction of expressing cells (size of the dot) and mean expression levels (dot color).* ***h****) UMAP of scRNA-seq showing the different cell-type clusters. Stem cells, regenerative progenitors, enterocytes 1, enterocytes 2, enteroendocrine and secretory progenitors. (Number of cells after filtering in each condition was Control: 1742; NRG1+SPP1: 2236)*

At single-cell resolution, we observed a statistically significant upregulation of regenerative/fetal/YAP signaling signatures (p-value<0.0001) upon NRG1 and SPP1 combined treatment, particularly within the enterocyte cluster (Figure 39a). To further characterize the effects induced by spp1, we employed a constitutive spp1 knockout (KO) model. Following radiation and bulk RNA sequencing of WT and spp1 KO, intestinal epithelium on day 6 post-irradiation, we observed a reduction in the intestinal stem cell signature in the mutant cells, underscoring the role of Spp1 in maintaining stemness (Figure 39b). However, in spp1 KO mice, neither survival nor the proliferative capacity of the intestine was affected (data not showed). These results combined with bulk RNA-seq suggest that NRG1 drives cells toward a more fetal, regenerative state, while SPP1 promotes stemness.

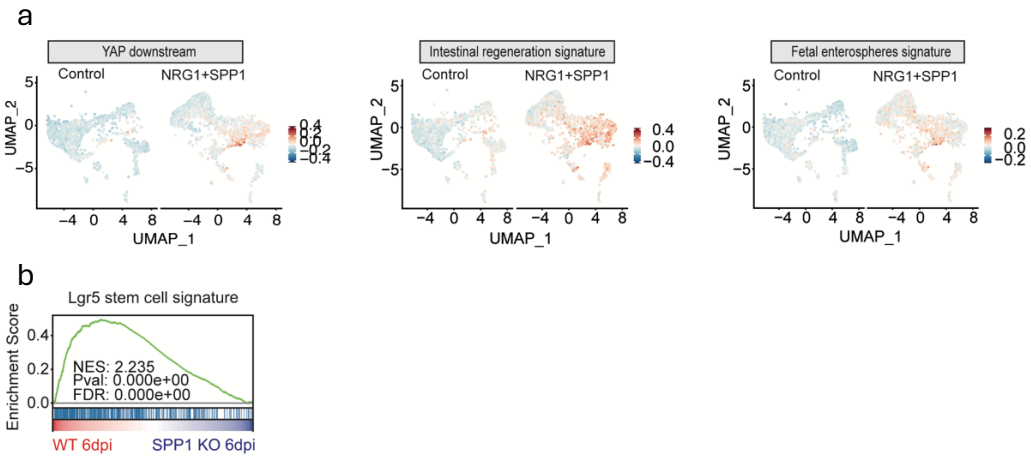

Figure 39: Nrg1+Spp1 induce a fetal-like regenerative program to organoids. ***a****) UMAP of scRNA-seq of the control and NRG1+SPP1 treated organoids demonstrate significant upregulation of the expression of published gene signatures associated with intestinal regeneration (p-val<0.001) [8], fetal spheroid (p-val<0.001) [13], and YAP (p-val<0.001) [18] in NRG1+SPP1 treated organoids (Wilcoxon test).* ***b****) Bulk RNA-seq of intestinal epithelial cells from SPP1 KO irradiated 6 days mice shows downregulation of intestinal stem cell signature [24] compared to WT 6days post irradiation mice as measured by GSEA. (n=3 mice per condition)*

4.5 Nrg1 and Spp1 rescue irradiated intestinal organoids *in vitro* and restored proliferative capacity *in vivo*

Given that Nrg1 and SPP1 factors can stimulate regenerative processes in intestinal organoids *in vitro*, we questioned whether these proteins might also help intestinal organoids recover from irradiation. Typically, intestinal organoids exposed to more than 6 Gy fail to reform after passaging [202]. To test this, organoids were irradiated with 8 Gy and treated with NRG1, SPP1, or a combination of both for three days, followed by passaging on day four. Three days after passaging, we

quantified the number of surviving organoids (Figure 40a). After irradiation most of the untreated organoids did not survive. However, organoids treated with NRG1 or the NRG1 and SPP1 combined treatment showed a significant increase in the organoid formation capacity (Figure 40b and c). These findings demonstrate that both NRG1 and SPP1 are able to rescue intestinal organoid formation following radiation damage.

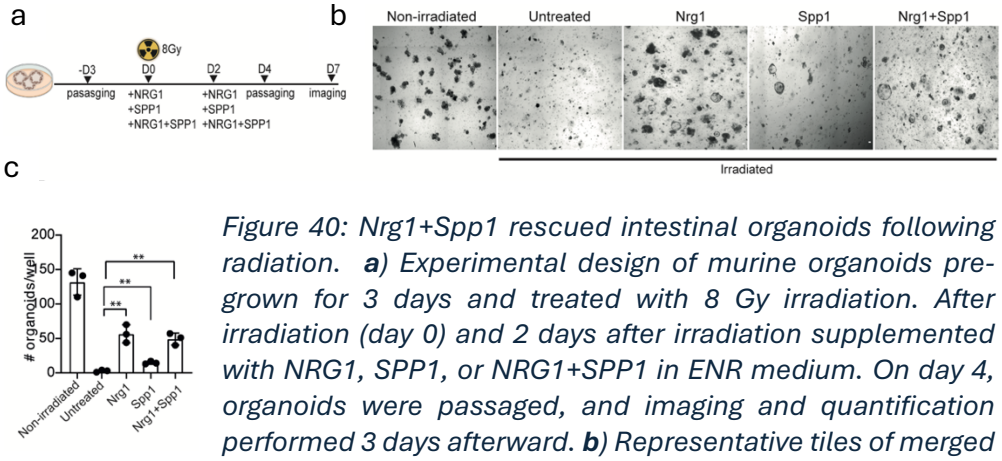

Figure 40: Nrg1+Spp1 rescued intestinal organoids following radiation. ***a****) Experimental design of murine organoids pre-grown for 3 days and treated with 8 Gy irradiation. After irradiation (day 0) and 2 days after irradiation supplemented with NRG1, SPP1, or NRG1+SPP1 in ENR medium. On day 4, organoids were passaged, and imaging and quantification performed 3 days afterward.* ***b****) Representative tiles of merged brightfield images of organoids; control (unirradiated and untreated), untreated (irradiated but not treated) and NRG1, SPP1 and NRG1+SPP1(irradiated and treated respectively). Scale bar 100 µm.* ***c****) quantification of the number of organoids in each well. (n=3 wells; unpaired t test **p < 0.01)*

To validate these results *in vivo* and to test whether these factors can restore the epithelial proliferation lost due to injury and macrophage ablation, we irradiated mice, followed by CD11c cell ablation. Mice were subsequently intraperitoneally injected with NRG1, SPP1, or a combined NRG1 and SPP1 treatment for three days. On day 5 post irradiation 1h before small intestine collection, mice were injected with EdU (Figure 41a). The number of EdU+ crypts increased in all treated groups compared to untreated control although it was not statistically significant

for NRG1 and NRG1+SPP1 treated group because of high deviation (Figure 41b and c). Interestingly, although the SPP1 treatment resulted in a significantly higher number of EdU+ crypts, the overall number of EdU+ cells per crypt was similar to untreated group. In contrast, both the NRG1 and NRG1+SPP1 groups demonstrated a statistically significant increase in EdU+ cells per crypt relative to untreated control resulting to larger crypts (Figure 41d). This further support different roles for nrg1 and spp1 in intestinal regeneration/repair with the nrg1 promoting processes like dedifferentiation and proliferation and spp1 pathways related to stemness.

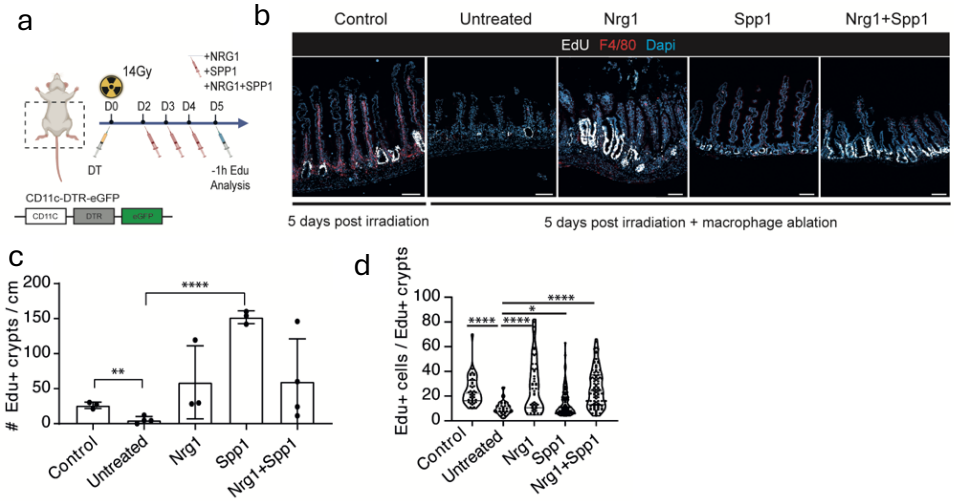

Figure 41:In vivo Nrg1+Spp1 treatment following radiation and macrophage ablation. **a**) Experimental design of induction protocol for deletion of CD11c+ cells followed by radiation injury. Mice were irradiated and subsequently injected with DT to ablate macrophages. At 2-, 3- and 4dpi mice were injected with NRG1, SPP1 or NRG1+SPP1. At 5dpi, mice injected with EdU and 1h after small intestines were collected. **b**) Detection of EdU, F4/80 and DAPI in tissue section from small intestine. scale bar 50 μm. **c**) Quantification of the number of EdU+ crypts per cm, 1 h after EdU labeling. (Each dot represents a mouse at the indicated group; unpaired t test; $**p < 0.01$, $***p < 0.001$ and $****$ $p < 0.0001$. **d**) Quantification of the number of EdU+ cells per crypt, 1 h after EdU labeling.

(control: 40 crypts, untreated: 28 crypts, Nrg1: 50 crypts, Spp1: 82 crypts Nrg1+Spp1: 80 crypts; unpaired t test; **p < 0.01, ***p <0.001 and **** p <0.0001).

Collectively, upon injury, macrophages are massively recruited to the ISC compartment acting as temporary niche for the dedifferentiating epithelial cells by secreting 2 critical factors that instruct cell fate. The secretion of NRG1 induces the activation of the regenerative genetic program that drives the process of regeneration and SPP1 promotes the acquisition of the ISCs transcriptional traits (Figure 42). These results underscore a critical role of macrophages beyond their involvement in the innate immune response and demonstrate they are indispensable to orchestrate the regenerative process.

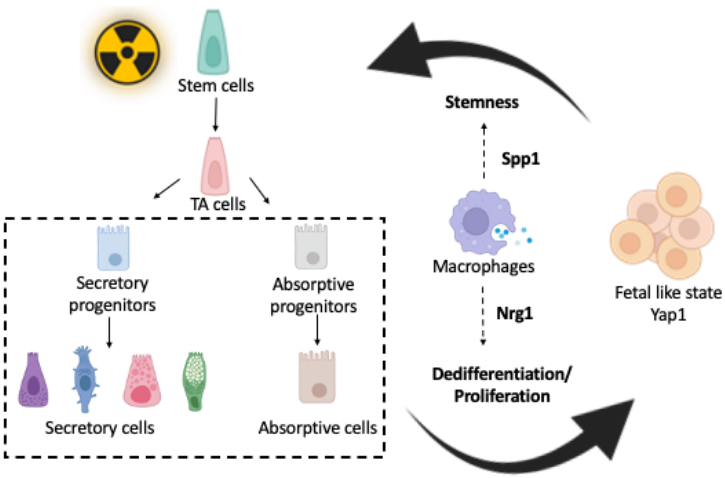

Figure 42: Graphical abstract. Following abdominal radiation injury, there is a significant loss of intestinal stem cells. However, progenitor and differentiated epithelial cells can de-differentiate and acquire a more fetal-like state, characterized by the activation of the YAP pathway. Concurrently, macrophages are massively recruited to the injured small intestine, expressing markers such as NRG1, among others, which promote the de-differentiation and proliferation

of epithelial cells. Additionally, a subset of macrophages expresses factors like SPP1, which facilitate the transition of epithelial cells from a fetal-like state to a more stem cell-like fate, supporting tissue repair.

4.6 Human macrophages induce changes in cell fate trajectory in human organoids.

In order to develop therapies that improve the quality of life of cancer patients and survivors that suffer the intestinal side-effects of radiotherapy, it is relevant to know if the mechanisms we identified in mice – demonstrating that macrophages are able to orchestrate the intestinal regenerative process – are conserved in humans. For this reason, we established 4 human intestinal organoid lines from the healthy ileum of patients that were subjected to a hemicolectomy. Next, we polarized human macrophages derived from purified CD14+ peripheral blood monocytes (Lonza, cat# ZW-400C) *in vitro*, towards pro-inflammatory macrophages and towards anti-inflammatory macrophages, using IFN-γ/LPS and IL-4, respectively (Figure 43a). Subsequently, polarized macrophages were embedded in Matrigel with the 4 multiplexed organoid lines. After 3 days in culture, cells were encapsulated to perform scRNA-seq (Figure 43b). UMAP visualization allowed the identification of 6 clusters (Figure 44a). Cluster 5 was positive for the CD45 immune cell marker, indicating macrophage contamination and was subsequently removed from the analysis (Figure 44b).

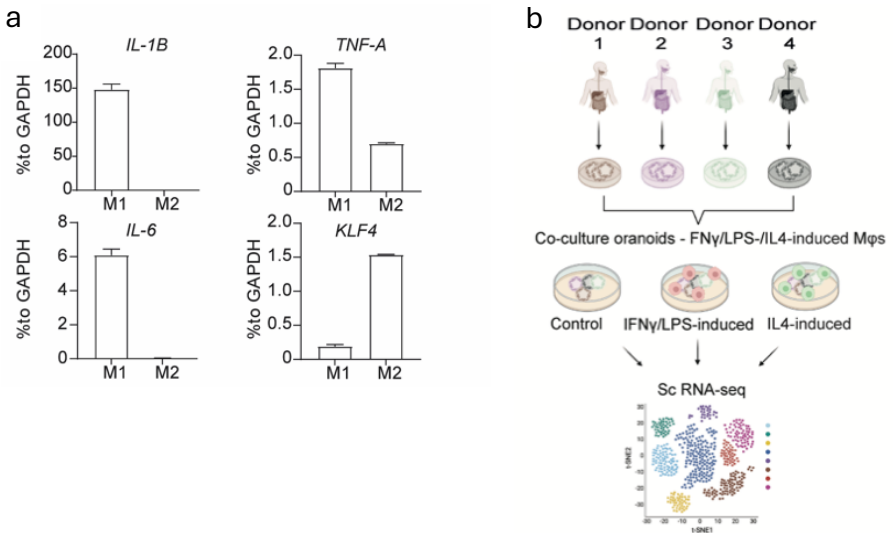

*Figure 43: Human macrophages polarization. **a**) qRT-PCR analysis of pro-inflammatory genes (Il-b, Il-6 and tnf-a) and anti-inflammatory gene (klf4) after the activation of macrophages toward to IFN-γ/LPS-induced and IL4-induced macrophages. **b**) Schematic of experimental degn of co-culture of human intestinal organoids with IFN-γ/LPS-induced or IL4-induced macrophages. 4 organoid lines from healthy ileum from patients that were subjected to a hemicolectomy were generated and subsequently multiplexed in the same culture. Purified CD14 peripheral blood monocytes were polarized in vitro towards IFN-γ/LPS-induced proinflammatory and towards IL4-induced macrophages using LPS, IFNγ and IL-4, respectively. Subsequently polarized macrophages were embedded in Matrigel with the multiplexed organoid lines. Co-cultures and control (only organoids) were collected for scRNA-seq on day 3.*

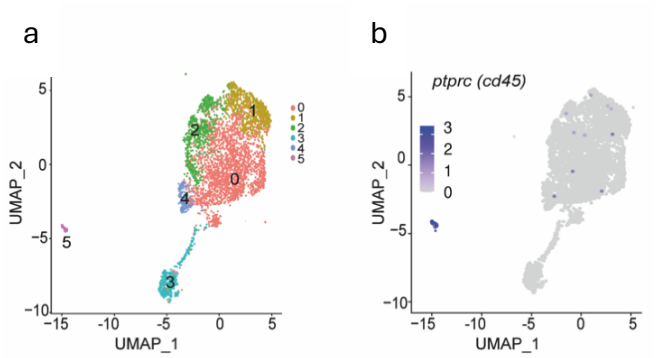

Figure 44: ScRNA-seq of human cocultures. ***a****) UMAP projection of all cells from scRNA-seq of co-cultures. (Number of cells after filtering in each condition was Control: 1543; IFN-γ/LPS-induced macrophages coculture: 1226; IL4-induced macrophages coculture: 947)* ***b****) The expression of CD45 marker specifically in the cluster 5 indicating the presence of immune cells.*

The 4 organoid lines were demultiplexed in silico [177], showing representation in different clusters (Figure 45a). It was previously reported that portions of transcriptomic signatures may be biased by cellular stress [203] , due to dissociation [204]. Therefore, we overlayed a stress gene signature on our data (*fos, jun, egr1, ubc, hspa1b, btg2, ier2* and *id3*) *[204, 205]* and detected elevated average expression in Cluster 3 (Figure 45b). Consequently, this cluster was excluded from the analysis. For the characterization of the cell clusters were used published gene signature indicating intestinal stem cells [12], proliferation [179], zonation signatures along the crypt-villus axis [69] and intermediate enterocytes [157] (Figure 46a). Therefore resulting in a UMAP with four clusters corresponding to proliferative stem cells (*smoc2*$^{+}$*, mki67*$^{+}$ and *top2a*$^{+}$), stem cells (*smoc2*$^{+}$*, mki67*^{low} and *top2a*^{low}) progenitors (*smoc2*$^{-}$*, mki67*$^{-}$ and *top2a*$^{-}$*, krt20*^{low}) and differentiated cells (*krt20*$^{+}$*, fabp1*$^{+}$) (Figure 46b and c).

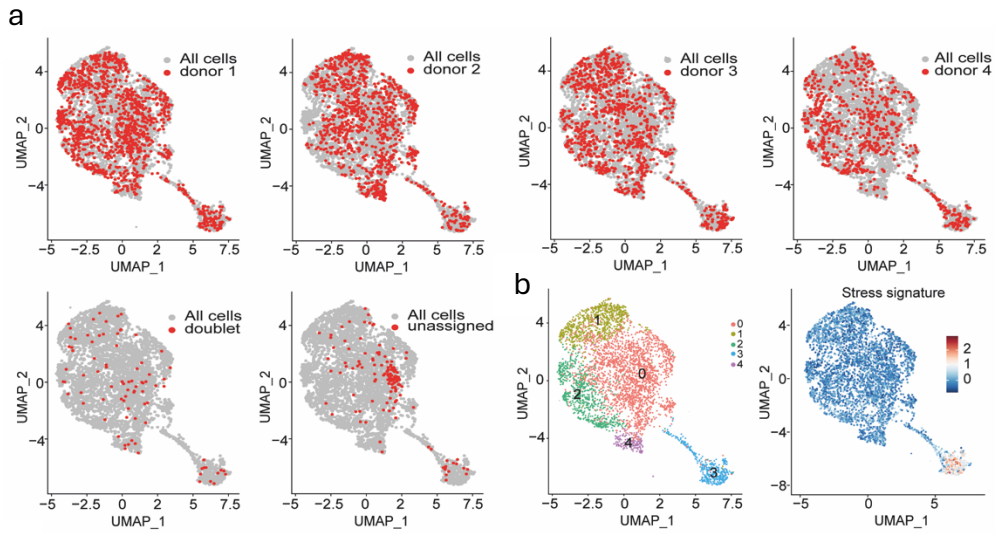

Figure 45: Characterization of ScRNA-seq of human cocultures. ***a****) Number of cells assigned to each donor by Vireo analysis.* ***b****) UMAP of scRNA-seq after sub clustering the epithelial cells resulted in the identification of five cell clusters and the expression of published gene signatures associated with stress in the cluster 3.*

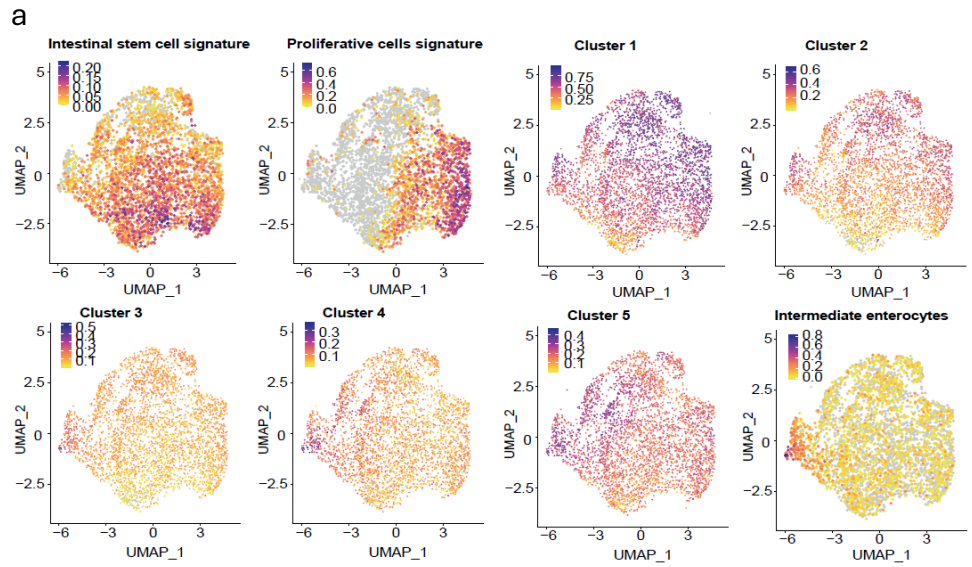

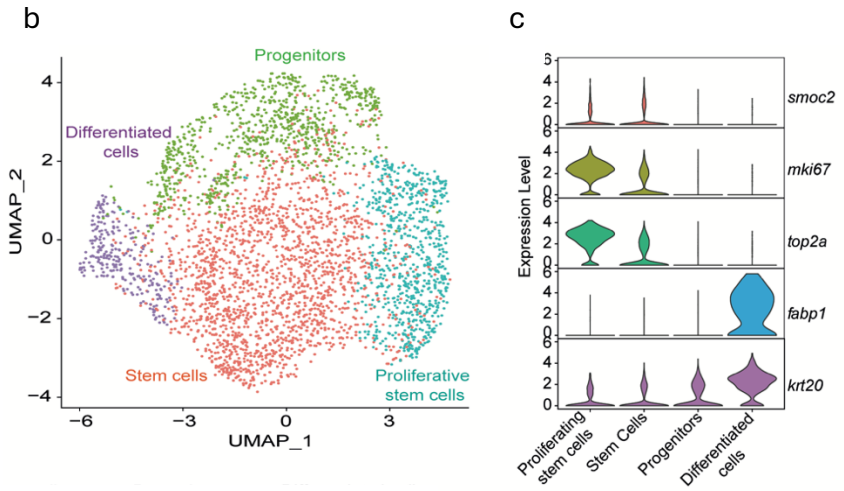

Figure 46: Characterization of ScRNA-seq of human cocultures. ***a****)UMAP of scRNA-seq of the epithelial cells after the removal of cluster 3 from the analysis show the expression of published gene signatures associated with intestinal stem cell [12], proliferative cells [179] zonation signature along the crypt-villus axis with cluster 1 be expressed close to the bottom part of the villi compartment and cluster 5 be expressed near the tip of the villi [69] and intermediated enterocytes [157].* ***b****) UMAP of scRNA-seq of human intestinal organoids co-cultures showing the different cell-type clusters. Stem cells, proliferative stem cells, progenitors and differentiated cells.* ***c****) Violin plot showing expression of known marker genes Smoc2, MKi67, Top2a, Fabp1 and Krt20 to distinguish the different cell-type clusters.*

Cluster distribution analysis with scCODA [178] revealed that IFN-γ/LPS-induced human macrophages inhibit differentiation, resulting in a significantly decreased enterocyte cluster and a significantly increased progenitor cluster when compared to the control (Figure 47a). The same tendency was observed with IL4-induced macrophages co-cultures. Progenitors have been proposed to provide a new source for ISCs through dedifferentiation during the process of intestinal regeneration [206]. Consequently, we posited that if macrophages are inducing the process of regeneration via dedifferentiation of progenitors, we should identify changes in cell fate trajectories in the scRNA-seq dataset.

Using RNA velocity cell trajectory analysis [148], we inferred that during steady state proliferative stem cells are the source of the stem cells, progenitors, and differentiated cells, as expected (Figure 47b). The cell trajectory in IFN-γ/LPS-induced macrophages coculture was similar to control. Interestingly when organoids were co-cultured with IL4-induced macrophages, progenitors became the predicted source of the other cell types (Figure 47b). Additionally, CellRank [149] confirmed these findings, predicting similar changes in origin and terminal states, imposed by IL4-induced macrophages (Figure 47c).

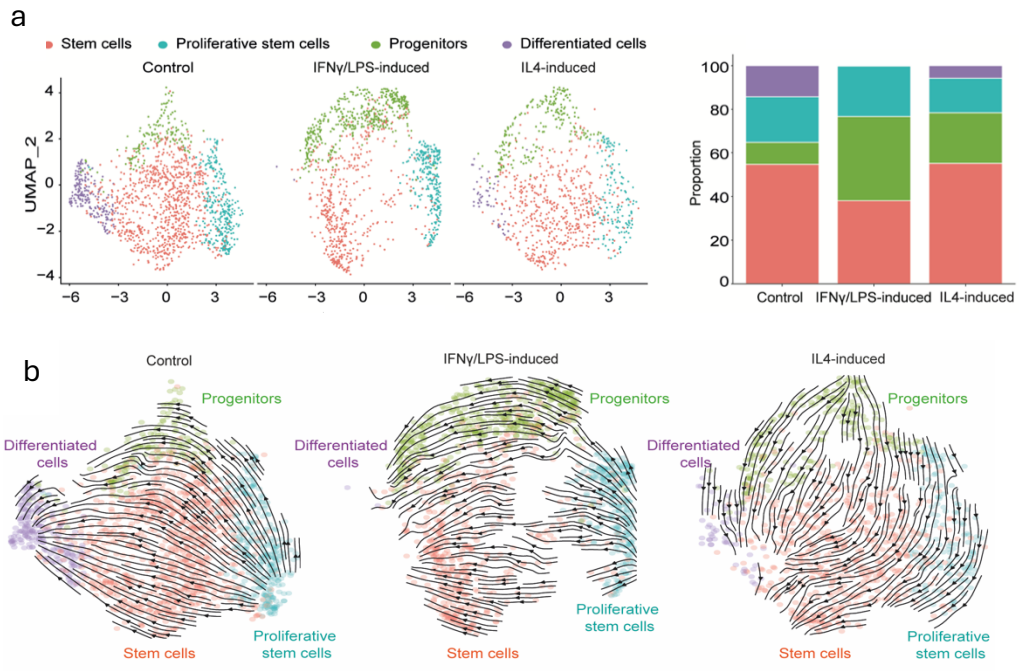

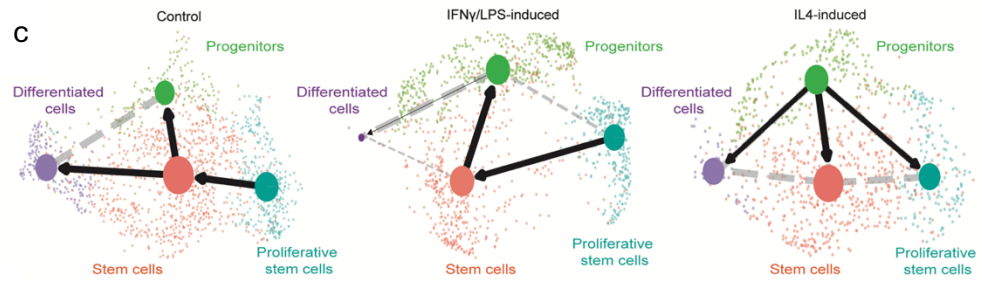

Figure 47: IFN-γ/LPS-induced macrophages inhibit the dedifferentiation and IL4-induced macrophages change the cell trajectory. ***a****) ScCODA analysis showing significant reduction of differentiated cluster (FDR < 0.05, in 10/10 ran tests) and increased progenitor cluster in IFN-γ/LPS-induced (FDR < 0.05, in 9/10 run tests). The same tendency in the reduction of differentiated cluster is observed also in IL4-induced co-culture (FDR < 0.05, in 5/10 ran tests).* ***b****) RNA velocity cell trajectory analysis identifies that in IL4-induced macrophage co-culture, the progenitor cluster is the source of the other cell lineages* ***c****) PAGA analysis shows the cell fate directionality.*

To assess the functional human macrophage relevance and their ability to promote human organoid recovery after injury, we irradiated 4 human intestinal organoid lines, multiplexed together and co-cultured them with IFN-γ/LPS-induced or IL4-induced macrophages for three days, followed by passaging. Three days after passaging, we quantified the number of surviving organoids (Figure 48a). Interestingly, both IFN-γ/LPS-induced and IL4-induced macrophages significantly enhanced organoid survival after radiation compared to untreated control (Figure 48b and c). Collectively, these results highlight the therapeutic potential of macrophages in promoting tissue repair after injury.

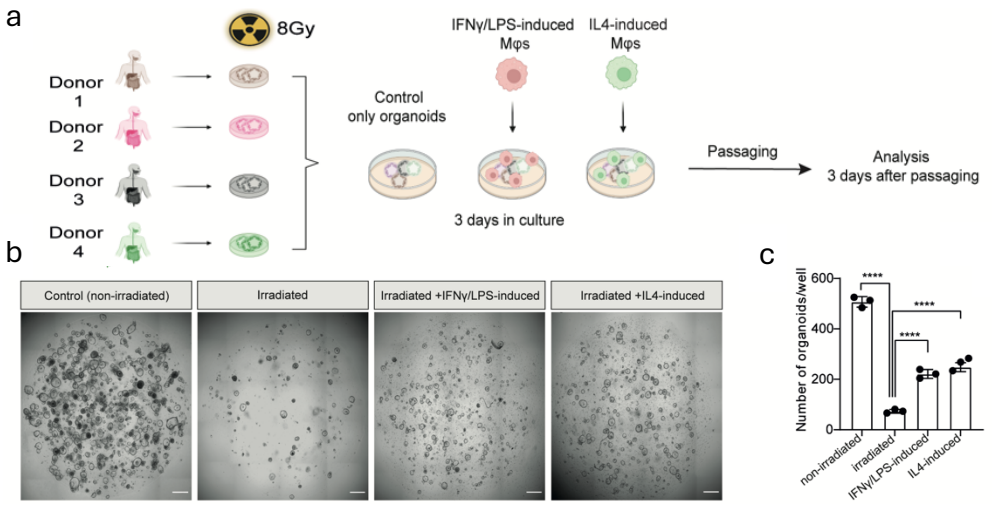

*Figure 48: Human polarized macrophages enhanced organoid survival after radiation. **a**) Schematic representation of experimental design of co-culture of human irradiated intestinal organoids with IFN-γ/LPS-induced or IL4-induced macrophages (Mϕs). 4 organoid lines (as described in figure 43b) were irradiated with 8Gy and subsequently multiplexed in the same culture with polarized IFN-γ/LPS-induced or IL4-induced macrophages for 3 days. On day 4, passaging of organoids was performed and 3 days later imaging and quantification. **b**) Representative tiles of merged brightfield images of organoids. Scale bar 500 µm. **c**) Quantification of the number of organoids in each well. (n=3 wells; unpaired t test; **** p <0.0001).*

Collectively, these results indicate that human polarized macrophages are able to inhibit intestinal differentiation and to revert the inferred cell trajectory in the human intestinal organoids (Figure 49).

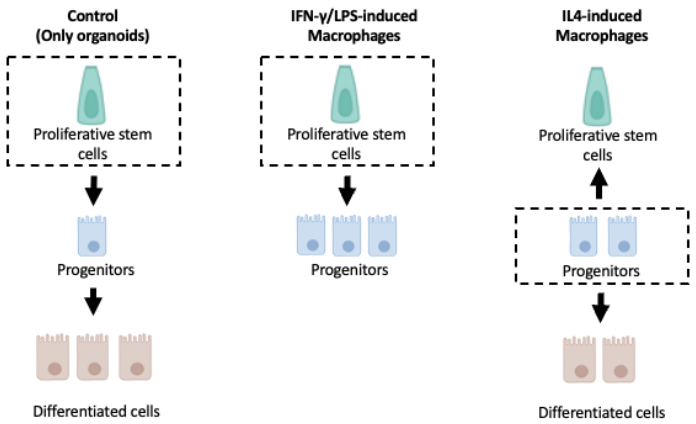

Figure 49: Graphical abstract of human experiments. IFN-γ/LPS-induced macrophages inhibit the differentiation resulting in an increased number of progenitors cells and IL4-induced macrophages shift the cell trajectory establishing progenitors as the new origin of intestinal stem cells. Dash box indicates the origin of the cells.

5 Discussion

The study of radiation-induced enteritis has historically been challenging due to the lack of physiologically relevant models. Standard whole-body irradiation at 8-10 Gy often results in hematological death by day 8, which limits the ability to investigate the disease during the healing phase or to study hematopoietic cells. In our system, we overcome this challenge by delivering 14 Gy exclusively to the posterior half of the mice, allowing them to recover from radiation-induced enteritis over two weeks. This approach preserves the hematopoietic system in non-irradiated bones, enabling the study of immune-epithelial crosstalk during tissue injury and repair in a more relevant physiological context. Although our dosing is higher than typical fractionated human regimens (1.8-2 Gy), the observed histopathological effects, such as villus shortening and degenerative crypts, are consistent across species, including mice, non-human primates, and humans [71, 75]. Thus, reinforcing the relevance of our model. Furthermore, while preclinical and clinical radiotherapy differ in energy levels and delivery systems[207, 208], the use of a 6 MeV photon beam from a linear accelerator (LINAC) in our study closely mimics human radiotherapy, enhancing the translational value of our findings.

Although the role of intestinal macrophages as key players of the gut immune system, regulation of gut motility and secretion [209] is well established, their contribution to the intestinal epithelial regeneration process is poorly characterized. Previous studies have mostly focused on observation and description of the phenotype and morphology of macrophages, as well as their role as regulators of intestinal inflammation and resolution [210], in the regulation of epithelial differentiation and homeostasis [210-213]. In the last decade, several

studies found that macrophages play a role in regulating homeostasis [213] and promoting the regeneration of different tissues, such as the heart, liver, skin, kidney, muscle, and nerve [141, 214-218] and provided evidence that macrophages participate in intestinal regeneration [219-222]. However, the mechanisms by which macrophages coordinate regeneration at the cellular and molecular level, their potential contribution to fetal-like reprogramming, and whether these processes are conserved in human, remain poorly understood. Here, using scRNA-seq combined with quantitative lineage tracing, *in vivo* ablation of macrophages and murine and human co-cultures of macrophages and intestinal organoids, we reveal that macrophages crosstalk with intestinal epithelial cells to i) orchestrate the regenerative program, ii) induce epithelial proliferation and iii) promote the *de novo* acquisition of the stem cell fate.

We demonstrate that the depletion of macrophages upon radiation impairs the process of intestinal dedifferentiation and proliferation and leads to a failure of epithelial recovery and regeneration. Performing scRNA-seq of epithelial cells, combined with fluorescent lineage tracing of $Krt20^{+}$ cells and EdU chase proliferation studies following radiation and macrophage ablation, we demonstrate that intestinal cell plasticity, dedifferentiation and proliferation of epithelial cells is impaired in the absence of macrophages. Using scRNA-seq of intestinal macrophages during homeostasis and after injury, we identify remarkable changes in their transcriptome including the significant overexpression of *nrg1* and *spp1*. This is in agreement with previous studies that have proposed macrophages as a source of intestinal microenvironment signals [101,

107, 223, 224], although they did not examine the precise role of macrophages on epithelial cells. We subsequently cultured intestinal organoids with NRG1 and SPP1 to demonstrate that those proteins promote the regenerative genetic program and simultaneously promote the acquisition of ISC traits in intestinal epithelial cells. This is in agreement with previous studies showing that NRG1 robustly stimulates proliferation in crypts, in part through elevated and sustained activation of mitogen-activated protein kinase (MAPK) and AKT [124, 199]. Furthermore, SPP1 has been linked to multiple signaling pathways, crucial for intestinal regeneration, such as the WNT, integrin, PI3K/AKT, MAPK, and NF-κB [196-198]. A role for SPP1 in intestinal regeneration is also aligned with many studies that have proposed SPP1 as a driver of regeneration and repair in heart, muscle and skin [225-227]. Interestingly, treatment of our organoids with SPP1 resulted in elevation of the WNT signaling pathway signature. This is noteworthy, considering that WNT signaling is critical for the maintenance of the intestinal epithelial stem cell compartment [201]. Therefore, following abdominal radiation injury, there is a significant loss of intestinal stem cells. However, progenitor and differentiated epithelial cells can de-differentiate and acquire a more fetal-like state, characterized by the activation of the YAP pathway. Concurrently, macrophages are massively recruited to the injured small intestine, expressing markers such as NRG1, among others, which promote the de-differentiation and proliferation of epithelial cells. Additionally, a subset of macrophages expresses factors like SPP1, which facilitate the transition of epithelial cells from a fetal-like state to a more stem cell-like fate, supporting tissue regeneration

To develop therapies that enhance the quality of life for cancer patients and survivors suffering from radiotherapy side effects, it is imperative to determine whether the regenerative mechanisms that we identified in mice, specifically the coordination by macrophages, is conserved in humans as well. It has been suggested that progenitor cells can serve as a novel source for intestinal stem cells (ISCs) during intestinal regeneration through a dedifferentiation process, as demonstrated by previous study [206]. Here we show with co-cultures experiments involving human intestinal organoids and polarized macrophages, that macrophages are indeed able to promote changes in organoid differentiation and in the inferred cell differentiation trajectory. Firstly, IFN-γ/LPS-induced macrophages inhibit differentiation, resulting in an augmented number of progenitors cells. Secondly, IL4-induced macrophages redirect cell trajectories, establishing progenitors as the new origin of ISCs. Moreover, macrophages enhance human organoid recovery in response to radiation injury. These findings enhance our understanding of intestinal regeneration, thereby laying the groundwork for novel regenerative therapies and interventions for intestinal diseases [228, 229]. Furthermore, with immunotherapy emerging as a promising and potentially transformative approach to cancer treatment in recent years, the role of macrophages as a putative target is highly relevant [230]. Therefore, these findings have key implications in the development of immunotherapy aimed at targeting macrophages.

Although the majority of CD11c+ cells in the intestine are macrophages, a small subset of these cells does not express macrophage-specific markers. As a result, the CD11c-DTR-eGFP model cannot distinguish

between the roles of macrophages and non-macrophage CD11c+ cells. Other mouse models, such as CD11b-DTR [231], CD206-DTR, or MafbCre;Cx3cr1DTR [232], allow for conditional macrophage ablation. However, these models also have limitations, as no single marker exclusively identifies macrophages. Additionally, while we polarized macrophages into pro- and anti-inflammatory-like phenotypes *in vitro*, macrophages exhibit significant plasticity and functional diversity *in vivo*. This adaptability enables them to respond dynamically to various signals in their microenvironment, making it difficult to classify them as pro- or anti-inflammatory.

Using radiation as an injury model introduces further complexity. It remains unclear whether transcriptional changes in macrophages result directly from radiation exposure or from the effects of the injured intestinal niche. Nevertheless, data (Figure 15) suggest that non-irradiated femur bones remain unaffected by radiation. Additionally, it is uncertain whether macrophages recruited to the injured intestine originate from the proliferation of tissue-resident macrophages or infiltration from other sources. Evidence (Figure 33h) indicates that most macrophages may be infiltrated, with a smaller proportion being tissue-resident. Employing a macrophage-tracking system, such as the CXCR4-inducible system [233], could provide valuable insights into the origin of macrophages following injury. Finally, macrophages are not the sole source of NRG1 and SPP1, as been expressed from other cell types. Moreover, additional markers may also contribute to processes related to intestinal regeneration, proliferation, or stem cell maintenance. Further characterization of single-cell RNA sequencing of macrophages during

both homeostasis and post-irradiation conditions would greatly enhance our understanding of their contributions to these processes.

In summary, we have conducted a comprehensive characterization of intestinal macrophages in relation to radiation-induced intestinal injury. Our findings reveal that upon injury, macrophages are massively recruited to the ISC compartment acting as temporary niche for the dedifferentiating epithelial cells by secreting 2 factors among others that instruct cell fate. The secretion of NRG1 induces the activation of the regenerative genetic program that drives the process of regeneration and SPP1 promotes the acquisition of the ISCs transcriptional traits. Our results underscore a critical role of macrophages beyond their involvement in the innate immune response and demonstrate they are indispensable to orchestrate the regenerative process. A deeper understanding of the factors that drive macrophage specialization, how this change following irradiation, and which alterations occur in the surrounding niche, will be vital. Such knowledge will inform therapeutic strategies targeting macrophage responses to irradiation damage, offering potential treatments for conditions marked by injury and epithelial deficiency such as necrotizing enterocolitis, ulcerative colitis, Crohn’s disease, and short gut syndrome.

6 Conclusions

Macrophages are indispensable to drive intestinal regeneration *in vivo*.

- Upon intestinal injury, macrophages are massively recruited along the entire crypt-villus axis and closely interact with hyperplastic crypts.
- Mice cannot survive abdominal radiation injury following macrophage ablation.
- The absence of macrophages upon radiation injury impairs the processes of dedifferentiation, regeneration, and proliferation.
- Single-cell RNA sequencing of macrophages revealed significant transcriptional differences compared to homeostatic macrophages, with the ¨injured¨ macrophages expressing factors related to intestinal regeneration and proliferation.
- Injury leads to elevated levels of SPP1 and NRG1 in the small intestine, particularly around hyperproliferative crypts.
  Macrophage ablation reduces the expression of NRG1 and SPP1 upon injury.

NRG1 and SPP1 induce the regenerative genetic program and promote the stem cell fate.

- NRG1 is involved in processes related to regeneration and proliferation, while SPP1 is more associated with stemness.
- Both NRG1 and SPP1 can rescue intestinal organoids after radiation.
- NRG1 can restore proliferation disrupted by injury and macrophage ablation, while SPP1 can sustain the crypt compartment.
- In SPP1 knockout models, there is a reduction in the intestinal stem cell signature upon injury compared to wild-type mice.

Polarized macrophages crosstalk with intestinal epithelial cells and induce the regenerative program *in vitro*.

- Polarized macrophages with pro- and anti-inflammatory phenotype interacting with epithelial cells and induce a spherical, fetal-like morphology in adult intestinal organoids, promoting a regenerative program *in vitro*.

Human macrophages induce changes in cell fate trajectory in human organoids.

- Human pro-inflammatory macrophages inhibit differentiation in human intestinal organoids, resulting in increased progenitor numbers.
- Human anti-inflammatory macrophages shift cell trajectories, establishing progenitors as the new origin of intestinal stem cells.
- Both human pro- and anti-inflammatory macrophages can rescue human intestinal organoids following radiation.

7 Graphical abstract

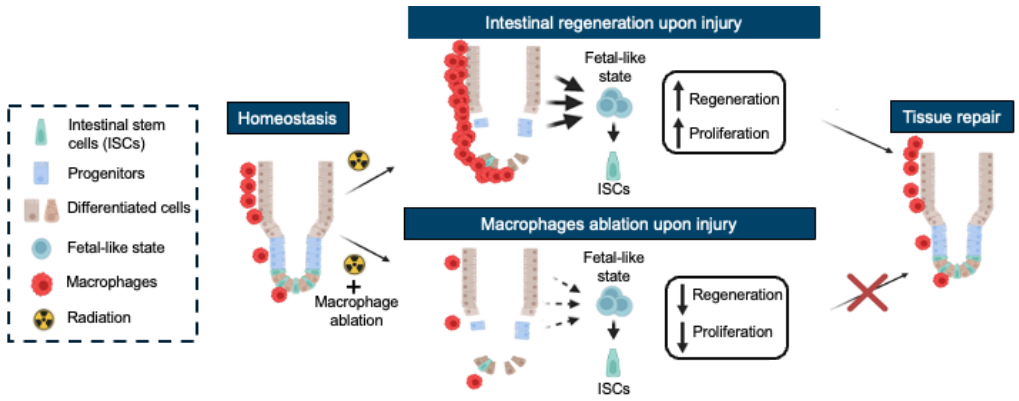

Figure 50: General graphical abstract of thesis. Upon radiation injury, the epithelium is transiently reprogrammed into a fetal-like primitive state. in addition, macrophages are massively recruit to the small intestine, appearing around the hyperplastic regenerative crypts and closely associating with the epithelium promoting intestinal regeneration and proliferation. The activation of this program resulting in the dedifferentiation of progenitors and committed cells to a fetal-like state in order to repopulate the ISCs that been loss during radiation. However, macrophages ablation impairs these processes upon injury reducing the proliferative and regenerative capacity of the intestine.

8 Bibliography

1. Moog, F., *The lining of the small intestine*. Sci Am, 1981. **245**(5): p. 154-8, 160, 162 et passiom.
2. Helander, H.F. and L. Fandriks, *Surface area of the digestive tract - revisited*. Scand J Gastroenterol, 2014. **49**(6): p. 681-9.
3. Collins, J.T., A. Nguyen, and M. Badireddy, *Anatomy, Abdomen and Pelvis, Small Intestine*, in *StatPearls*. 2024: Treasure Island (FL).
4. Johansson, M.E., H. Sjovall, and G.C. Hansson, *The gastrointestinal mucus system in health and disease*. Nat Rev Gastroenterol Hepatol, 2013. **10**(6): p. 352-61.
5. Crosnier, C., D. Stamataki, and J. Lewis, *Organizing cell renewal in the intestine: stem cells, signals and combinatorial control*. Nat Rev Genet, 2006. **7**(5): p. 349-59.
6. van der Flier, L.G. and H. Clevers, *Stem cells, self-renewal, and differentiation in the intestinal epithelium*. Annu Rev Physiol, 2009. **71**: p. 241-60.
7. Lopez-Garcia, C., et al., *Intestinal stem cell replacement follows a pattern of neutral drift*. Science, 2010. **330**(6005): p. 822-5.
8. Snippert, H.J., et al., *Intestinal crypt homeostasis results from neutral competition between symmetrically dividing Lgr5 stem cells*. Cell, 2010. **143**(1): p. 134-44.
9. Cheng, H. and C.P. Leblond, *Origin, differentiation and renewal of the four main epithelial cell types in the mouse small intestine. V. Unitarian Theory of the origin of the four epithelial cell types*. Am J Anat, 1974. **141**(4): p. 537-61.
10. Bjerknes, M. and H. Cheng, *Clonal analysis of mouse intestinal epithelial progenitors*. Gastroenterology, 1999. **116**(1): p. 7-14.
11. van der Flier, L.G., et al., *OLFM4 is a robust marker for stem cells in human intestine and marks a subset of colorectal cancer cells*. Gastroenterology, 2009. **137**(1): p. 15-7.
12. Munoz, J., et al., *The Lgr5 intestinal stem cell signature: robust expression of proposed quiescent '+4' cell markers*. EMBO J, 2012. **31**(14): p. 3079-91.
13. Tian, H., et al., *A reserve stem cell population in small intestine renders Lgr5-positive cells dispensable*. Nature, 2011. **478**(7368): p. 255-9.
14. Jadhav, U., et al., *Dynamic Reorganization of Chromatin Accessibility Signatures during Dedifferentiation of Secretory*

Precursors into Lgr5+ Intestinal Stem Cells. Cell Stem Cell, 2017. **21**(1): p. 65-77 e5.
15. Buczacki, S.J., et al., *Intestinal label-retaining cells are secretory precursors expressing Lgr5*. Nature, 2013. **495**(7439): p. 65-9.
16. Ritsma, L., et al., *Intestinal crypt homeostasis revealed at single-stem-cell level by in vivo live imaging*. Nature, 2014. **507**(7492): p. 362-365.
17. Capdevila, C., et al., *Time-resolved fate mapping identifies the intestinal upper crypt zone as an origin of Lgr5+ crypt base columnar cells*. Cell, 2024. **187**(12): p. 3039-3055 e14.
18. Baulies, A., N. Angelis, and V.S.W. Li, *Hallmarks of intestinal stem cells*. Development, 2020. **147**(15).
19. Farin, H.F., et al., *Visualization of a short-range Wnt gradient in the intestinal stem-cell niche*. Nature, 2016. **530**(7590): p. 340-3.
20. Clevers, H., *The intestinal crypt, a prototype stem cell compartment*. Cell, 2013. **154**(2): p. 274-84.
21. Kabiri, Z., et al., *Stroma provides an intestinal stem cell niche in the absence of epithelial Wnts*. Development, 2014. **141**(11): p. 2206-15.
22. Gregorieff, A., et al., *Expression pattern of Wnt signaling components in the adult intestine*. Gastroenterology, 2005. **129**(2): p. 626-38.
23. Farin, H.F., J.H. Van Es, and H. Clevers, *Redundant sources of Wnt regulate intestinal stem cells and promote formation of Paneth cells*. Gastroenterology, 2012. **143**(6): p. 1518-1529 e7.
24. Koo, B.K., et al., *Tumour suppressor RNF43 is a stem-cell E3 ligase that induces endocytosis of Wnt receptors*. Nature, 2012. **488**(7413): p. 665-9.
25. Degirmenci, B., et al., *GLI1-expressing mesenchymal cells form the essential Wnt-secreting niche for colon stem cells*. Nature, 2018. **558**(7710): p. 449-453.
26. Valenta, T., et al., *Wnt Ligands Secreted by Subepithelial Mesenchymal Cells Are Essential for the Survival of Intestinal Stem Cells and Gut Homeostasis*. Cell Rep, 2016. **15**(5): p. 911-918.
27. Shoshkes-Carmel, M., et al., *Author Correction: Subepithelial telocytes are an important source of Wnts that supports intestinal crypts*. Nature, 2018. **560**(7718): p. E29.

28. Czerwinski, M., N.F. Shroyer, and J.R. Spence, *Chapter 7 - WNT Signaling in the Intestine: Development, Homeostasis, Disease*, in *Physiology of the Gastrointestinal Tract (Sixth Edition)*, H.M. Said, Editor. 2018, Academic Press. p. 185-196.
29. Stamataki, D., et al., *Delta1 expression, cell cycle exit, and commitment to a specific secretory fate coincide within a few hours in the mouse intestinal stem cell system*. PLoS One, 2011. **6**(9): p. e24484.
30. Kim, T.H., et al., *Broadly permissive intestinal chromatin underlies lateral inhibition and cell plasticity*. Nature, 2014. **506**(7489): p. 511-5.
31. Shroyer, N.F., et al., *Intestine-specific ablation of mouse atonal homolog 1 (Math1) reveals a role in cellular homeostasis*. Gastroenterology, 2007. **132**(7): p. 2478-88.
32. Takahashi, T. and A. Shiraishi, *Stem Cell Signaling Pathways in the Small Intestine*. Int J Mol Sci, 2020. **21**(6).
33. Demitrack, E.S. and L.C. Samuelson, *Notch regulation of gastrointestinal stem cells*. J Physiol, 2016. **594**(17): p. 4791-803.
34. van Es, J.H., et al., *Notch/gamma-secretase inhibition turns proliferative cells in intestinal crypts and adenomas into goblet cells*. Nature, 2005. **435**(7044): p. 959-63.
35. Fre, S., et al., *Notch signals control the fate of immature progenitor cells in the intestine*. Nature, 2005. **435**(7044): p. 964-8.
36. Carulli, A.J., et al., *Notch receptor regulation of intestinal stem cell homeostasis and crypt regeneration*. Dev Biol, 2015. **402**(1): p. 98-108.
37. Zhang, Y. and J. Que, *BMP Signaling in Development, Stem Cells, and Diseases of the Gastrointestinal Tract*. Annu Rev Physiol, 2020. **82**: p. 251-273.
38. He, X.C., et al., *BMP signaling inhibits intestinal stem cell self-renewal through suppression of Wnt-beta-catenin signaling*. Nat Genet, 2004. **36**(10): p. 1117-21.
39. Kosinski, C., et al., *Gene expression patterns of human colon tops and basal crypts and BMP antagonists as intestinal stem cell niche factors*. Proc Natl Acad Sci U S A, 2007. **104**(39): p. 15418-23.
40. Davis, H., et al., *Aberrant epithelial GREM1 expression initiates colonic tumorigenesis from cells outside the stem cell niche*. Nat Med, 2015. **21**(1): p. 62-70.

41. Sato, T., et al., *Single Lgr5 stem cells build crypt-villus structures in vitro without a mesenchymal niche*. Nature, 2009. **459**(7244): p. 262-5.
42. Kosinski, C., et al., *Indian hedgehog regulates intestinal stem cell fate through epithelial-mesenchymal interactions during development*. Gastroenterology, 2010. **139**(3): p. 893-903.
43. Walton, K.D. and D.L. Gumucio, *Hedgehog Signaling in Intestinal Development and Homeostasis*. Annu Rev Physiol, 2021. **83**: p. 359-380.
44. Rohatgi, R., L. Milenkovic, and M.P. Scott, *Patched1 regulates hedgehog signaling at the primary cilium*. Science, 2007. **317**(5836): p. 372-6.
45. Madison, B.B., et al., *Epithelial hedgehog signals pattern the intestinal crypt-villus axis*. Development, 2005. **132**(2): p. 279-89.
46. van Es, J.H., et al., *Wnt signalling induces maturation of Paneth cells in intestinal crypts*. Nat Cell Biol, 2005. **7**(4): p. 381-6.
47. Durand, A., et al., *Functional intestinal stem cells after Paneth cell ablation induced by the loss of transcription factor Math1 (Atoh1)*. Proc Natl Acad Sci U S A, 2012. **109**(23): p. 8965-70.
48. Lueschow, S.R. and S.J. McElroy, *The Paneth Cell: The Curator and Defender of the Immature Small Intestine*. Front Immunol, 2020. **11**: p. 587.
49. Sato, T., et al., *Paneth cells constitute the niche for Lgr5 stem cells in intestinal crypts*. Nature, 2011. **469**(7330): p. 415-8.
50. Garabedian, E.M., et al., *Examining the role of Paneth cells in the small intestine by lineage ablation in transgenic mice*. J Biol Chem, 1997. **272**(38): p. 23729-40.
51. Mori-Akiyama, Y., et al., *SOX9 is required for the differentiation of paneth cells in the intestinal epithelium*. Gastroenterology, 2007. **133**(2): p. 539-46.
52. Gribble, F.M. and F. Reimann, *Function and mechanisms of enteroendocrine cells and gut hormones in metabolism*. Nat Rev Endocrinol, 2019. **15**(4): p. 226-237.
53. Sternini, C., L. Anselmi, and E. Rozengurt, *Enteroendocrine cells: a site of 'taste' in gastrointestinal chemosensing*. Curr Opin Endocrinol Diabetes Obes, 2008. **15**(1): p. 73-8.
54. Sanchez, J.G., J.R. Enriquez, and J.M. Wells, *Enteroendocrine cell differentiation and function in the intestine*. Curr Opin Endocrinol Diabetes Obes, 2022. **29**(2): p. 169-176.

55. Beumer, J., et al., *High-Resolution mRNA and Secretome Atlas of Human Enteroendocrine Cells*. Cell, 2020. **181**(6): p. 1291-1306 e19.
56. Beumer, J., et al., *Enteroendocrine cells switch hormone expression along the crypt-to-villus BMP signalling gradient*. Nat Cell Biol, 2018. **20**(8): p. 909-916.
57. van Es, J.H., et al., *Enteroendocrine and tuft cells support Lgr5 stem cells on Paneth cell depletion*. Proc Natl Acad Sci U S A, 2019. **116**(52): p. 26599-26605.
58. Kim, Y.S. and S.B. Ho, *Intestinal goblet cells and mucins in health and disease: recent insights and progress*. Curr Gastroenterol Rep, 2010. **12**(5): p. 319-30.
59. Beumer, J. and H. Clevers, *Cell fate specification and differentiation in the adult mammalian intestine*. Nat Rev Mol Cell Biol, 2021. **22**(1): p. 39-53.
60. Strugala, V., P.W. Dettmar, and J.P. Pearson, *Thickness and continuity of the adherent colonic mucus barrier in active and quiescent ulcerative colitis and Crohn's disease*. Int J Clin Pract, 2008. **62**(5): p. 762-9.
61. Gustafsson, J.K., et al., *Intestinal goblet cells sample and deliver lumenal antigens by regulated endocytic uptake and transcytosis*. Elife, 2021. **10**.
62. Knoop, K.A., et al., *Microbial sensing by goblet cells controls immune surveillance of luminal antigens in the colon*. Mucosal Immunol, 2015. **8**(1): p. 198-210.
63. McDonald, K.G., et al., *CCR6 promotes steady-state mononuclear phagocyte association with the intestinal epithelium, imprinting and immune surveillance*. Immunology, 2017. **152**(4): p. 613-627.
64. Bergstrom, K.S., et al., *Goblet Cell Derived RELM-beta Recruits CD4+ T Cells during Infectious Colitis to Promote Protective Intestinal Epithelial Cell Proliferation*. PLoS Pathog, 2015. **11**(8): p. e1005108.
65. Beumer, J., et al., *BMP gradient along the intestinal villus axis controls zonated enterocyte and goblet cell states*. Cell Rep, 2022. **38**(9): p. 110438.
66. von Moltke, J., et al., *Tuft-cell-derived IL-25 regulates an intestinal ILC2-epithelial response circuit*. Nature, 2016. **529**(7585): p. 221-5.

67. Mabbott, N.A., et al., *Microfold (M) cells: important immunosurveillance posts in the intestinal epithelium*. Mucosal Immunol, 2013. **6**(4): p. 666-77.
68. Knoop, K.A., et al., *RANKL is necessary and sufficient to initiate development of antigen-sampling M cells in the intestinal epithelium*. J Immunol, 2009. **183**(9): p. 5738-47.
69. Moor, A.E., et al., *Spatial Reconstruction of Single Enterocytes Uncovers Broad Zonation along the Intestinal Villus Axis*. Cell, 2018. **175**(4): p. 1156-1167 e15.
70. Calvo, F., et al., *Cancer Core Europe: A European cancer research alliance realizing a research infrastructure with critical mass and programmatic approach to cure cancer in the 21st century*. Eur J Cancer, 2018. **103**: p. 155-159.
71. Hauer-Jensen, M., J.W. Denham, and H.J. Andreyev, *Radiation enteropathy--pathogenesis, treatment and prevention*. Nat Rev Gastroenterol Hepatol, 2014. **11**(8): p. 470-9.
72. Bhutta, B.S., R. Fatima, and M. Aziz, *Radiation Enteritis*, in *StatPearls*. 2024: Treasure Island (FL).
73. Le, Q.T., et al., *Emerging Treatment Paradigms in Radiation Oncology*. Clin Cancer Res, 2015. **21**(15): p. 3393-401.
74. Shadad, A.K., et al., *Gastrointestinal radiation injury: symptoms, risk factors and mechanisms*. World J Gastroenterol, 2013. **19**(2): p. 185-98.
75. Singh, V.K., et al., *Pathology of acute sub-lethal or near-lethal irradiation of nonhuman primates prophylaxed with the nutraceutical, gamma tocotrienol*. Sci Rep, 2024. **14**(1): p. 13315.
76. Gu, J., et al., *At What Dose Can Total Body and Whole Abdominal Irradiation Cause Lethal Intestinal Injury Among C57BL/6J Mice?* Dose Response, 2020. **18**(3): p. 1559325820956783.
77. Chua, H.L., et al., *Long-term hematopoietic stem cell damage in a murine model of the hematopoietic syndrome of the acute radiation syndrome*. Health Phys, 2012. **103**(4): p. 356-66.
78. Booth, C., et al., *Evidence of delayed gastrointestinal syndrome in high-dose irradiated mice*. Health Phys, 2012. **103**(4): p. 400-10.
79. Booth, C., et al., *Acute gastrointestinal syndrome in high-dose irradiated mice*. Health Phys, 2012. **103**(4): p. 383-99.
80. Guiu, J., et al., *Tracing the origin of adult intestinal stem cells*. Nature, 2019. **570**(7759): p. 107-111.

81. van Es, J.H., et al., *Dll1+ secretory progenitor cells revert to stem cells upon crypt damage*. Nat Cell Biol, 2012. **14**(10): p. 1099-1104.
82. Nusse, Y.M., et al., *Parasitic helminths induce fetal-like reversion in the intestinal stem cell niche*. Nature, 2018. **559**(7712): p. 109-113.
83. Yui, S., et al., *YAP/TAZ-Dependent Reprogramming of Colonic Epithelium Links ECM Remodeling to Tissue Regeneration*. Cell Stem Cell, 2018. **22**(1): p. 35-49 e7.
84. Tetteh, P.W., et al., *Replacement of Lost Lgr5-Positive Stem Cells through Plasticity of Their Enterocyte-Lineage Daughters*. Cell Stem Cell, 2016. **18**(2): p. 203-13.
85. Tomic, G., et al., *Phospho-regulation of ATOH1 Is Required for Plasticity of Secretory Progenitors and Tissue Regeneration*. Cell Stem Cell, 2018. **23**(3): p. 436-443 e7.
86. Malagola, E., et al., *Isthmus progenitor cells contribute to homeostatic cellular turnover and support regeneration following intestinal injury*. Cell, 2024. **187**(12): p. 3056-3071 e17.
87. Yu, S., et al., *Paneth Cell Multipotency Induced by Notch Activation following Injury*. Cell Stem Cell, 2018. **23**(1): p. 46-59 e5.
88. Yan, K.S., et al., *Intestinal Enteroendocrine Lineage Cells Possess Homeostatic and Injury-Inducible Stem Cell Activity*. Cell Stem Cell, 2017. **21**(1): p. 78-90 e6.
89. Westphalen, C.B., et al., *Long-lived intestinal tuft cells serve as colon cancer-initiating cells*. J Clin Invest, 2014. **124**(3): p. 1283-95.
90. Sheaffer, K.L., et al., *DNA methylation is required for the control of stem cell differentiation in the small intestine*. Genes Dev, 2014. **28**(6): p. 652-64.
91. Kaaij, L.T., et al., *DNA methylation dynamics during intestinal stem cell differentiation reveals enhancers driving gene expression in the villus*. Genome Biol, 2013. **14**(5): p. R50.
92. Yu, D.H., et al., *Postnatal epigenetic regulation of intestinal stem cells requires DNA methylation and is guided by the microbiome*. Genome Biol, 2015. **16**: p. 211.
93. Okamoto, R., et al., *Requirement of Notch activation during regeneration of the intestinal epithelia*. Am J Physiol Gastrointest Liver Physiol, 2009. **296**(1): p. G23-35.

94. Gasnier, M., H.Y.G. Lim, and N. Barker, *Role of Wnt signaling in the maintenance and regeneration of the intestinal epithelium*. Curr Top Dev Biol, 2023. **153**: p. 281-326.
95. Harnack, C., et al., *R-spondin 3 promotes stem cell recovery and epithelial regeneration in the colon*. Nat Commun, 2019. **10**(1): p. 4368.
96. Gregorieff, A., et al., *Yap-dependent reprogramming of Lgr5(+) stem cells drives intestinal regeneration and cancer*. Nature, 2015. **526**(7575): p. 715-8.
97. Serra, D., et al., *Self-organization and symmetry breaking in intestinal organoid development*. Nature, 2019. **569**(7754): p. 66-72.
98. Kim, H.B., et al., *Prostaglandin E(2) Activates YAP and a Positive-Signaling Loop to Promote Colon Regeneration After Colitis but Also Carcinogenesis in Mice*. Gastroenterology, 2017. **152**(3): p. 616-630.
99. Fu, M., et al., *The Hippo signalling pathway and its implications in human health and diseases*. Signal Transduct Target Ther, 2022. **7**(1): p. 376.
100. Goldsmith, J.R., et al., *TNFAIP8 controls murine intestinal stem cell homeostasis and regeneration by regulating microbiome-induced Akt signaling*. Nat Commun, 2020. **11**(1): p. 2591.
101. Chen, L., et al., *TGFB1 Induces Fetal Reprogramming and Enhances Intestinal Regeneration*. bioRxiv, 2023.
102. Kurokawa, K., Y. Hayakawa, and K. Koike, *Plasticity of Intestinal Epithelium: Stem Cell Niches and Regulatory Signals*. Int J Mol Sci, 2020. **22**(1).
103. Shoshkes-Carmel, M., et al., *Subepithelial telocytes are an important source of Wnts that supports intestinal crypts*. Nature, 2018. **557**(7704): p. 242-246.
104. Greicius, G., et al., *PDGFRalpha(+) pericryptal stromal cells are the critical source of Wnts and RSPO3 for murine intestinal stem cells in vivo*. Proc Natl Acad Sci U S A, 2018. **115**(14): p. E3173-E3181.
105. Wang, P., et al., *Adrenergic nerves regulate intestinal regeneration through IL-22 signaling from type 3 innate lymphoid cells*. Cell Stem Cell, 2023. **30**(9): p. 1166-1178 e8.

106. Biton, M., et al., *T Helper Cell Cytokines Modulate Intestinal Stem Cell Renewal and Differentiation*. Cell, 2018. **175**(5): p. 1307-1320 e22.
107. Saha, S., et al., *Macrophage-derived extracellular vesicle-packaged WNTs rescue intestinal stem cells and enhance survival after radiation injury*. Nat Commun, 2016. **7**: p. 13096.
108. Hume, D.A., V.H. Perry, and S. Gordon, *The mononuclear phagocyte system of the mouse defined by immunohistochemical localisation of antigen F4/80: macrophages associated with epithelia*. Anat Rec, 1984. **210**(3): p. 503-12.
109. Lee, S.H., P.M. Starkey, and S. Gordon, *Quantitative analysis of total macrophage content in adult mouse tissues. Immunochemical studies with monoclonal antibody F4/80*. J Exp Med, 1985. **161**(3): p. 475-89.
110. Yona, S., et al., *Fate mapping reveals origins and dynamics of monocytes and tissue macrophages under homeostasis*. Immunity, 2013. **38**(1): p. 79-91.
111. Hashimoto, D., et al., *Tissue-resident macrophages self-maintain locally throughout adult life with minimal contribution from circulating monocytes*. Immunity, 2013. **38**(4): p. 792-804.
112. Shaw, T.N., et al., *Tissue-resident macrophages in the intestine are long lived and defined by Tim-4 and CD4 expression*. J Exp Med, 2018. **215**(6): p. 1507-1518.
113. Mills, C.D., et al., *M-1/M-2 macrophages and the Th1/Th2 paradigm*. J Immunol, 2000. **164**(12): p. 6166-73.
114. Mulder, K., et al., *Cross-tissue single-cell landscape of human monocytes and macrophages in health and disease*. Immunity, 2021. **54**(8): p. 1883-1900 e5.
115. Nahrendorf, M. and F.K. Swirski, *Abandoning M1/M2 for a Network Model of Macrophage Function*. Circ Res, 2016. **119**(3): p. 414-7.
116. Delfini, M., et al., *Macrophages in the gut: Masters in multitasking*. Immunity, 2022. **55**(9): p. 1530-1548.
117. Epelman, S., K.J. Lavine, and G.J. Randolph, *Origin and functions of tissue macrophages*. Immunity, 2014. **41**(1): p. 21-35.
118. Bain, C.C. and A. Schridde, *Origin, Differentiation, and Function of Intestinal Macrophages*. Front Immunol, 2018. **9**: p. 2733.
119. Lynch, S.V. and O. Pedersen, *The Human Intestinal Microbiome in Health and Disease*. N Engl J Med, 2016. **375**(24): p. 2369-2379.

120. Niechcial, A., et al., *Spermidine Ameliorates Colitis via Induction of Anti-Inflammatory Macrophages and Prevention of Intestinal Dysbiosis*. J Crohns Colitis, 2023. **17**(9): p. 1489-1503.
121. Schridde, A., et al., *Tissue-specific differentiation of colonic macrophages requires TGFbeta receptor-mediated signaling*. Mucosal Immunol, 2017. **10**(6): p. 1387-1399.
122. Kumawat, A.K., et al., *Expression and characterization of alphavbeta5 integrin on intestinal macrophages*. Eur J Immunol, 2018. **48**(7): p. 1181-1187.
123. Muller, P.A., et al., *Crosstalk between muscularis macrophages and enteric neurons regulates gastrointestinal motility*. Cell, 2014. **158**(2): p. 300-313.
124. Jarde, T., et al., *Mesenchymal Niche-Derived Neuregulin-1 Drives Intestinal Stem Cell Proliferation and Regeneration of Damaged Epithelium*. Cell Stem Cell, 2020. **27**(4): p. 646-662 e7.
125. Shouval, D.S., et al., *Interleukin-10 receptor signaling in innate immune cells regulates mucosal immune tolerance and anti-inflammatory macrophage function*. Immunity, 2014. **40**(5): p. 706-19.
126. Shaw, M.H., et al., *Microbiota-induced IL-1beta, but not IL-6, is critical for the development of steady-state TH17 cells in the intestine*. J Exp Med, 2012. **209**(2): p. 251-8.
127. Denning, T.L., et al., *Functional specializations of intestinal dendritic cell and macrophage subsets that control Th17 and regulatory T cell responses are dependent on the T cell/APC ratio, source of mouse strain, and regional localization*. J Immunol, 2011. **187**(2): p. 733-47.
128. Denning, T.L., et al., *Lamina propria macrophages and dendritic cells differentially induce regulatory and interleukin 17-producing T cell responses*. Nat Immunol, 2007. **8**(10): p. 1086-94.
129. Willenborg, S., et al., *CCR2 recruits an inflammatory macrophage subpopulation critical for angiogenesis in tissue repair*. Blood, 2012. **120**(3): p. 613-25.
130. Lucas, T., et al., *Differential roles of macrophages in diverse phases of skin repair*. J Immunol, 2010. **184**(7): p. 3964-77.
131. Leoni, G., et al., *Wound repair: role of immune-epithelial interactions*. Mucosal Immunol, 2015. **8**(5): p. 959-68.

132. Kurashima, Y. and H. Kiyono, *Mucosal Ecological Network of Epithelium and Immune Cells for Gut Homeostasis and Tissue Healing*. Annu Rev Immunol, 2017. **35**: p. 119-147.
133. Piccolo, S., S. Dupont, and M. Cordenonsi, *The biology of YAP/TAZ: hippo signaling and beyond*. Physiol Rev, 2014. **94**(4): p. 1287-312.
134. Dupont, S., et al., *Role of YAP/TAZ in mechanotransduction*. Nature, 2011. **474**(7350): p. 179-83.
135. Yao, H. and G. Tang, *Macrophages in intestinal fibrosis and regression*. Cell Immunol, 2022. **381**: p. 104614.
136. Qiao, L., et al., *Total Flavone of Abelmoschus manihot Ameliorates TNBS-Induced Colonic Fibrosis by Regulating Th17/Treg Balance and Reducing Extracellular Matrix*. Front Pharmacol, 2021. **12**: p. 769793.
137. Gao, Y., et al., *The Roles of Macrophages in Heart Regeneration and Repair After Injury*. Front Cardiovasc Med, 2021. **8**: p. 744615.
138. Tonkin, J., et al., *Monocyte/Macrophage-derived IGF-1 Orchestrates Murine Skeletal Muscle Regeneration and Modulates Autocrine Polarization*. Mol Ther, 2015. **23**(7): p. 1189-1200.
139. Chamoto, K., et al., *Alveolar macrophage dynamics in murine lung regeneration*. J Cell Physiol, 2012. **227**(9): p. 3208-15.
140. Rodero, M.P. and K. Khosrotehrani, *Skin wound healing modulation by macrophages*. Int J Clin Exp Pathol, 2010. **3**(7): p. 643-53.
141. Ding, J., et al., *Macrophages are necessary for skin regeneration during tissue expansion*. J Transl Med, 2019. **17**(1): p. 36.
142. Zhang, Y., et al., *Lineage tracing: technology tool for exploring the development, regeneration, and disease of the digestive system*. Stem Cell Res Ther, 2020. **11**(1): p. 438.
143. Kretzschmar, K. and F.M. Watt, *Lineage tracing*. Cell, 2012. **148**(1-2): p. 33-45.
144. Wang, T., et al., *Cre-loxP-mediated genetic lineage tracing: Unraveling cell fate and origin in the developing heart*. Front Cardiovasc Med, 2023. **10**: p. 1085629.
145. Barker, N., et al., *Identification of stem cells in small intestine and colon by marker gene Lgr5*. Nature, 2007. **449**(7165): p. 1003-7.
146. Indra, A.K., et al., *Temporally-controlled site-specific mutagenesis in the basal layer of the epidermis: comparison of the recombinase activity of the tamoxifen-inducible Cre-ER(T) and*

Cre-ER(T2) recombinases. Nucleic Acids Res, 1999. **27**(22): p. 4324-7.
147. Chong, J.J., E. Forte, and R.P. Harvey, *Developmental origins and lineage descendants of endogenous adult cardiac progenitor cells*. Stem Cell Res, 2014. **13**(3 Pt B): p. 592-614.
148. Gao, M., C. Qiao, and Y. Huang, *UniTVelo: temporally unified RNA velocity reinforces single-cell trajectory inference*. Nat Commun, 2022. **13**(1): p. 6586.
149. Lange, M., et al., *CellRank for directed single-cell fate mapping*. Nat Methods, 2022. **19**(2): p. 159-170.
150. Haber, A.L., et al., *A single-cell survey of the small intestinal epithelium*. Nature, 2017. **551**(7680): p. 333-339.
151. Wang, Y.C., et al., *Intestinal cell type-specific communication networks underlie homeostasis and response to Western diet*. J Exp Med, 2023. **220**(5).
152. Dimitrov, D., et al., *LIANA+ provides an all-in-one framework for cell-cell communication inference*. Nat Cell Biol, 2024. **26**(9): p. 1613-1622.
153. Garrido-Trigo, A., et al., *Macrophage and neutrophil heterogeneity at single-cell spatial resolution in human inflammatory bowel disease*. Nat Commun, 2023. **14**(1): p. 4506.
154. Joanito, I., et al., *Single-cell and bulk transcriptome sequencing identifies two epithelial tumor cell states and refines the consensus molecular classification of colorectal cancer*. Nat Genet, 2022. **54**(7): p. 963-975.
155. Canellas-Socias, A., et al., *Metastatic recurrence in colorectal cancer arises from residual EMP1(+) cells*. Nature, 2022. **611**(7936): p. 603-613.
156. Kim, S.S., et al., *Leveraging single-cell ATAC-seq and RNA-seq to identify disease-critical fetal and adult brain cell types*. Nat Commun, 2024. **15**(1): p. 563.
157. Burclaff, J., et al., *A Proximal-to-Distal Survey of Healthy Adult Human Small Intestine and Colon Epithelium by Single-Cell Transcriptomics*. Cell Mol Gastroenterol Hepatol, 2022. **13**(5): p. 1554-1589.
158. Date, S. and T. Sato, *Mini-gut organoids: reconstitution of the stem cell niche*. Annu Rev Cell Dev Biol, 2015. **31**: p. 269-89.

159. Pikkupeura, L.M., et al., *Transcriptional and epigenomic profiling identifies YAP signaling as a key regulator of intestinal epithelium maturation*. Sci Adv, 2023. **9**(28): p. eadf9460.
160. Szvicsek, Z., et al., *Extracellular vesicle release from intestinal organoids is modulated by Apc mutation and other colorectal cancer progression factors*. Cell Mol Life Sci, 2019. **76**(12): p. 2463-2476.
161. Taelman, J., M. Diaz, and J. Guiu, *Human Intestinal Organoids: Promise and Challenge*. Front Cell Dev Biol, 2022. **10**: p. 854740.
162. Nozaki, K., et al., *Co-culture with intestinal epithelial organoids allows efficient expansion and motility analysis of intraepithelial lymphocytes*. J Gastroenterol, 2016. **51**(3): p. 206-13.
163. Rogoz, A., et al., *A 3-D enteroid-based model to study T-cell and epithelial cell interaction*. J Immunol Methods, 2015. **421**: p. 89-95.
164. Noel, G., et al., *A primary human macrophage-enteroid co-culture model to investigate mucosal gut physiology and host-pathogen interactions*. Sci Rep, 2017. **7**: p. 45270.
165. Staab, J.F., et al., *Co-Culture System of Human Enteroids/Colonoids with Innate Immune Cells*. Curr Protoc Immunol, 2020. **131**(1): p. e113.
166. Lindemans, C.A., et al., *Interleukin-22 promotes intestinal-stem-cell-mediated epithelial regeneration*. Nature, 2015. **528**(7583): p. 560-564.
167. Pavlidis, P., et al., *Cytokine responsive networks in human colonic epithelial organoids unveil a molecular classification of inflammatory bowel disease*. Cell Rep, 2022. **40**(13): p. 111439.
168. Jowett, G.M., et al., *ILC1 drive intestinal epithelial and matrix remodelling*. Nat Mater, 2021. **20**(2): p. 250-259.
169. Beaurivage, C., et al., *Development of a human primary gut-on-a-chip to model inflammatory processes*. Sci Rep, 2020. **10**(1): p. 21475.
170. Valiei, A., J. Aminian-Dehkordi, and M.R.K. Mofrad, *Gut-on-a-chip models for dissecting the gut microbiology and physiology*. APL Bioeng, 2023. **7**(1): p. 011502.
171. Brassard, J.A., et al., *Recapitulating macro-scale tissue self-organization through organoid bioprinting*. Nat Mater, 2021. **20**(1): p. 22-29.

172. Ewels, P.A., et al., *The nf-core framework for community-curated bioinformatics pipelines*. Nat Biotechnol, 2020. **38**(3): p. 276-278.
173. Love, M.I., W. Huber, and S. Anders, *Moderated estimation of fold change and dispersion for RNA-seq data with DESeq2*. Genome Biol, 2014. **15**(12): p. 550.
174. Subramanian, A., et al., *Gene set enrichment analysis: a knowledge-based approach for interpreting genome-wide expression profiles*. Proc Natl Acad Sci U S A, 2005. **102**(43): p. 15545-50.
175. Dobin, A., et al., *STAR: ultrafast universal RNA-seq aligner*. Bioinformatics, 2013. **29**(1): p. 15-21.
176. Huang, X. and Y. Huang, *Cellsnp-lite: an efficient tool for genotyping single cells*. Bioinformatics, 2021. **37**(23): p. 4569-4571.
177. Huang, Y., D.J. McCarthy, and O. Stegle, *Vireo: Bayesian demultiplexing of pooled single-cell RNA-seq data without genotype reference*. Genome Biol, 2019. **20**(1): p. 273.
178. Buttner, M., et al., *scCODA is a Bayesian model for compositional single-cell data analysis*. Nat Commun, 2021. **12**(1): p. 6876.
179. Tirosh, I., et al., *Dissecting the multicellular ecosystem of metastatic melanoma by single-cell RNA-seq*. Science, 2016. **352**(6282): p. 189-96.
180. Fordham, R.P., et al., *Transplantation of expanded fetal intestinal progenitors contributes to colon regeneration after injury*. Cell Stem Cell, 2013. **13**(6): p. 734-44.
181. Mustata, R.C., et al., *Identification of Lgr5-independent spheroid-generating progenitors of the mouse fetal intestinal epithelium*. Cell Rep, 2013. **5**(2): p. 421-32.
182. Ying, W., et al., *Investigation of macrophage polarization using bone marrow derived macrophages*. J Vis Exp, 2013(76).
183. Viola, M.F. and G. Boeckxstaens, *Niche-specific functional heterogeneity of intestinal resident macrophages*. Gut, 2021. **70**(7): p. 1383-1395.
184. Jung, S., et al., *In vivo depletion of CD11c+ dendritic cells abrogates priming of CD8+ T cells by exogenous cell-associated antigens*. Immunity, 2002. **17**(2): p. 211-20.
185. Bradford, B.M., et al., *Defining the anatomical localisation of subsets of the murine mononuclear phagocyte system using integrin alpha X (Itgax, CD11c) and colony stimulating factor 1*

receptor (Csf1r, CD115) expression fails to discriminate dendritic cells from macrophages. Immunobiology, 2011. **216**(11): p. 1228-37.
186. Mann, L., et al., *CD11c.DTR mice develop a fatal fulminant myocarditis after local or systemic treatment with diphtheria toxin*. Eur J Immunol, 2016. **46**(8): p. 2028-42.
187. Ayyaz, A., et al., *Single-cell transcriptomes of the regenerating intestine reveal a revival stem cell*. Nature, 2019. **569**(7754): p. 121-125.
188. Chan, C.W., et al., *Gastrointestinal differentiation marker Cytokeratin 20 is regulated by homeobox gene CDX1*. Proc Natl Acad Sci U S A, 2009. **106**(6): p. 1936-41.
189. Merlos-Suarez, A., et al., *The intestinal stem cell signature identifies colorectal cancer stem cells and predicts disease relapse*. Cell Stem Cell, 2011. **8**(5): p. 511-24.
190. Orecchioni, M., et al., *Macrophage Polarization: Different Gene Signatures in M1(LPS+) vs. Classically and M2(LPS-) vs. Alternatively Activated Macrophages*. Front Immunol, 2019. **10**: p. 1084.
191. Martinez, F.O. and S. Gordon, *The M1 and M2 paradigm of macrophage activation: time for reassessment*. F1000Prime Rep, 2014. **6**: p. 13.
192. Zhang, Y., et al., *ErbB2 and ErbB3 regulate recovery from dextran sulfate sodium-induced colitis by promoting mouse colon epithelial cell survival*. Lab Invest, 2012. **92**(3): p. 437-50.
193. Bartus, K., et al., *Neuregulin-1 controls an endogenous repair mechanism after spinal cord injury*. Brain, 2016. **139**(Pt 5): p. 1394-416.
194. Gemberling, M., et al., *Nrg1 is an injury-induced cardiomyocyte mitogen for the endogenous heart regeneration program in zebrafish*. Elife, 2015. **4**.
195. Jarde, T., et al., *Wnt and Neuregulin1/ErbB signalling extends 3D culture of hormone responsive mammary organoids*. Nat Commun, 2016. **7**: p. 13207.
196. Pang, X., et al., *SPP1 Promotes Enzalutamide Resistance and Epithelial-Mesenchymal-Transition Activation in Castration-Resistant Prostate Cancer via PI3K/AKT and ERK1/2 Pathways*. Oxid Med Cell Longev, 2021. **2021**: p. 5806602.

197. Sun, G., Z. Shang, and W. Liu, *SPP1 Regulates Radiotherapy Sensitivity of Gastric Adenocarcinoma via the Wnt/Beta-Catenin Pathway*. J Oncol, 2021. **2021**: p. 1642852.
198. Zeng, B., et al., *SPP1 promotes ovarian cancer progression via Integrin beta1/FAK/AKT signaling pathway*. Onco Targets Ther, 2018. **11**: p. 1333-1343.
199. Lemmetyinen, T.T., et al., *Fibroblast-derived EGF ligand neuregulin 1 induces fetal-like reprogramming of the intestinal epithelium without supporting tumorigenic growth*. Dis Model Mech, 2023. **16**(4).
200. Liberzon, A., et al., *The Molecular Signatures Database (MSigDB) hallmark gene set collection*. Cell Syst, 2015. **1**(6): p. 417-425.
201. Krausova, M. and V. Korinek, *Wnt signaling in adult intestinal stem cells and cancer*. Cell Signal, 2014. **26**(3): p. 570-9.
202. Montenegro-Miranda, P.S., et al., *A Novel Organoid Model of Damage and Repair Identifies HNF4alpha as a Critical Regulator of Intestinal Epithelial Regeneration*. Cell Mol Gastroenterol Hepatol, 2020. **10**(2): p. 209-223.
203. Ascension, A.M., M.J. Arauzo-Bravo, and A. Izeta, *The need to reassess single-cell RNA sequencing datasets: the importance of biological sample processing*. F1000Res, 2021. **10**: p. 767.
204. van den Brink, S.C., et al., *Single-cell sequencing reveals dissociation-induced gene expression in tissue subpopulations*. Nat Methods, 2017. **14**(10): p. 935-936.
205. Hao, Y., et al., *Integrated analysis of multimodal single-cell data*. Cell, 2021. **184**(13): p. 3573-3587 e29.
206. Morral, C., et al., *Zonation of Ribosomal DNA Transcription Defines a Stem Cell Hierarchy in Colorectal Cancer*. Cell Stem Cell, 2020. **26**(6): p. 845-861 e12.
207. Dilworth, J.T., et al., *Preclinical models for translational research should maintain pace with modern clinical practice*. Int J Radiat Oncol Biol Phys, 2014. **88**(3): p. 540-4.
208. Krause, M., et al., *Specific requirements for translation of biological research into clinical radiation oncology*. Mol Oncol, 2020. **14**(7): p. 1569-1576.
209. Yip, J.L.K., et al., *The Role of Intestinal Macrophages in Gastrointestinal Homeostasis: Heterogeneity and Implications in Disease*. Cell Mol Gastroenterol Hepatol, 2021. **12**(5): p. 1701-1718.

210. Na, Y.R., et al., *Macrophages in intestinal inflammation and resolution: a potential therapeutic target in IBD*. Nat Rev Gastroenterol Hepatol, 2019. **16**(9): p. 531-543.
211. Sehgal, A., et al., *The role of CSF1R-dependent macrophages in control of the intestinal stem-cell niche*. Nat Commun, 2018. **9**(1): p. 1272.
212. Fritsch, S.D., et al., *Metabolic support by macrophages sustains colonic epithelial homeostasis*. Cell Metab, 2023. **35**(11): p. 1931-1943 e8.
213. Chakrabarti, R., et al., *Notch ligand Dll1 mediates cross-talk between mammary stem cells and the macrophageal niche*. Science, 2018. **360**(6396).
214. Aurora, A.B., et al., *Macrophages are required for neonatal heart regeneration*. J Clin Invest, 2014. **124**(3): p. 1382-92.
215. Kraiczy, J., et al., *Graded BMP signaling within intestinal crypt architecture directs self-organization of the Wnt-secreting stem cell niche*. Cell Stem Cell, 2023. **30**(4): p. 433-449 e8.
216. Liu, P., et al., *Role of macrophages in peripheral nerve injury and repair*. Neural Regen Res, 2019. **14**(8): p. 1335-1342.
217. Mamilos, A., et al., *Macrophages: From Simple Phagocyte to an Integrative Regulatory Cell for Inflammation and Tissue Regeneration-A Review of the Literature*. Cells, 2023. **12**(2).
218. Wang, X. and L. Zhou, *The Many Roles of Macrophages in Skeletal Muscle Injury and Repair*. Front Cell Dev Biol, 2022. **10**: p. 952249.
219. D'Angelo, F., et al., *Macrophages promote epithelial repair through hepatocyte growth factor secretion*. Clin Exp Immunol, 2013. **174**(1): p. 60-72.
220. Morhardt, T.L., et al., *IL-10 produced by macrophages regulates epithelial integrity in the small intestine*. Sci Rep, 2019. **9**(1): p. 1223.
221. Pull, S.L., et al., *Activated macrophages are an adaptive element of the colonic epithelial progenitor niche necessary for regenerative responses to injury*. Proc Natl Acad Sci U S A, 2005. **102**(1): p. 99-104.
222. Quiros, M., et al., *Macrophage-derived IL-10 mediates mucosal repair by epithelial WISP-1 signaling*. J Clin Invest, 2017. **127**(9): p. 3510-3520.

223. Na, Y.R., *Prostaglandin E2 receptor PTGER4-expressing macrophages promote intestinal epithelial barrier regeneration upon inflammation*. Gut, 2021. **70**(12).
224. Zhu, P., et al., *Gut microbiota drives macrophage-dependent self-renewal of intestinal stem cells via niche enteric serotonergic neurons*. Cell Res, 2022. **32**(6): p. 555-569.
225. Rotem, I., et al., *Osteopontin promotes infarct repair*. Basic Res Cardiol, 2022. **117**(1): p. 51.
226. Wang, W., et al., *Osteopontin activates mesenchymal stem cells to repair skin wound*. PLoS One, 2017. **12**(9): p. e0185346.
227. Wang, Y., et al., *Osteopontin May Improve Postinjury Muscle Repair Via Matrix Metalloproteinases And tgf-beta Activation in Regular Exercise*. Int J Med Sci, 2023. **20**(9): p. 1202-1211.
228. Rutherford, D. and G.T. Ho, *Therapeutic Potential of Human Intestinal Organoids in Tissue Repair Approaches in Inflammatory Bowel Diseases*. Inflamm Bowel Dis, 2023. **29**(9): p. 1488-1498.
229. Zhang, F.L., et al., *Organoids transplantation attenuates intestinal ischemia/reperfusion injury in mice through L-Malic acid-mediated M2 macrophage polarization*. Nat Commun, 2023. **14**(1): p. 6779.
230. Duan, Z. and Y. Luo, *Targeting macrophages in cancer immunotherapy*. Signal Transduct Target Ther, 2021. **6**(1): p. 127.
231. Duffield, J.S., et al., *Selective depletion of macrophages reveals distinct, opposing roles during liver injury and repair*. J Clin Invest, 2005. **115**(1): p. 56-65.
232. McKendrick, J.G., et al., *CSF1R-dependent macrophages in the salivary gland are essential for epithelial regeneration after radiation-induced injury*. Sci Immunol, 2023. **8**(89): p. eadd4374.
233. Gohagan, J.K., et al., *Prostate cancer screening in the prostate, lung, colorectal and ovarian cancer screening trial of the National Cancer Institute*. J Urol, 1994. **152**(5 Pt 2): p. 1905-9.